A DISTINCT SUBPOPULATION OF MELANOPSIN GANGLION CELLS IN THE DORSAL RETINA: PHOTORECEPTION, DISTRIBUTION, AND CENTRAL INNERVATION

By

Michael H. Berry

THESIS DISSERTATION

Oregon Health & Science University - School of Medicine

Department of Physiology & Pharmacology
Casey Eye Institute

In partial fulfillment of the requirements for the degree of
Doctor of Philosophy

March 2022

TABLE OF CONTENTS i

I also appreciate the amazing members of the Sivyer, Allen, and Schultz labs, past and present, for creating an environment of learning, advancement and comradery. I am especially grateful to Ben Sivyer, Tavita Garrett, Joe Leffler, Charles Allen, Michael Moldavan, Olga Cravetchi, and Marc Meadows for their intellectual discussions and scientific contributions to my thesis. This work could not have been done without them.

Dr. Beth Edmunds has served as my clinical mentor and a source of career advice and personal support during my training. Through her dedication, kindness, expansive knowledge and 1-on-1 teaching, she has instilled in me the skills of patient management and provided a foundation in the identification, description and treatment of eye disease. My time with her has brought clinical perspective to my past work and established exciting avenues for my future research interests. I am immensely grateful for her support and for nurturing my passion for training in Ophthalmology.

Thank you to Udi Isacoff from UC Berkeley who inspired me to pursue a scientific career and has continued to serve as a source of support and mentorship throughout my medical and graduate training. Udi also kindly provided the MEA that I employed in experiments described in Chapter 4. This equipment allowed me to further develop my skills in multi-electrode recording techniques.

ABSTRACT

Technological changes to modern society have lead to circadian misalignment in a significant portion of the population, resulting in numerous metabolic, sleep, and mood disorders. This dysfunction is due to alterations in the vast range of biological clocks that regulate our physiology. Clock entrainment is achieved through the light and dark of the day-night cycle, sensed by a unique class of photoreceptors in the retina called intrinsically photosensitive retinal ganglion cells (ipRGCs). Distinct from rod and cone photoreceptors classically involved in visual perception, ipRGCs form direct connections primarily with non-image forming areas of the brain, influencing numerous neuroendocrine modulators throughout the body. IpRGC mediated entrainment is important for health maintenance and interruptions can cause dysregulation of our endogenous clocks. This significant health burden demonstrates a clear need for more integrated medical practices and methods of circadian realignment. However, much about ipRGCs remains unknown and a deeper understanding of their diversity, distribution, and function is still required.

IpRGCs are responsible for encoding changes in ambient light but are more complex than originally anticipated. Although they only make up a small percentage of the retinal population, it is now evident that ipRGCs consist of multiple distinct 'types' that project to more than a dozen discrete brain regions. Furthermore, it appears that ipRGCs express different amounts of melanopsin and receive variable synaptic input. This together suggests that ipRGC

subpopulations are extracting, encoding, and projecting different aspects of visual information to influence a separate collection of light-driven behaviors. However, the specific functional role of the majority of ipRGCs remains unclear.

My thesis work has focused on the study of a previously undescribed subpopulation of ipRGCs. These cells form an evenly-spaced mosaic and are restricted to the dorsal retina, coding for luminance reflected off the ground. Although they share some morphological similarity with other ipRGCs, I demonstrate this subpopulation has unique central projects to areas of circadian pacemaking, and form the exclusive innervation to the supraoptic nucleus (SON-ipRGCs); a site involved in systemic fluid homeostasis, maternal behavior, and appetite.

I also examined the light encoding capacity of SON-ipRGCs and compared them with other ipRGCs of the dorsal retina, without disturbing their photosensitivity. To achieve this I used a multi-electrode array (MEA) to record rod, cone and melanopsin mediated photoresponses, in combination with a novel 'OptoTaging' approach to selectively localize Chanelrodopsin expressing retinal cells at the end of the recordings. I found that SON-ipRGCs are one of eight functional subtypes of ipRGCs, each with distinct photosensitivity and response timing. The photoresponses from SON-ipRGCs are highly uniform and sensitive, exhibiting the most sustained photoresponses of all ipRGCs. They respond over a wide

range of light intensities from starlight to bright daylight and encode constant light levels under conditions that activate melanopsin.

My graduate work has extended our understanding of ipRGC diversity and described a novel population of non-image forming cells. Although the behavioral function of SON-ipRGCs is unknown, their localized distribution in the dorsal retina might underlie the increased reliance on reflected luminance in diurnal and nocturnal environments.

LIST OF TABLES & FIGURES

LIST OF TABLES

LIST OF FIGURES

CHAPTER 1: INTRODUCTION

1.1 – Preface

The retina is a paper-thin layer of tissue responsible for encoding our visual environment. Despite its slender appearance, the retina is organized into both morphologically and functionally distinct layers that contribute significantly to image computation, extraction, and processing. When light enters the eye electrical signals are generated from the absorbance of photons by opsin proteins found in the rod and cone photoreceptors of the outer retina. These signals are passed through bipolar cells, with neighboring input from a complex network of additional interneurons (amacrine and horizontal cells) before summating onto retinal ganglion cells (RGCs) in the inner retina. Unlike the majority of other retinal cells, RGCs are capable of producing action potentials and posses long axons that leave the eye via the optic nerve to deliver visual information centrally with high spatial and temporal resolution. Signals from individual RGC axons integrate at higher order visual areas in the brain, allowing for visual perception. However, the behavioral function of light sensation is not exclusively used for navigating the environment. Many biological processes as diverse as sleep regulation, pupillary constriction, hormonal adjustment, neuromodulation, mood, and learning and are influenced by the subconscious ability to sense illumination changes throughout the solar day and night cycle. As a result, vision can be clearly organized into image and non-image forming functions.

For most of the last century it was believed that both image and non-image forming visual functions were encoded by the photosensitive rods and cones of the outer retina. But, through a series of exciting and impactful studies beginning in late 90s[1], a third photoreceptor, expressing the photosensitive protein melanopsin, was discovered to be primarily responsible for non-image forming vision[2-5]. These melanopsin expressing photoreceptors are a small population (0.5% in human) of retinal ganglion cells in the inner retina and referred to as intrinsically photosensitive retinal ganglion cells (ipRGCs). In addition to the high spatiotemporal signal encoding of canonical RGCs, the melanopsin driven ipRGCs also respond to illumination slowly with sustained summative responses, encoding absolute intensity of luminance[6]. IpRGC axons directly convey these signals to more than 17 distinct areas in the brain[7,8], serving as the body's main biochemical synchronizer and exercising control over hormonal and neuronal modulators all over the body. Studies have also identified ipRGCs as the regulator of photo-entrainment to the day night cycle[9,10], establishing their importance in circadian maintenance. IpRGCs have defied many established expectations of retinal ganglion cells, here I will discuss their discovery, function, and diversity; components that make them among the most fascinating cell populations in the mammalian retina.

1.2 – The discovery of a third photoreceptor in the retina

Although the most substantial gains in the understanding of ipRGCs only occurred at the recent turn of the century, there have been hints of a third type of non-rod and non-cone photoreceptor for far longer. In 1927 a Harvard graduate student, Clyde Keeler, made an interesting observation in a family of white house mice he had collected for an anatomical study of eye diversity among vertebrates. Upon sectioning the retina for histological examination, he found that a small cohort of mice were missing their outer retina, lacking all rod and cone photoreceptors. This serendipitous discovery, now known to be caused by an autosomal recessive mutation in phosphodiesterase 6B enzyme used in rod photoreceptor phototransduction, was identified in humans as a cause of retinitis pigmentosa ~70 years later[11,12]. Despite this aberrant phenotype Clyde Keeler observed that these mice still retained the ability to constrict the pupil (pupillary light reflex) when exposed to light. He went on to describe this presumed form of inherited blindness[13] as well as the conundrum of a retained pupillary light reflex in animals without canonical photoreceptors[14]. As the field of Ophthalmology matured, hints of an additional retinal photoreceptor emerged in clinical patients. Throughout the 1900s physicians observed that some patients with late stages of inherited retinal disease were functionally blind but retained a sleep schedule and remained synchronized to a 24-hour day night cycle[15-17]. This entrainment could have been provided by other environmental cues, such as regularly scheduled meals; however, remaining photosensitivity was confirmed in 1995 when Czeisler et al. showed that melatonin, the sleep regulation hormone, could be suppressed

by light in a group of completely blind patients suffering from late stage photoreceptor dystrophies[18]. Though these observations were striking, skeptics could argue that a small number of residual rod and cone photoreceptors in the periphery of the outer retina might account for this remaining yet subconscious vision. This left the possibility of a third type of retinal photoreceptor in contentious debate until a discovery in 1998, made outside of the retina and in a tangential scientific discipline.

In Bethesda, Maryland, Iggy Provencio and colleagues, working on the dermal cells of frog skin, identified a new type of light sensitive molecule[1]. Responsible for light induced redistribution of melanin pigment used in amphibian camouflage, they named this protein melanopsin and designed mRNA primers to identify it in other cell types of the body using in situ hybridization. In a surprise discovery, they found a small subset of melanopsin expressing RGCs in the mouse and human retina[19]. As RGCs, including melanopsin-expressing RGCs, are located in the inner retina, Iggy Provencio and colleagues provided a potential explanation for the retained photosensitivity in rod and cone dystrophic diseases[20]. It also hinted at the illusive third type of retinal photoreceptor predicted by Clyde Keeler in 1927. This discovery contextualized previous work and motivated a flurry of studies by individuals that have now become pioneers in the field. Lucas et al. and Freedman et al. generated a transgenic mouse without rods and cones (*rd*) and demonstrated that both circadian rhythm and pupillary light reflex remained intact but are lost when the eyes are enucleated[2,3]. Multiple groups identified

direct retinal projections to hypothalamic and thalamic structures associated with image and non-image forming[21,22] vision and described the association with lighting intensity dependent changes in homeostatic functions such as body temperature, circadian rhythm and alertness behaviors[9,23,24]. Although supportive, the definitive evidence of intrinsically photosensitive RGCs came in back-to-back publications from Hattar et al. and Berson et al.[4,5]. In this work they first revealed the morphological identity and distribution of melanopsin expressing RGCs across the retina using immunostaining against the melanopsin protein[5]. Second, by designing a transgenic mouse line localizing melanopsin-expressing RGCs they identified direct axonal innervation to the supraciasmatic nucleus (SCN) and olivery pretectal nucleus, the sites of circadian pacemaking and pupillary constriction[5,10]. Third, they confirmed the intrinsic photosensitivity of these RGCs by performing retrograde brain injections in the SCN of mice and then targeting retrolabled RGCs in the retina for single cell recordings[4]. Excitingly, RGCs remained photosensitive when pharmacologically isolated under a cocktail of synaptic blockers or when their cell bodies were physically isolated from the retina.

Although circuitous, these pioneering studies collectively lead to the discovery of a third photoreceptor in the mammalian retina. A small population of intrinsically photosensitive retinal ganglion cells or "ipRGCs", distinct from the established rod and cone photoreceptors of the outer retina, primarily convey light information to non-image forming brain regions. In the last 20 years the study of

ipRGCs, melanopsin, and non-image forming vision has expanded dramatically, revealing a far more extensive relationship between retinal function, visual behavior and body homeostasis.

1.3 – Photoactivation of ipRGCs

Since the initial discovery, ipRGCs have been identified across most vertebrate species and all mammals so far examined, including human and non-human primates[25]. The intrinsic photosensitivity of ipRGCs is attributed to the melanopsin protein that is encoded by the *OPN4* gene[19]. The *OPN4* gene is surprisingly penetrant across evolutionary time and phylogenic studies suggest that melanopsin-like homologs (rhabdomeric opsins) likely comprised the sole photosensitivity of the primitive eye of vertebrates 500 million years ago[26-28]. Like rhodopsin and the cone opsins found in the photoreceptors of the outer retina, melanopsin is a 7-transmembrane G-protein coupled receptor (GPCR) that absorbs light through the isomerization of *11-cis* retinal into *trans*-retinal[29]. Interestingly, melanopsin can perform its own transisomerase activity[30], requiring replenishment from the retinal pigment epithelium (RPE) or Müller glia cells only under bright or continual light exposure[31,32]. Light activation of melanopsin initiates a series of intracellular second messengers. However, unlike the opsins of ciliary photoreceptors, whose activation leads to closure of cGMP-gated cation channels and a hyperpolarized membrane potential[33], melanopsin activation instead leads to the opening of cation channels and a membrane depolarization[34]. Previously, this was believed to be mediated exclusively through

7

the well established Gq/11 second messenger pathway used in other rhabdomeric photoreceptors, yet recent studies suggest that melanopsin may promiscuously couple to multiple signaling pathways, with interaction of second messengers being determined by the intracellular environment of the ipRGC[35-37]. Though these down stream signaling pathways are actively being explored, it is clear that melanopsin activation leads to sustained light responses critical to ipRGC function[37-39].

The photoresponse generated in rods and cones and transmitted to conventional RGCs are used for resolving detail, tracking movement, and guiding actions, amongst many other functions. As a result, these electrical responses are fast, with a rapid onset and decay on the order of milliseconds. The intrinsic photoresponses of ipRGCs however, are slow lasting seconds to minutes even following brief periods of illumination. Though not suited for the spatiotemporal requirements of image forming vision, ipRGC kinetics allow for integration of light levels over time[40]. This provides ipRGC recipient brain regions with an accurate representation of irradiance in the visual environment; a periodic count of photons rather than the instantaneous resolved image[38]. Numerous behavioral processes rely on determining environmental luminance in order to predict behaviorally relevant changes. These include the rhythmic timing of sleep-wake cycles and feeding behaviors[41]. The unique response capacity of ipRGCs allows this information to be reliably encoded. An early example provided by Nelson and Takahashi in 1991, and recently discussed by Milner & Do[42], identified that

changes to the circadian clock of laboratory animals responded to a given number of total photons, regardless of whether this quantity was presented in bulk over milliseconds or titrated over minutes[43]. This time independent nature distinguishes intrinsic and extrinsic photoreception in ipRGCs.

Like conventional RGCs, ipRGCs also receive synaptic input from the up-stream rod and cone photoreceptor mediated pathways. Therefore, sluggish intrinsic (melanopsin) and fast extrinsic (ciliary) photoresponses are combined in ipRGCs, resulting in a primarily ON-light responsive spike induction. The functional role of this dual sensitivity is currently unknown, however a couple advantages are apparent. Rhodopsin, the cone opsins, and melanopsin each exhibit differences in their sensitivity to light and action spectrum. The signaling capacity of all three types of photoreceptors allows ipRGCs to respond to light at a range spanning at least 8 log units of light intensity and considerably broadens the wavelength spectrum of visible light encoded. This could allow ipRGCs to encode luminance levels throughout the solar cycle, accounting for seasonal or weather related changes to the light. As the organization of the melanopsin protein in the cell body, dendrites and axon of RGCs have less efficient photon capture[44] compared to the disk-like lamellae of ciliary photoreceptors, the sensitivity of the melanopsin photoresponse is reduced under light exposure at short intervals. Given the importance of many sustained functions, such as continued pupillary constriction under bright light, these temporal characteristics of melanopsin likely have substantial behavioral relevance.

1.4 - ipRGC diversity in the retina

Though initially considered to be a single type of RGC[5], two decades of ipRGC studies has identified at least 6 distinct types (M1-M6) in the mouse, primarily organized by their morphological characteristics (Figure 1a). Differences in these types include their dendritic size, complexity and stratification in the inner plexiform layer, as well as their expression of melanopsin, which underlies their intrinsic photosensitivity. All of these features aid in their anatomical differentiation in the retina.
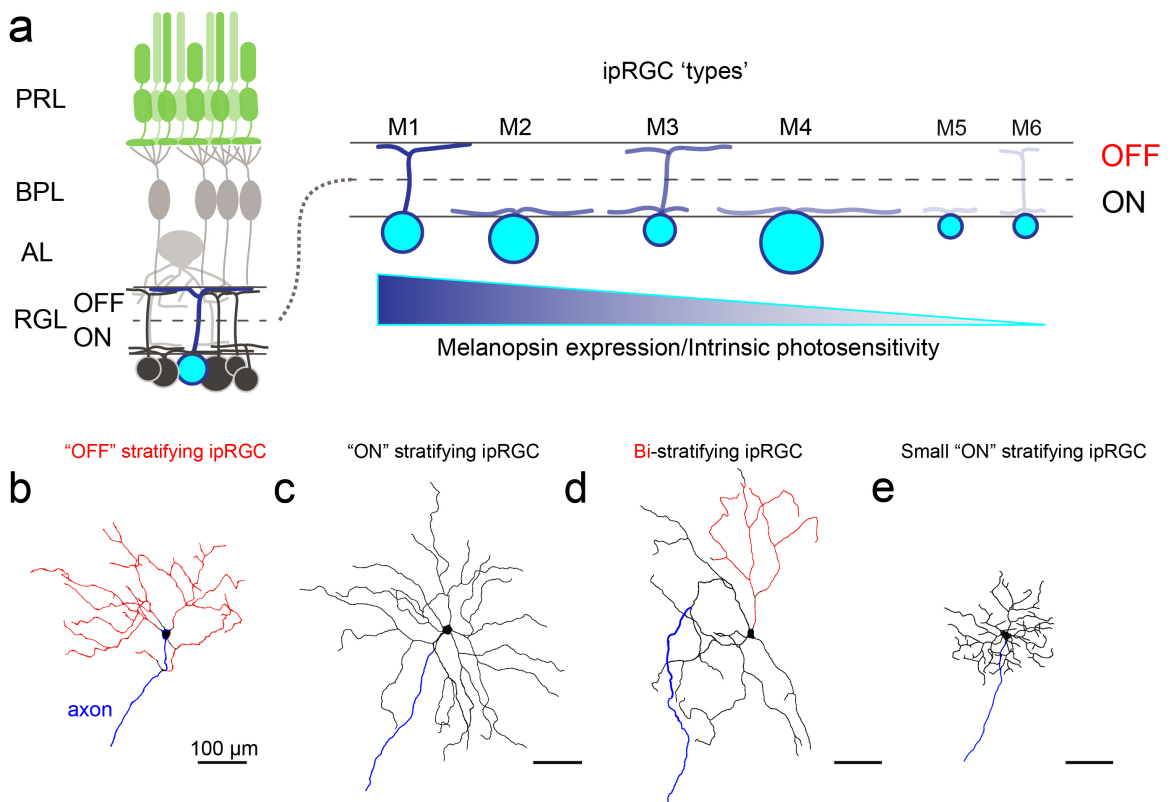
Figure 1: Illustration of ipRGC diversity
(a) Illustrative representation of the 6 current 'types' of ipRGCs, differing in their dendritic size, soma size, dendritic stratification in the ON and/or OFF layer of the IPL, and amount of melanopsin expression. (b-e) Dendritic tracings of

Neurobiotin filled ipRGCs in the GlyT2Cre:Ai9 mouse, with OFF stratifying (b) (red) M1 ipRGCs and a mixed population of ON stratifying (c-e) (black) ipRGCs.

M1 ipRGCs have small cell bodies and relatively simple dendritic structure that occupy the OFF layer of the IPL[45]. They also express the highest concentrations of melanopsin, making them the easiest to identify through immunostaining[45,46]. M2 ipRGCs have larger cell bodies and dendritic arbors compared to M1s but instead stratify in the ON layer of the IPL[6,47]. M3 ipRGCs are a significantly understudied subpopulation that share many characteristics with M2 ipRGCs but instead asymmetrically bi-stratify in both the ON and OFF layers of the IPL with variable levels of melanopsin expression. Due to their rarity and the lack of functional distinction, the M3 ipRGCs may simply represent an intermediary or partially differentiated ipRGC rather a distinct subtype[48]. M4 ipRGCs, originally defined as a subtype of Alpha cells[49,50], have the largest somas, highly complex dendritic structure, and express low levels of melanopsin[45,51,52]. A recent study found that the dendritic size of M4 ipRGCs actually differ substantially across the nasal temporal axis of the retina[53], making identification on morphology alone quite tricky. Thankfully, M4s can also be uniquely distinguished from other ipRGCs using an antibody against the non-phosphorylated neuro-filament heavy chain protein (SMI-32)[35,51]. M5 ipRGCs are also ON stratifying, and share similar structure to the M4[53] but have small tight and more highly branching dendrites[54,55]. M6 ipRGCs, though equal to the M5 in dendritic size and complexity, instead have truly bi-stratified dendritic arbors and the smallest soma

size of all ipRGCs[56]. M5 and M6 ipRGCs were originally discovered in transgenic mouse lines and express exceptionally low levels of melanopsin making them difficult to identify with immnostaining[54-56]. As a result, their study has been more protracted and currently little is known about their functional contribution to vision[57].

Unsurprisingly, the morphological diversity among ipRGC types results in functional differences in response to light. Single cell recordings have revealed that sensitivity, response latency and duration of photoresponses differ between most ipRGC types (M1-M6)[58]. M1 ipRGCs for example, due to their abundant melanopsin expression, display the highest intrinsic photosensitivity and shortest delay in response to light compared to non-M1 ipRGCs[58]. Their simple dendritic structures also means they receive less complex synaptic input from upstream rod and cone photoreceptors[45,46]. M2-M6 ipRGCs, on the other hand have less intrinsic photosensitivity but are governed by a stronger synaptic drive from rod and cone photoreceptors[6,59]. M4 ipRGCs for example, have well established center surround receptive fields, an organization that allows them to participate in the encoding of contrast and spatial frequency tuning[35,45]. M5 ipRGCs also have tuned receptive fields but display wavelength dependent color opponency in their center and surround features[55], meaning that this antagonistic circuit can encode the difference between opposing colors. As at least some M5 ipRGCs project to image-forming areas in the thalamus[55], it suggests M5 ipRGCs play a role in conscious color vision[45,60].

IpRGC types also appear to have different patterns of central projections to the brain, predicting type dependent influence over ipRGC driven behaviors. M1 ipRGCs primarily project to non-image forming areas such as the suprachiasmatic nucleus (SCN), which is the master biological pacemaker,[2,4,7,61,62], the shell of the olivery pretectal nucleus (OPN), which serves as the primary site of light dependent pupillary constriction[10,63,64], as well as a number of hypothalamic brain regions, the function of which remain unknown[45,62,65]. M4-M6 subtypes appear to project to image forming brain regions similar to conventional RGCs[54]. These include the dorsal region of the lateral geniculate nucleus (dLGN) and the superior colliculus (SC)[8,54,55,66]. The functional role of ipRGCs in image forming vision is unclear, however some exciting recent discoveries have made it an active area of investigation. Transgenic mice lacking rod and cone photoreceptors were able to discriminate course contrast gratings in a learned two choice y-maze, illustrating that the photoreception of remaining ipRGCs allows some level of conscious visual acuity to the conventionally "blind" mouse[54]. Correspondingly, animals lacking the melanopsin protein or animals lacking all non-M1 ipRGCs displayed normal visual acuity but reductions in contrast sensitivity measured using eye tracking in an Optokinetic drum[51]. M2 and M3 ipRGCs appear more mysterious with some limited evidence that they project to both image and non-image forming areas [24,45,54,67]. The lack of clearly defined sites of central innervation for ipRGC types,

emphasizes the need for more sophisticated methods and expanded tools for discriminating and studying ipRGCs[45].

M1 ipRGCs are the most well studied type in the retina and were originally identified as the first type of ipRGC[68]. There are ~800 M1 ipRGCs in the mouse retina, with dendrites that abundantly overlap with other M1 ipRGCs (~4-fold)[69]. Interestingly, the distribution of M1 ipRGCs across the retina is asymmetric, with a higher concentration located in the dorsal retina, suggesting an additional significance to the encoding of light in the ventral visual field[70]. Though morphologically similar across the retina, recent studies suggest that M1 ipRGCs are physiologically heterogenous. Using careful quantitative analysis of individual M1 cells, Michael Do's group identified vast dissimilarities in membrane properties, synaptic input, and photoresponses, even in neighboring cells recorded simultaneously in the same region of the retina[71]. Samer Hattar's group found that M1 ipRGCs can also be separated by their expression of the transcription factor *Brn3b (Pou4f2)*[64]. These two populations (Brn3b+ & Brn3b-) have distinct patterns of central innervation[62] and it is thought they underlie different behavioral functions[64,72]. Finally, the recent discovery of a subpopulation of GABAergic ipRGCs innervating the SCN, LGN, and OPN by Tiffany Schmidt's group, suggest ipRGCs with the same central target can differ in their neurotransmission[73]. These studies provide compelling evidence that additional, functionally distinct subtypes of ipRGCs exist within our current morphological organization.

1.5 - The description of a novel subtype of ipRGCs

The vertebrate visual system is complex and retinal ganglion cells (RGCs) are remarkably diverse. Among cells of the nervous system, the computational units or 'functional subtypes' possess shared spatial, structural, and physiological properties, allowing input stimuli to be ideally encoded and to elicit common responses for a coordinated purpose[74,75]. For instance, the subtypes of mechanoreceptor nerve endings in the skin encode different aspects of somatosensory touch, allowing texture and object discrimination[76]. In the retina selective synaptic connectivity and intrinsic biophysical uniformity allow RGCs to encode specific features of a visual scene. Subtypes – or individual computational units – of RGCs are thought to be defined most accurately by their spatial distribution. Rodents are believed to have more than 40 distinct functional subtypes of RGCs[3] and their spatial organization, structural morphology and physiological properties are key features that define and distinguish their membership[77,78]. RGC subtypes each form tiling 'mosaic' distributions in the retina, serving to reduce encoding of redundant information among cells of the same subtype and allow an equal visual representation of specific features to be encoded at each location of the retina[79,80]. RGCs within a subtype also exhibit similar physiological responses to a common light stimulus, and innervate similar brain regions, important for conveying consistent information from the visual environment. As discussed above (Chapter 1.4) IpRGC types instead, display significant dendritic overlap[69], variable photoresponse properties[71], and influence

different brain regions[71]. My thesis work provides evidence that ipRGCs comprise multiple functional subtypes, with shared morphological features but distinct functions. This is primarily addressed through the characterization of a novel subtype of ipRGC.

Thesis overview & Summary

During an unrelated study of glycinergic amacrine cells using a transgenic mouse where *Cre* is driven by the inhibitory glycine transporter (*GlyT2*), we discovered a population of RGCs labeled in the ganglion cell layer. While tracing their axons, we noticed that they only entered the optic nerve from a single hemisphere of the retina. Follow-up melanopsin immunostaining and electrophysiological recordings confirmed them as a small population of intrinsically photosensitive melanopsin cells. My graduate work has focused on characterizing this novel population of ipRGCs. What is the identity of these cells, where are they located in the retina and what do they innervate in the brain? This portion of my thesis work has resulted in the following major conclusions:

- 1) GlyT2Cre ipRGCs are localized exclusively to the dorsal retina where they capture reflected luminance off the ground.
- 2) GlyT2Cre ipRGCs consist of a primary morphological subtype, with M1-like structure. However, GlyT2Cre ipRGCs overlap with other M1 ipRGCs in the dorsal retina, accounting for the asymmetric distribution of M1 ipRGCs across the dorso-ventral axis.

- 3) They project to non-image forming brain regions and display patterns of innervation distinct from other ipRGCs. They also represent the sole retinal projection to the supraoptic nucleus (SON-ipRGCs) and project to a previously undescribed sub-region of the SCN we call the 'outer core'.
- 4) SON-ipRGCs are evenly spaced, forming a tiling mosaic across the dorsal retina, representing the first 'true' ipRGC subtype.

The glycine transporter 2 is a neuronal reuptake pump that moves sodium ions and chloride ions along their electrical gradient in exchange for glycine[81]. The retina has an abundant number of glycinergic and GABAergic amacrine cells and GlyT2-Cre[82] and Glyt2-GFP[83] are present in both glycinergic and GABAergic amacrine cells. However, we were surprised to find ipRGCs in an inhibitory Cre line, as RGCs were thought to be predominantly glutamatergic. However, a recent discovery of GABAergic ipRGCs[73] suggest that inhibitory release from the retinohypothalamic tract (RHT) might be a feature of non-image forming vision circuits. Are SON-ipRGCs an inhibitory population of ganglion cells? SCN and SON recordings were performed by Michael Moldavan (Allen lab). IGL recordings were performed by Marc Meadows (von Gersdorff lab), and Tavita Garrett (Sivyer lab).

- 1) SON-ipRGCs have direct synaptic connectivity with neurons in the SON
- 2) SON-ipRGCs are glutamatergic and excite downstream neurons in the SCN and in the IGL, suggesting that GlyT2 in this subset of ipRGCs may perform some other function outside of direct neurotransmission.

SON-ipRGCs are a unique subtype of M1 ipRGCs that overlap with other M1 ipRGCs with shared morphology, sampling the same area of visual space. An explanation for this overlap is that different subtypes of M1 ipRGCs are extracting different aspects of illumination from the visual environment similar to subtypes of traditional RGCs. What are the photoresponses of SON-ipRGCs and how do they compare with neighboring ipRGCs that sample a similar visual space? To access this required that I characterize the light-evoked responses of ipRGCs at the population level. Recording from ipRGCs is uniquely challenging, due to their rarity, response diversity, and their direct and prolonged activation by fluorescent targeting strategies. To address this, I performed Multielectrode Array (MEA) recordings on dark-adapted retina dissected under infrared light, and developed an 'OptoTagging' strategy to retroactively identify channelrhodopsin 2 (ChR2) expressing SON-ipRGCs. This novel approach allows long, stable recordings from several ipRGCs simultaneously, and avoids the need to expose the retina to fluorescent light. To organize ipRGCs into functional subtypes I performed unbiased clustering which ignored morphological and molecular characteristics, and instead classified ipRGCs based on their intrinsic light responses. This portion of my thesis work resulted in the following major conclusions:

- 1) ipRGCs cluster into 8 distinct functional groups, which differ in their sensitivity, response onset, and duration.

- 2) Two fast responding and highly photosensitive 'M1-like' ipRGC clusters differ in their responses to prolonged illumination, producing either transient or sustained responses.

- 3) SON-ipRGCs produce the most sustained responses and are predominantly localized to one functional cluster.

- 4) SON-ipRGCs are photoresponsive from moonlight to day lighting conditions, in contrast to the other M1-like cells that only responded to moonlight conditions and become suppressed at light levels equivalent to sunrise through daylight.

- 5) Given their site of projection, it suggests that sustained photoresponses are necessary for SON-dependent behavioral function.

Since the discovery of ipRGCs, knowledge of their critical involvement in physiology and behavior has grown rapidly. We know that ipRGCs function as the body's main biochemical synchronizer, aligning most bodily functions with the day night cycle. Changes to this entrainment can have significant health consequences. The last portion of my thesis (Chapter 5) is a wider discussion on the biological, clinical, and environmental significance of ipRGCs; a challenging exercise that contextualizes the broader implications of non-image forming vision on human health.

CHAPTER 2: METHODS USED FOR THE STUDY OF IPRGCS

2.1 – Chapter preface

The methods used in my thesis work are described here, in a separate chapter in order to provide an expanded technical description without detracting from the results and discussion of subsequent chapters. The motivations, applications and advancements of these techniques were inspired by the desire to describe a novel subpopulation of ipRGCs. However, many of these approaches can be broadly applied to the study of other cell types in the retina, and therefore the details may be of interest to future students. The techniques can be broadly separated into anatomical (Chapter 2.2) and physiological (Chapter 2.3) approaches and should be used for reference throughout the other chapters.

2.2 – Anatomical approaches

Ethical approval and animal use

Experiments involving animals were in accordance with the National Institutes of Health guidelines, and all procedures were approved by the Oregon Health and Science University Institutional Animal Care and Use Committee. *GlyT2^{Cre}* mice (Tg(Slc6a5-cre)KF109Gsat/Mmucd) were a kind gift from Larry Trussell, prior to being cryo-recovered by the OHSU Transgenic Mouse Model Core using sperm purchased from the Mutant Mouse Resource and Research Center (Stock 030730-UCD). Ai32 (RCL-ChR2(H134R)/EYFP) and Ai9 (RCL-tdT) mice were obtained from The Jackson Laboratories. OPN4Cre (tm1.1(cre)Saha/J) were a gift from Samer Hattar and The Johns Hopkins University. Animals were bred and housed on a 12-h light/dark cycle with food and water ad libitum.

Eye and brain injections

To trace ipRGC projections and sites of central innervation, anterograde tracers were delivered in the eye through intravitreal injection. AAV-FLEX-tdTomato (Catalog# 28306 AAV2 & PHPeB) and AAV1-DF-ChR2-mcherry (Catalog# 18916) were purchased through Addgene. For this procedure, animals were anesthetized by intraperitoneal injection of 100mg/kg ketamine and 15mg/kg xylazine. Proparacaine (anesthetic) and tropicamide (anticholinergic) drops were applied topically to the eye for local anesthesia and to improve visualization of the surgical field, respectively. Under stereo microscopic control, a small hole was made at the ora serrate using a 32G needle. AAV vectors containing ~10^{13}-10^{14} viral genomes were delivered in 1.5 µL volumes to the vitreous of the eye

using a 5 µL Hamilton microinjection syringe. Animals were allowed to recover from anesthetic on a heat pad before being returned to their cage. AAV injections were performed between P30–P60. To aid in visualizing retino-recipient brain structures animals also received a follow up eye injection of 1uL cholera toxin beta subunit (CTB) 488 one week before sacrifice. In order to identify ipRGCs that innervate specific central locations, stereotactic brain injections of retrograde tracers were performed using a Kopf stereotic instrument (performed by Olga Cravetchi, Charles Allen lab). For the supraoptic nucleus (SON), 100nL of AAVRG-DF-ChR2-mcherry (Catalog# 18916) was injected bisymmetrically at 0.5mm from Bregma, +/- 1.3mm from the midline at a depth of 5.0mm, determined from the Franklin & Paxinos Mouse Brain Coordinate Atlas, 4th ed. Animals were sacrificed three-four weeks following injections for brain and eye histology.
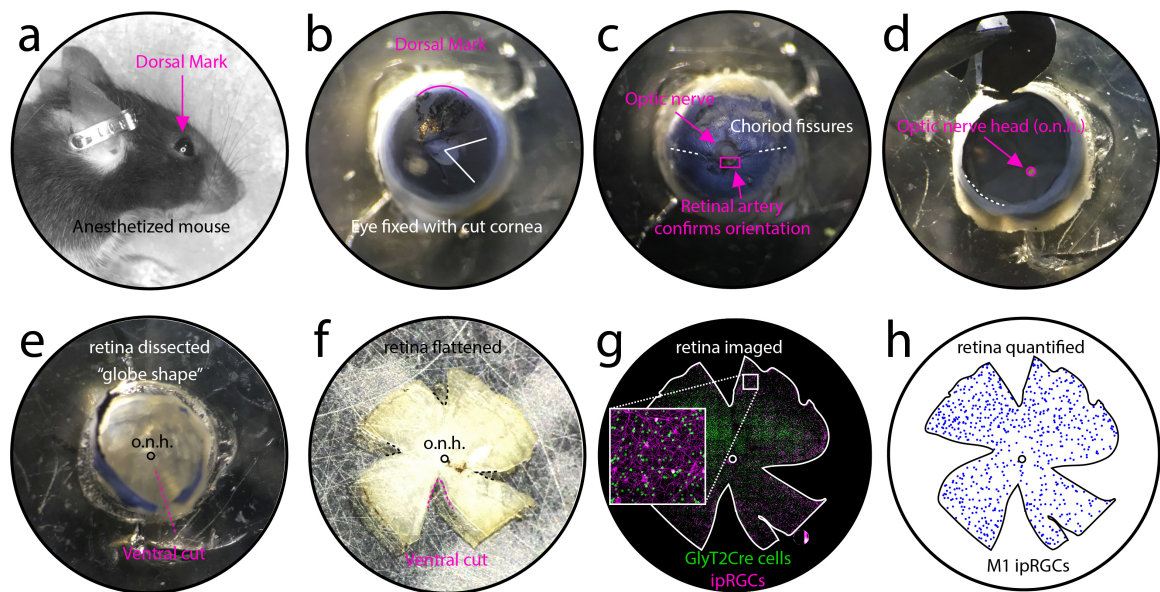
Figure 2: Generating whole retina tile maps
(a) Dorsal portion of the cornea and sclera marked with a felt tip pen, before eye removal to aid in dorso-ventral orientation. (b) Cornea cut and partially removed to allow paraformaldehyde to adequately fix the tissue. (c) Posterior side of the eye inspected for the orienting vascular supply, located ventral to the optic nerve and the choroid fissures flanking the optic nerve. (d) Iris, lens, and vitreous removed exposing the fixed retina in the eyecup and centrally located optic nerve head (o.n.h.). (e) Retina with orienting ventral cut, separated from the sclera by delicately cutting along the rim of retinal attachment and transecting the optic nerve from its scleral bed. (f) Whole retina flat-mounted RGC side up on a glass slide with additional relieving cuts. (g) whole retina tiling confocal z-stack captured with 40x oil objective and stitched together into a high resolution image. (h) Whole retina map generated by systematically identified ipRGCs across the entire retina. M1 ipRGCs were distinguished by their characteristic OFF stratifying dendrites (in IPL) and abundant melanopsin expression.

Tissue preparation and immunohistochemistry

For retinal histology, animals were euthanized with 200 mg/kg ketamine and 30 mg/kg xylazine followed by cervical dislocation. The dorsal portion of the cornea and sclera were marked a felt tip pen to aid in orientation (Figure 2a,b). Eyes were then removed with curved surgical scissors and placed in 4% paraformaldehyde (PFA) (Electron Microscopy Sciences Catalog#: IC993M31) + PBS for 30 mins with the cornea partially removed (Figure 2b). Eyes were then washed thoroughly in PBS for 24hrs. To dissect the retina from the eye, the lens and tissue up to the trabecular meshwork was removed leaving an exposed globe (Figure 2d,e). Dorsal ventral orientation, marked with a ventral cut (Figure 2e), was established using the choroid fissures and retinal artery (Figure 2d), which can be visualized (in posterior view) entering the back of the eye, inferior to the optic nerve. The retina was then separated from the sclera by delicately cutting along the rim of retinal attachment and transecting the optic nerve from its

scleral bed (Figure 2e). Whole retina was then transferred to a 1.5ml eppendorf tube for immunohistochemistry. The details, including the timing and concentration of primary and secondary antibodies used for specific experiments are described in Table 1. Once immunostaining was complete, 3 additional relieving cuts were made at cardinal positions (4-leaf clover shape) to allow the whole retina to be flat-mounted RGC side up on glass slides (Figure 2f). Retinas were dried on the slide until transparent, then mounted with a cover slip using Vectashield mounting medium.

For brain histology, animals were heavily anesthetized by IP injection of ketamine/xylazine and transcardially perfused with 50μL Heparin + 30 mL PBS followed by 40mL 4% paraformaldehyde (PFA) + PBS. Brains were removed and post-fixed in 4% PFA + PBS for 2-4 hrs. Brains were then washed thoroughly in PBS azide for 24hrs, mounted in 4% agar and sectioned at 200μm from rostral to caudal using a Leica VT1000S vibratome. Sections were collected in PBS and transferred to glass slides. Retinas and brain slices were immuno-stained in a mixture of 5% Donkey serum, 5% Triton X-100 and 2.5% PBS azide at room temperature. Details, including the timing and concentration of primary and secondary anti-bodies used for specific experiments are described in Table 1. Both brain slice and whole-mount retina were coversliped using Vectashield mounting medium (Vector laboratories) and imaged on a Leica SP8 scanning confocal microscope.

Quantification of retina histology

To generate retina maps, whole retina tiling confocal z-stacks were captured using a Leica SP8 confocal microscope with a 40x oil objective (Figure 2g). Tiles were stitched together in Leica LAS X Life Sciences software and analyzed in ImageJ. IpRGCs were manually identified across the entire retina by systematically localizing all melanopsin positive cell bodies in 200x200um square increments (Figure 2h). Somas were marked as regions of interest (ROI) in a separate overlay image using ImageJ's multipoint tool (2d axis image). M1 ipRGCs were identified by their characteristic dendritic stratification in the "OFF" sublamina, their small somas, and bright melanopsin staining. GlyT2Cre ipRGCs were identified by the co-localization of GFP and melanopsin in their cell bodies (GLyT2Cre::Tigre[GFP]). Distribution maps of ipRGCs were generated from the x/y coordinates extracted from the axis image. Due to their abundance, UV cone distribution maps were generated using the trainable Weka segmentation plugin for ImageJ[84] (imagej.net/plugins/tws/). This machine learning software allows structures of similar appearance to be identified in a semi-automated manner. Images were processed with a binary threshold and segmentation was trained to identify fluorescent cells (UV+ cone outer segments) in the photoreceptor layer. Segmentation can be challenging when the proximity of cells is small or overlapping. As a result, the density of UV cones reported in the ventral retina is likely an underestimate.

Neighbor density maps and density recovery profiles were generated using the Neighbor density analysis application within the BioVoxxel_Toolbox plugin for ImageJ (imagej.net/plugins/biovoxxel-toolbox). Axis images denoting cell bodies were converted to 8-bit and applied with a binary threshold. Particle neighbor analysis was used to identify the number of cell bodies within a given radius from each soma. Neighbor density maps were generated with density radius of 110um to approximate the average dendritic diameter of RGCs. Density recovery profiles were calculated similarly using radii from 0 to 400um in 20um increments. Population per hemisphere were calculated by dividing oriented retinas through the optic nerve head along the naso-temporal axis and quantifying # of cells per hemisphere. Density of cells per mm^2 was determined by quantifying the number of cells within $1mm^2$ areas of dorsal and ventral retina.

2.3 – Physiological approaches

Multi-electrode array recordings & light stimulation

The MEA is an extracellular recording device, consisting of multiple electrodes that allow action potentials of proximal neurons to be monitored and recorded simultaneously. MEA recordings in retinal explants provide a method of recording photoresponses from RGCs at a population level. The motivation for recording ipRGCs with this approach was to avoid the fluorescent light exposure used in single cell targeting techniques, which can activate the melanopsin protein and cause light adaptation of the rod and cone photoreceptors. As MEA recordings of

RGCs are non-specific, pharmacological and optogenetic approaches were added in order to localize the cells of interest.

GlyT2Cre::Ai32 mice were dark adapted overnight and anesthetized with ketamine/xylazine. To help with removal of the vitreous during dissection and improve tissues proximity to the MEA electrodes, each eye received a 1µL intravitreal injection of 15 u/µL purified Hyaluronidase (Worthington Chemicals) 2.5 u/µL purified collagenase (Worthington Chemicals) in Balanced Salt Solution (BSS). Anesthetized animals were left on a heatpad for 15 mins then euthanized by cervical dislocation. Orientation of the eye was indicated by lightly marking the dorsal portion of the cornea and sclera with a felt tip marker. Eyes were removed and dissected in Ames solution (US Biological) under infrared illumination. Retinas were mounted on millicell membranes (Millipore, PICMORG50), and placed in an incubator under 95% C02 until recording (~30 min). Recordings were acquired on a 256-channel MEA-2100-System (Multichannel systems) at 20kHz using MC_Experimenter (Multichannel systems acquisition software). All experiments were conducted in the dark under dim red headlamps. Retinas were placed retinal ganglion side down on the MEA electrodes and a MultiChannel Systems harp weight (Scientific Instruments) was placed on top. In order improve connectivity and stability of the recording, the retina was allowed to settle for 1hr under constant Ames perfusion and a gradual increase in temperature (room temp to 32C degrees).

Illumination was presented by (1) a custom built LED array (Luxeon Star LEDs, Arduino controlled; built by Ben Sivyer) with 405nm, 470nm, and 535nm LEDs, (2) a lightcrafter projector controlled by custom software Pystim (available at github: https://github.com/SivyerLab/pystim) and (3) a 483nm LED with collimator and control box (Thorlabs) for optogenetic stimulation. Stimuli were generally presented at increasing light intensities in order to retain photoresponses throughout the recording. See Table 2 for illumination and experimental details.

A combination of illumination and pharmacological bath application was used to identify ipRGCs within the GlyT2Cre::Ai32 retina in three steps. Step 1: illuminations were presented and light responses were recorded from all RGCs in regular Ames media. Step 2: synaptic blockers (50µm DL-AP-5 (Tocris #0105), 40µm L-AP4 (Tocris #0103), 100µm CNQX (Tocris #0190) and 2µM ACET (Tocris #2728) were added to the Ames solution, pharmacologically isolating RGCs. Extended illuminations (20 sec) of increasing intensity were then used to identify the ipRGCs through their sluggish intrinsic photoresponses under blockade. Step 3: A melanopsin inhibitor[85,86] (opsinamide) (Sigma AA92593) was added to the synaptic blocking solution (10µm) and a high frequency flicker (18Hz) was used to identify "OptoTagged" or ChR2 expressing GlyT2-ipRGCs by their instantaneous time locked responses (Table 2).

During step 1, four different types of light stimuli were used (i-iv). (i) A full field illumination of 3 sec (470nm – Thor Labs) for $1.3x10^8$ to $1.3x10^{14}$ photons cm^{-2} s$^-$

[1] at log unit steps, with 5 min of dark in between each exposure. (ii) A full field illumination of 60 sec (470nm – Thor Labs) for 1.3×10^8 to 1.3×10^{12} photons cm^{-2} s^{-1} at 2 log unit steps. (iii) (iv) Full field illumination of 405nm then 535nm presented in 3 sec intervals from 1.7×10^7 to 1.7×10^{13} photons cm^{-2} s^{-1} at 1 log unit steps. In step 2 extended illumination of 20 sec (470nm – Thor Labs) was used at light intensities from 7.9×10^{10} to 7.9×10^{14} photons cm^{-2} s^{-1} at half log unit steps with 90 sec of dark between exposures. During step 3 high frequency flicker (40x 5ms flashes at 18Hz over 9 repeated trials) was presented at 2×10^{17} photons cm^{-2} s^{-1} (483nm LED) (Thor Labs), the light intensity necessary for robust ChR2 activation[87].
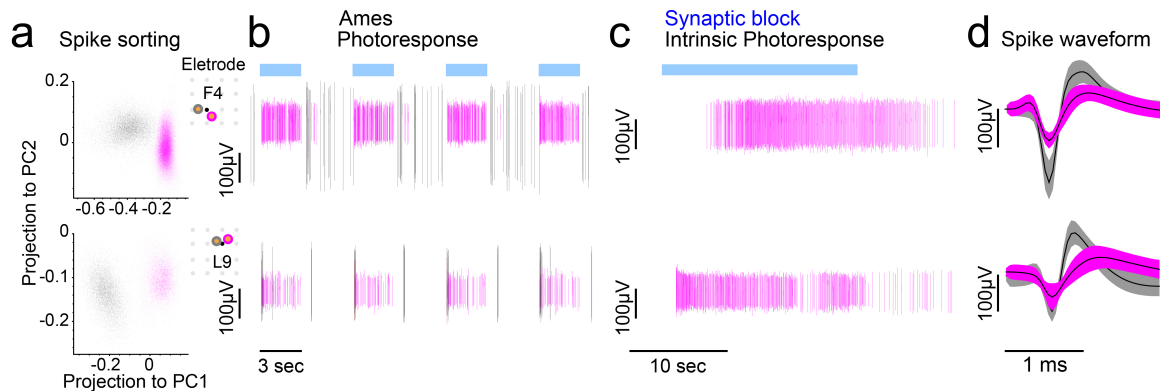
Figure 3: Spike sorting of ipRGCs on the MEA
(a-d) Each electrode on the MEA often records spikes from multiple cells that can be distinguished by their waveform shape and amplitude. Principle component analysis (PCA) of the waveforms attribute individual spikes to a localized "unit" (cell). (a) RGC spike waveforms of 1st and 2nd principal component from two example electrodes on the MEA, analyzed in the component space using Plexon Offline Spike Sorter V3 (Plexon). Each electrode identified two cells (magenta and black). (b,c) Photoresponses from individual units examined before (b) and after synaptic block (c). IpRGCs identified by their photosensitivity under block (Magenta). (d) Average waveform shapes (with standard deviation) for each unit per electrode exemplifies waveform differences of neighboring cells.

MEA data extraction and analysis

Raw voltage traces per retina were merged in sequential order using Multichannel data manager (MCS) and Plexutility (Plexon), generating one file with all light responses. Voltage traces per channel were then bandpass filtered (Butterworth 100 and 3000 Hz). Spikes were extracted at a spike threshold of 4.5 SD from baseline with minor adjustments to insure appropriate extraction of spikes in channels with amplitudes at or near the deviation. Spikes were then rerecorded in Multichannel Analyzer (MCS). Channels with no connectivity or channels with small spiking amplitudes (typically below 20µV) were removed in order to reduce the size of the extraction file. Spike waveforms (Figure 3d) per channel were then template sorted into individual 'units' we call cells, via principal component analysis (PCA) using Plexon Offline Spike Sorter V3 (Plexon) (Figure 3a). Stringent thresholding of spikes during extraction (above), together with a large signal to noise during the recording results in each electrode commonly identifying only 1–3 cells but with well circumscribed localization in the PCA component space. Channels with more than one cell were individually confirmed to insure that spikes are well attributed. Cells with ambiguous sorting or overlapping waveforms in the PCA component space were removed from the analysis. Trigger time points of visual stimuli were then synchronized using Multi-channel data manager and cell responses were visualized in Neuroexplorer (Plexon) (Figure 3b,c). Spike timestamps were exported directly for graphing (Profit and Prism) or imported to MATLAB for further analysis using the Mathworks toolbox.

IpRGCs were identified within the MEA recordings through their photoresponses to physiological light intensities under synaptic blockade. In *GlyT2Cre::Ai32* mice, the ipRGC population, were further divided into GlyT2Cre ipRGCs (aka 'opto'Tagged ipRGCs, SON-ipRGCs) and surrounding ipRGCs (non-GlyT2 ipRGCs). GlyT2-ipRGCs (13%±4.6 SEM of ipRGCs sorted) were identified as cells with fast, repeatable, and time locked responses to optogenetic stimulation (18Hz at 2×10^{17} photons cm^{-2} s^{-1}) under synaptic block + melanopsin antagonist.

Perievent histograms of dark-adapted photoresponses and intrinsic photoresponses were generated from averaged firing rate across repeated trials. Changes in firing rate for dark-adapted photoresponses during (solid lines) and following illumination (dotted lines) were calculated by subtracting the baseline (spontaneous mean before illumination) and normalizing to the peak firing rate during illumination. Changes in firing rate for intrinsic photoresponses were calculated similarly but normalizing to the peak firing rate after the start of illumination as some ipRGCs took longer than the illumination window to reach a peak firing rate. Maintained firing rate was measured as average firing rate from 1 sec after illumination to the end of illumination. Sustained firing rate during extended illumination (60 sec) was measured as average firing rate during the entire illumination period. Time to peak was measured as time from illumination onset to peak firing rate. Response duration after illumination was measured as time from peak firing rate to return to spontaneous mean firing rate. Response

duration during illumination was calculated similarly but limited to the duration of the illumination period (60 sec). Intrinsic responses following ChR2 activation (per trial) were calculated by subtracting the baseline (spontaneous mean) and normalizing to the average firing rate following 18Hz high frequency train (10 seconds). Perievent rasters for ChR2 responses display all spikes across all trials. Peristimulus time histograms (PSTH) graph the average normalized firing rate displayed as Z-score. Interspike interval (ISI) histogram was calculated as the frequency (occurrence) in spikes per second (instantaneous bin counts/(number of spike intervals in the spike train x bin size) per interspike interval across the entire optogenetic recording window (10 seconds before to 30 sec after 18Hz flicker across all trials). Interspike-interval (ISI) was shown as equivalent Hz as a comparison with stimulus frequency (18Hz). ISI mode histograms were plotted as the peak occurrence (mode) of ISI.

Unbiased clustering of intrinsic photoresponses

The functional classification of ipRGCs using the clustering of photoresponses involves extracting sparse principle components (sPCA) then clustering these components using Gaussian mixture models. The approach is similar to previous studies that performed unsupervised clustering on calcium fluorescence transients from RGCs[77], and recently ipRGCs of the neonatal mouse[88]. We applied similar methods to identify ipRGCs of the adult mouse retina using electrical responses recorded from the MEA.

Functional classification of ipRGCs was based on the clustering of intrinsic photoresponses to increases in full-field illumination. Each light response was trimmed to a window of 10 sec before and 80 sec after the start of illumination. All responsive cells were then combined into a single response matrix (cells x time points). Baseline firing rates were subtracted and each cell was normalized to its maximum value (cell normalization). Each column was also normalized to have a mean of zero; insuring that all changes in firing rate contribute variance equally (time point normalization). The sparse principle component algorithm (sPCA) from the SpaSM Matlab toolbox[89] was then employed on our normalized response matrix, obtaining the first 10 sparse principle components. Visualizing the % of individual variance explained by each sPCA, we observed a sharp drop off of explained variance after principle component 3. Therefore we chose to restrict the subsequent steps of the analysis to the first 3 components that each explained more than 5% of the variance within the response matrix. The weights of these sPCAs where then multiplied by the response matrix to obtain a matrix of weighted features (cells x sPCAs) with each sPCA representing a dimension. To cluster cells we fit Gaussian Mixture Models (GMMs) to the feature matrix using Matlab's fitgmdist algorithm, specifying 1-16 potential clusters. Each candidate cluster number was performed at 500 iterations (500x16 candidate clusters). To identify the optimal number of clusters we implemented the Bayesian (Schwarz) Information Criterion (BIC), a method of model selection that penalizes over-fitting of the data. We selected the GMM with 8 clusters as it represented the model with the lowest BIC. Clusters were constructed from the

GMM distribution, cell identities were localized within each cluster and photoresponses across visual stimuli were extracted for further analysis.

Single cell patch clamp recordings in the retina

Single cell current clamp recordings were performed in the GlyT2Cre::Ai9 mouse using a HEKA EPC800 amplifier, ITC-18 digitizer and Axograph software. Fluorescent ipRGCs were targeted using brief 554nm exposure (<100ms) and a high sensitivity camera (Andor technologies – DU-888E-COO-#BV). Recordings were performed in Ames medium with synaptic blockers 20uM L-AP4, 25uM DAP5, 20uM CNQX to isolate RGCs. Five second illumination of blue (445nm) light was used to illicit intrinsic melanopsin responses at 5×10^{13} log photons cm^{-2} s^{-1} using a Lightcrafter projector.

Single cell patch clamp recordings monitoring synaptic release in the brain (Michael Moldavan, Allen lab)

To study synaptic transmission mediated by the axons of SON-ipRGCs, GlyT2-Cre mice were crossed with the Ai32 reporter mouse driving channelrodopsin expression in Cre expressing ipRGCs. Male and female GlyT2::Ai32 mice were housed in an environmental chamber (Percival Scientific, Perry, IA) maintained at 20 - 21°C on a 12:12 hr light:dark (LD) cycle, with free access to food and water. The ChR2 expressing axonal terminals projecting to the SCN were activated by white light passing through a Chroma excitation filter (BP 470/40). The estimated intensity of the light was 16.5 to 17 log photons cm^{-2} s^{-1}. The ChR2 expressing RHT projection were observed using YFP filter (Chroma, ET-EYFP C212572,

Cat.# 49003). The recordings were performed at the end of the day and the beginning of the night. SCN neurons were voltage-clamped in the whole-cell and cell-attached patch clamp modes. The cells were filled with neurobiotin (0.5%), which made it possible to determine their localization after the experiment. The internal solution consisted of (in mM): 87 CH_3O_3SCs, 15 CsCl, 1 $CaCl_2$, 10 HEPES, 11 EGTA, 31.5 CsOH, 3 MgATP, 0.3 TrisGTP, 10 Phosphocreatine di(tris) salt and 5 N-(2,6-dimethylphenylcarbamoylmethyl)triethylammonium chloride (QX-314); pH 7.25, 278 mOsm. The extracellular recording solution (ACSF) was (in mM): 132.5 NaCl, 2.5 KCl, 1.2 NaH2PO4, 2.4 CaCl2, 1.2 MgCl2, 11 glucose, and 22 NaHCO3, saturated with 95% O2 and 5% CO2; pH 7.3–7.4, 300–305 mOsm. The equilibrium potential for chloride was -50 mV. For additional details see Moldavan et al., 2010[90]; 2018[91]. During recordings the inhibitors of glycine, $GABA_A$, and ionotropic glutamate receptors, respectively strychnine (1 µM), gabazine (10 µM), CNQX (20 µM) + AP-5 (DL-AP5, 50 µM), and TTX (1 µM) an inhibitor of voltage-dependent Na^+ currents were applied (n = 6 neurons). EPSCs evoked by electric stimulation of the optic chiasm were also used in order to confirm the recorded cell received retinal inputs (n = 5 neurons).

CHAPTER 3: A SUBTYPE OF MELANOPSIN GANGLION CELLS ENCODES REFELCTED LUMINANCE

Michael H. Berry[1,2], Michael Moldavan[3,4], Marc Meadows[5,6], Tavita Garrett[1,5], Olga Cravetchi[3,4] Elizabeth White[1], Charles Allen[3,4], Henrique von Gersdorff[6], Kevin Wright[6], Benjamin Sivyer[1,2,#] A subtype of melanopsin ganglion cells encodes reflected luminance

1. *Department of Ophthalmology, Casey Eye Institute*
2. *Department of Chemical Physiology and Biochemistry*
3. *Oregon Institute of Occupational Health Sciences*
4. *Department of Behavioral Neuroscience*
5. *Neuroscience Graduate program*
6. *Vollum Institute*
Oregon Health & Science University, Portland, OR, 97239

3.1 - Abstract

Visual input to the hypothalamus from intrinsically photosensitive retinal ganglion cells (ipRGCs) influences several functions including circadian entrainment, body temperature, and sleep. ipRGCs also project to nuclei such as the supraoptic nucleus (SON), which is involved in systemic fluid homeostasis, maternal behavior, and appetite. However, little is known about the SON-projecting ipRGCs or their relationship to well-characterized ipRGC subtypes. Using a *GlyT2*^{Cre} mouse line, we identify a subtype of M1 ipRGCs restricted to the dorsal retina that selectively project to the SON. These ipRGCs form a non-overlapping tiled mosaic that is limited to a dorsal region of the retina, representing a feature map encoding reflected luminance. Optogenetic activation of their axons demonstrates they release the neurotransmitter glutamate and that the SON is retinorecipient, receiving synaptic input from dorsal ipRGCs. Our results challenge the idea that ipRGC dendrites overlap to optimize photon capture and challenge the canonical rule that each RGC subtype independently encodes the entire visual scene.

3.2 - Introduction

In addition to the rod and cone photoreceptors that are used for image-forming vision, the mammalian retina contains intrinsically photosensitive retinal ganglion cells (ipRGCs) that primarily drive non-image forming behaviors[92,93]. ipRGCs express their own photopigment, melanopsin[5], and project to over 17 central brain regions[45,65,94] influencing many homeostatic functions including circadian entrainment, pupil constriction, body temperature, and mood[4,9,10,72,95]. There are six main 'types' of ipRGCs (M1-M6), which are categorized according to their dendritic morphology, melanopsin expression, gene expression, and central projection locations[45,96]. The most studied of these, the M1 ipRGCs, have dendrites that occupy the OFF layer of the inner plexiform layer (IPL). They form the primary projections to the suprachiasmatic nucleus (SCN), which is the master circadian clock[2,4,7,61,62], and the shell of the olivary pretectal nucleus (OPN), which serves as the primary site of light dependent pupillary constriction[10,63,64]. They also project to a number of lateral hypothalamic brain regions, such as the supraoptic nucleus (SON), ventral lateral preoptic area (VLPO), and medial amygdaloid nucleus, though the functional role of these projections remains unclear[45,62,65].

The retinal responses of M1 ipRGCs are suited to their primary role in non-image forming vision; their long and sustained responses to bright illumination reflect their comparatively high expression of melanopsin and weak photoreceptor-mediated synaptic drive from retinal bipolar cells[45,46]. These light responses are

optimal for signaling absolute light intensity and driving behaviors that are slow, such as circadian entrainment, and the maintained component of the pupillary light reflex [63,97,98]. M1 ipRGCs were first thought to comprise a single, homogenous population however, the discovery of a sub-population lacking *Brn3b* expression[64], the divergent projection patterns of M1 ipRGCs according to *Brn3b* expression[62,64], and the diversity of light responses within M1 ipRGCs[71,99] illustrate there are likely multiple M1 subtypes that mediate different roles in non-image forming behavior.

The density of M1 ipRGCs in the retina also suggests they might comprise multiple subtypes. Conventional RGCs within a functional subtype are commonly arranged in evenly spaced mosaics where their dendrites form territories with minimal overlap[100,101]. This arrangement is thought to optimize the sampling of visual space[79,80,102] and reduces the encoding of redundant information, where each RGC subtype samples an even component of the visual field across the retina. Previous reports indicate M1 ipRGC dendrites are not territorial and they overlap considerably - about 4 fold[69]. This might be due to their non-image forming role, where the even representation of visual space is forgone in favor of increasing their dendritic surface area, optimizing the capture of photons. Alternately they might comprise multiple functional subtypes, each of which independently tiles the retina. We provide evidence for the latter, illustrating that like conventional RGCs, ipRGCs are arranged in mosaics optimal for the even

representation of visual space. But the retinal distribution of ipRGCs and how this relates to specific subtypes of M1 ipRGCs remains unclear.

Here, we use a combination of mouse genetics, confocal microscopy, anterograde and retrograde labelling and optogenetics to describe a subtype of M1 ipRGCs that are found only in the peripheral dorsal retina. They form a regularly spaced mosaic within this region suggesting mice devote additional melanopsin-dependent processing power to their ventral visual field. This subtype of M1 ipRGCs forms the primary visual projection to the SON, and project to unique sub-regions of other non-image forming brain nuclei, where they release the excitatory neurotransmitter glutamate, despite having *Cre* expression driven by the promotor of the inhibitory transporter GlyT2.

3.3 - Results

A population of ipRGCs encoding ventral vision

We discovered RGCs in mice where *Cre* is driven by a BAC encoding the inhibitory glycine transporter GlyT2 (slc6a5 KF109;[103] Fig. 4a). In these mice, *Cre* is expressed both in GABAergic and glycinergic neurons in the retina and brain[104]. In retina, *Cre* expression is overwhelmingly restricted to inhibitory amacrine cells[82]. However, we also observed fluorescent axons in the ganglion cell layer (Fig. 4a), and when following them to the optic nerve head discovered they originated solely from RGCs in the dorsal retina (Fig. 4c). Reasoning these RGCs likely represent a unique feature selective population in the retina, we

sought to determine their functional identity by mapping their central axonal projections in the brain with *Cre*-dependent anterograde labelling of their axon terminals and their light responses and dendritic morphology with targeted electrophysiological recordings and Neurobiotin fills.
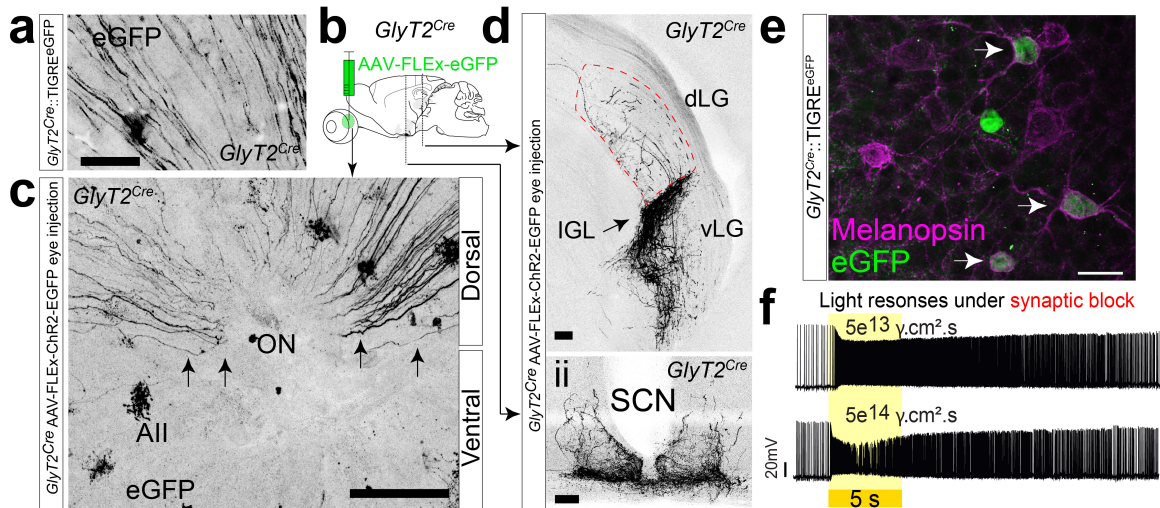
Figure 4: A subpopulation of ipRGCs in dorsal retina
(a) RGC axons identified in the dorsal portion of *GlyT2^Cre^;Ai140* whole mount retina. **(b-d)** *GlyT2^Cre^* RGC axons project from the dorsal retina via the optic nerve (ON) **(c)** to non-image forming central areas **(d)**: Intergeniculate leaflet (i) and suprachiasmatic nucleus (ii) following Cre-dependent AAV eye injection **(b)**. **(e)** Confocal imaging of *GlyT2^Cre^* RGC cell bodies and dendrites (dim green) in the Retinal Ganglion Layer (RGL) are immuno-positive for the photosensitive G-protein coupled receptor, melanopsin (magenta). **(f)** Current clamp recording of light responses to 5 sec illumination under synaptic block confirm that *GlyT2^Cre^* RGCs are intrinsically photosensitive (ipRGCs). scale bar = (a);20 µm, (c); 100 µm, (d); 100 µm.

To determine the location of the central projections of their axon terminals, we injected an AAV into the eye enabling the *Cre*-dependent expression of fluorescent protein (Fig. 4b). The axons of RGCs labeled using this method predominantly innervated non-image forming brain regions such as the intergeniculate leaflet (IGL) and suprachiasmatic nucleus or nuclei (SCN) (Fig.

4d), suggesting they arose from ipRGCs, which form the predominant projections to these regions. To confirm their identity in the retina, we performed melanopsin antibody co-staining in *GlyT2^{Cre};Ai140* mice (Fig. 4e) and *GlyT2^{Cre};Ai9* mice and found that fluorescent RGCs in the dorsal retina co-expressed melanopsin. We subsequently targeted fluorescent cell bodies in isolated preparations of dorsal retina from *GlyT2^{Cre};Ai9* mice for electrophysiological spike recordings. Current clamp recordings from fluorescent somas allowed us to confirm intrinsically photosensitive spike responses in the presence of a cocktail of excitatory synaptic blockers (Fig. 4f; 20 µM L-AP4, 25 µM DAP5, 20 µM CNQX).
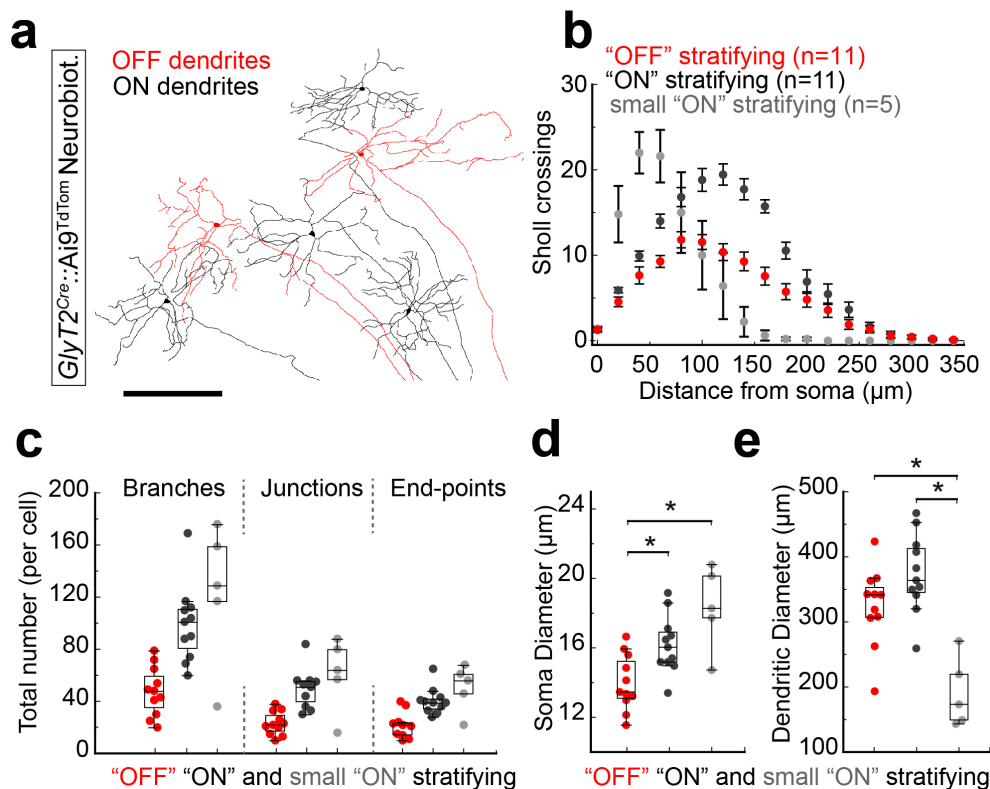
Figure 5: Morphological characterization of *GlyT2^{Cre}* ipRGCs

(a) Tracings of Neurobiotin electroporated *GlyT2^{Cre}* ipRGCs consist of morphological subtypes with dendritic stratification in the OFF (red) or ON (black) inner nuclear layer (INL). **(b)** Dendritic crossings at radial distances from each soma (Sholl analysis) **(c)**, number of branches, junctions and end-points **(f)**, as well as total soma **(d)** and dendritic diameter **(e)** quantified per morphologically

distinct subpopulation. n = 11 OFF stratifying ipRGCs (M1), 11 ON or partially bi-stratified, and 5 small ON stratifying cells (mixed "ON" stratifying/non-M1 ipRGCs). Values are mean+SEM. Statistical significance assessed using one-way Anova with Bonferroni correction for comparisons between multiple groups (*$p \leq 0.05$). Scale bar = (a);300 μm

To examine the dendritic morphology of these ipRGCs, we performed cell targeted Neurobiotin fills in the RGC layer of *GlyT2^Cre;*Ai9 retina. These experiments revealed they are predominantly comprised of an OFF stratifying type, a structural feature of M1 ipRGCs[6,105] (Fig. 5a). We also found they contained a secondary population stratifying in the ON layer, with variable morphologies, resembling a mixture of non-M1 ipRGCs [53,59,66,106]. Characterizing their dendritic structure using Sholl analysis (Fig. 5b), we found that the morphological complexity of the OFF stratifying cells, including the total number of branching points, junctions, and end-points are distinct from the mixture of ON stratifying cells (Fig. 5b,c). Furthermore, the soma diameter (Fig. 5d), dendritic diameter (Fig. 5e), and pattern of Sholl crossings (Fig. 5b) measured in the OFF stratifying cells are consistent with previous studies of M1 type morphology.

To determine the spatial location of *GlyT2^Cre*-positive ipRGCs, we generated distribution maps in wholemount preparations of *GlyT2^Cre;Ai140* retina using melanopsin antibody co-staining and confocal microscopy. *GlyT2^Cre*-expressing cells (Fig. 6a,b), and melanopsin expressing ipRGCs (Fig. 6c,d) were found across the entire retina (Fig. 6b,d). However, GFP-positive ipRGCs (Fig. 6e) were localized to the dorsal periphery of the retina (Fig. 6f), interspersed among other dorsal ipRGCs (Fig. 6e). Their location in the dorsal retina resembles the

asymmetric distribution of cone photoreceptors, more specifically the region of retina that contains predominately green cones and few UV cones[107,108]. Co-staining with the mouse S-opsin antibody that selectively labels UV opsin we show that *GlyT2^Cre*-positive expressing ipRGCs are located above the UV cone transition zone (Fig. 6g,h), occupying the dorsal region of retina with low UV cone density (Fig. 6f,h,g).
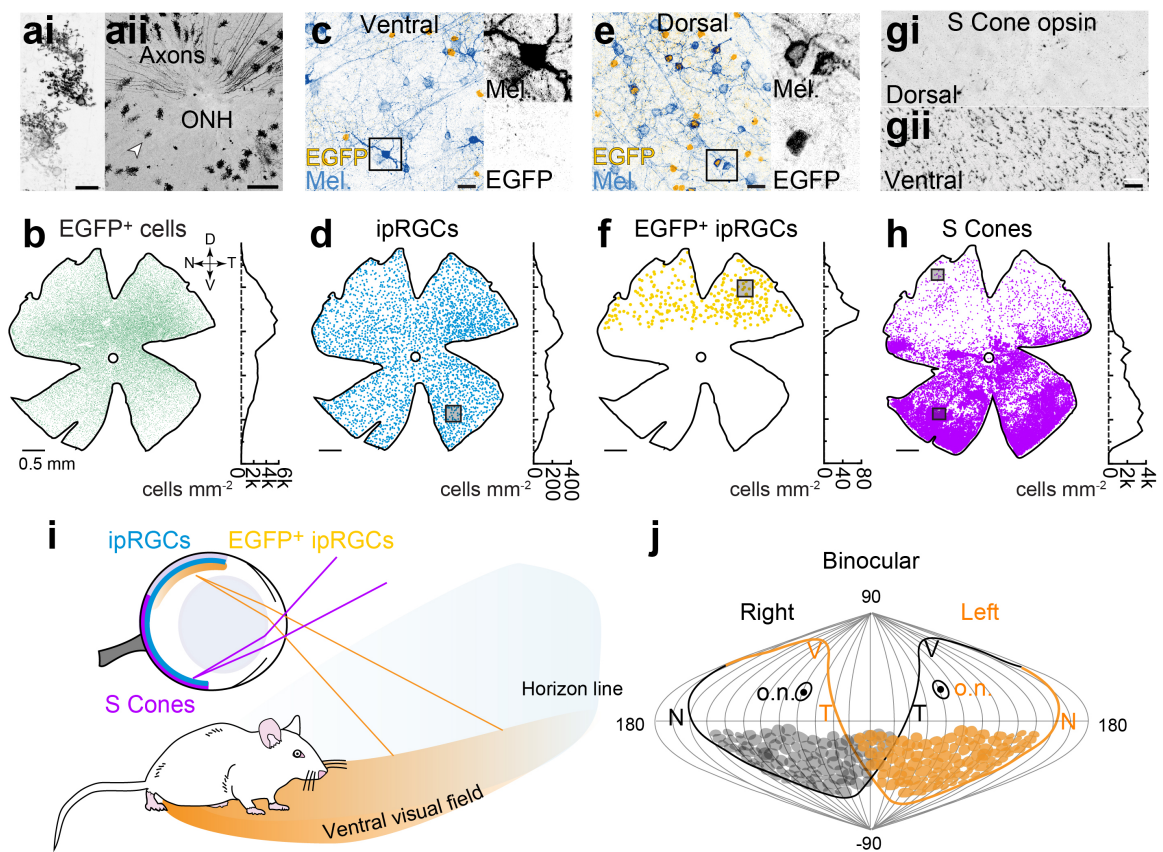
Figure 6: Localized distribution of ipRGCs capture reflected light
(a-h) Confocal images (top) and density maps (bottom) of transgenic EGFP+ cells (a,b), all ipRGCs (melanopsin+) (c,d), EGFP+ ipRGCs (EGFP+ & melanopsin+) (e,f) and S cones (short wavelength opsin expressing cones photoreceptors) (g,h) within the same *GlyT2^Cre;Ai140* retina. Dorso-ventral density curves (right of maps) measured in cell mm^{-2} along the y-axis emphasizes the asymmetric distribution of cells within the mouse retina. **(a,b)** Cells labeled in the *GlyT2^Cre;Ai140* mouse line consist primarily of AII amacrine cells (ai & aii;arrow). **(c-f)** IpRGCs (melanopsin+;blue) (c,d) and the small

population of *GlyT2^Cre* ipRGCs (melanopsin+;blue, GFP+;orange) (e,f) in whole mount retina. **(g,h)** S cone photoreceptors in the dorsal (di) and ventral (dii) retina emphasize their asymmetric distribution. (i) illustration of the *GlyT2^Cre* ipRGCs in the dorsal retina of the mouse encoding light in the ventral visual field (reflected off the ground), High density of S cones aligned with the dorsal visual field (purple). purple = density of S cones, blue = all ipRGCs, orange = *GlyT2^Cre* ipRGCs. **(j)** distribution of *GlyT2^Cre* ipRGCs in both eyes plotted in a sinusoidal projection. Orange outline = edge of left retina; black outline = edge of right retina. ONH = the location of the optic nerve. Labels N, D, T, V indicate the direction of the corresponding retinal poles. Scale bar = (ai);20,100 µm (c,e,g); 25 µm, (b,d,f,h); 0.5 mm.
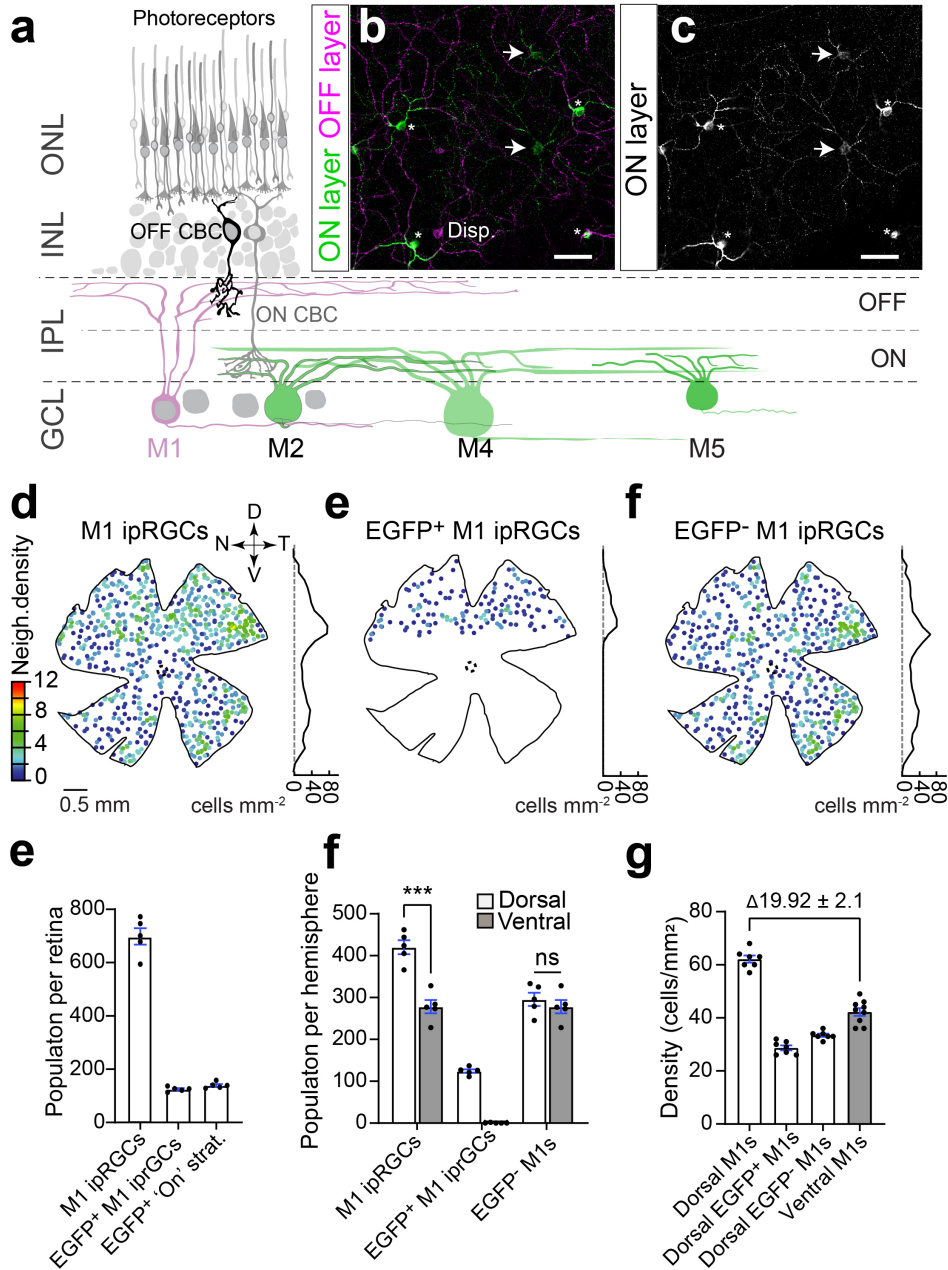
Figure 7: An additional M1 ipRGC visual channel dedicated to the dorsal retina

(**a**) Schematic of the retinal circuit with rod and cone photoreceptors located in the outer nuclear layer (ONL) and photosensitive ipRGCs localized to the retinal ganglion layer (RGL). Morphologically identified ipRGC types differ in their dendritic size and stratification in the ON (green) and OFF (magenta) inner plexiform layer (IPL). (a-inlay) Population of ipRGCs localized in the *GlyT2^Cre* mouse exhibit M1 type morphology. (**b-d**) Neighbor density maps of morphologically identified (b) all M1 ipRGCs (melanopsin+), (**c**) *GlyT2^Cre* M1 ipRGCs (EGFP+ & melanopsin+), (d) and M1 ipRGCs without *GlyT2^Cre* M1 ipRGCs (GFP- & melanopsin+). (**e**) Bar graph of quantified M1 ipRGCs, *GlyT2^Cre*

M1 ipRGCs, and 'ON' stratifying *GlyT2^{Cre}* ipRGCs in retina whole mount. (f) Bar graph of population per hemisphere and (g) density (dorsal; white vs. ventral; gray) for morphologically identified M1 ipRGCs per 1 mm^{-2}. Non- *GlyT2^{Cre}* M1s = (All) M1 ipRGCs – *GlyT2^{Cre}* M1 ipRGCs. Values are mean$\pm$SEM. Statistical significance assessed using one-way Anova. *** = p <0.001, n = 4 retina. Scale bar = (b-d); 0.50 mm

Previous studies report that M1 ipRGCs are denser in the dorsal retina[5,70,78,109], so we reasoned that GlyT2^{Cre}-expressing M1 ipRGCs might be a unique subtype that accounts for the asymmetry. If our hypothesis is correct, the density of M1 ipRGCs in the dorsal and ventral retinas should be the same if we discount the GlyT2^{Cre}-positive M1 ipRGCs. To test this hypothesis we examined the retinal distribution of all M1 ipRGCs using confocal microscopy. M1 ipRGCs have sparse dendritic arbors stratifying in the OFF IPL (Fig. 7a) and express the highest amount of melanopsin[69,105], making them easier to identify using immunohistochemistry and confocal microscopy. Whole retina density maps of M1 ipRGCs (n ≈ 800 cells) confirm their increased dorsal density (Fig. 7b)[70] and they were evenly interspersed with *GlyT2^{Cre}* M1 ipRGCs (Fig. 7c, n ≈ 150 cells). When we subtracted *GlyT2^{Cre}*-positive ipRGCs (Fig. 7d-g), the density of M1 ipRGCs between the dorsal and ventral retina were equivalent, confirming our hypothesis (Fig 7e,f,g). These results suggest the mouse visual system dedicates an additional M1 ipRGC visual channel to the ventral visual field. We reasoned this anatomical segregation in the retina might be mirrored in their central axonal projections, which are segregated in previously identified subtypes of M1 ipRGCs. These distinct separations of ipRGC central projections underlie distinct behavioral functions[62,64,72].
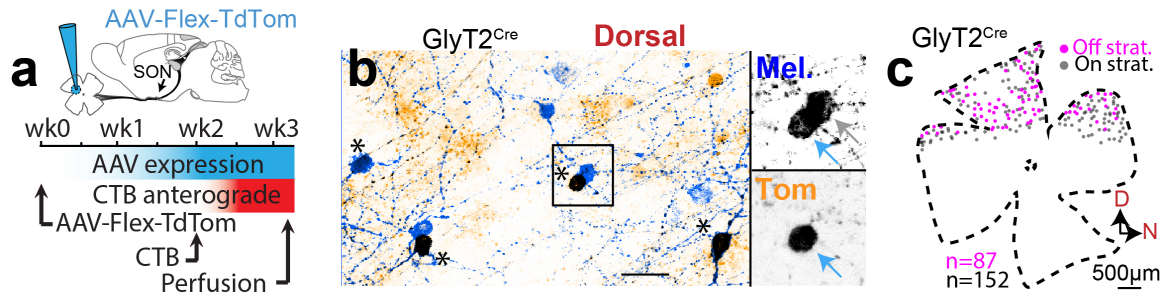
Figure 8: Labeling *GlyT2^Cre* ipRGCs using Cre-dependent anterograde AAV
(a) Schematic of the aterograde eye injection protocol used for identifying the central projections of GlyT2^Cre ipRGCs (Cre-dependent AAV - TdTomato) among RGC recipient areas (CTB labeling of all RGC axons). (b) A Cre-dependent AAV-TdTomato was used to drive fluorescent expression (orange) in the Cre+ retinal neurons. Melanopsin (blue) staining confirmed that all virally labeled RGCs are ipRGCs (black). (c) Retina map and subtype distribution of AAV labeled GlyT2 ipRGCs in the retina. OFF stratified (Magenta) and ON stratified (Gray) refers to the layer of the inner plexiform layer (INL) in which the dendrites terminate. Scale bars: (b); 25 μm. (c); 500 μm.
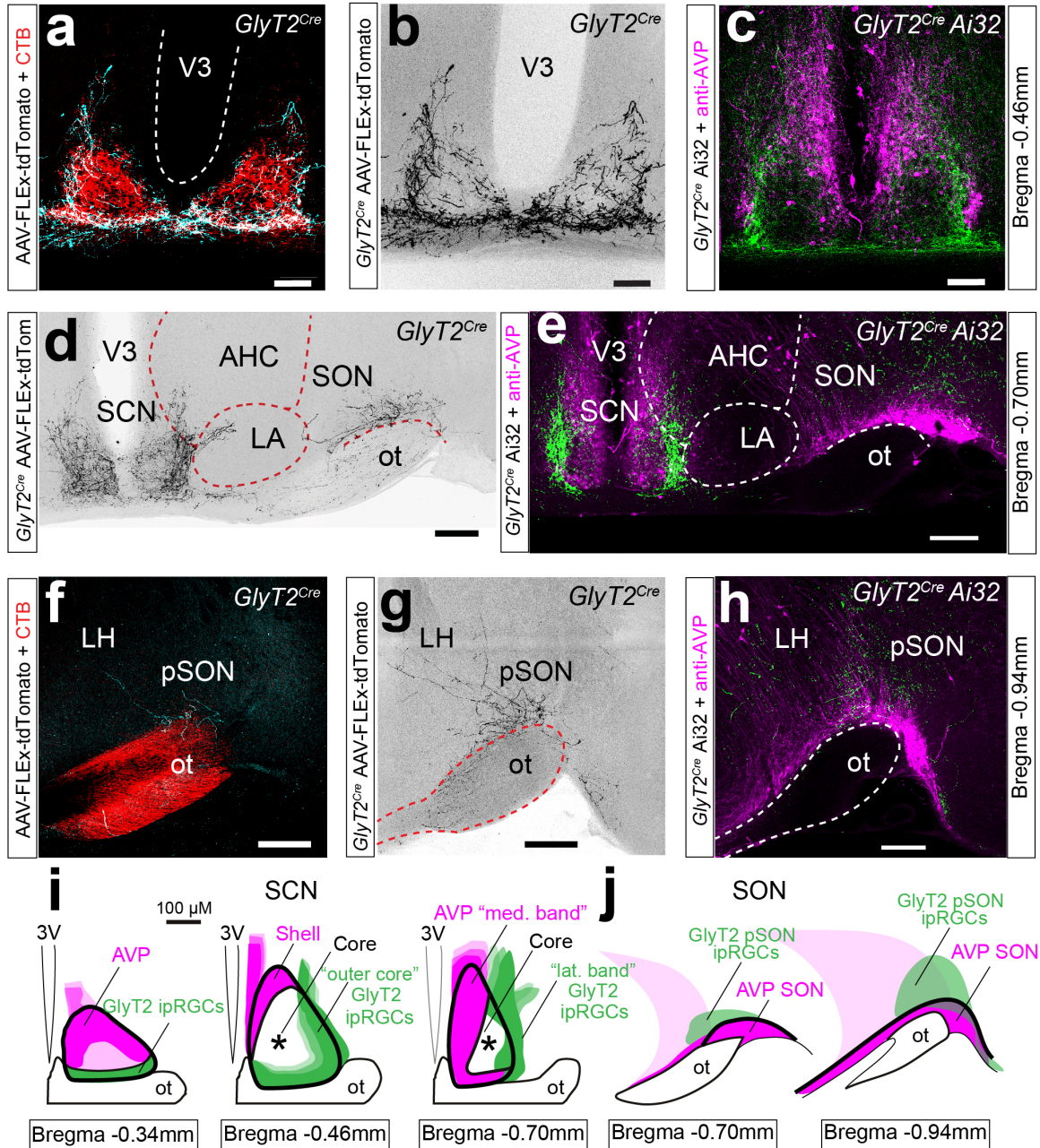
Figure 9: GlyT2^{Cre} ipRGCs project to the SON and a SCN sub-region

(a-n) Intravitreal eye injections of Cre-dependent AAV (AAV-FLEX-tdTomato) in the *GlyT2^{Cre}* mouse allowed anterograde tracing of central projections in confocal images of coronal brain slice (200µm). Cholera toxin subunit B (CTB), which labels all RGC axons, was also injected for anatomical assistance. **(a)** SCN receives dense ipRGC input at its central core (a – red) via the retinohypothalamic tract (RTH) **(a)** *GlyT2^{Cre}* ipRGCs also innervate the SCN but largely avoid the central core and instead innervate the outer core (medial SCN) and lateral band (caudal SCN) (a,b,c). **(c)** outer core and lateral band localized in the *GlyT2Cre;Ai32* (green = YFP of *GlyT2^{Cre}* ipRGC terminals) is distinct from the

50

anatomical shell of the SCN localized by arginine vasopressin neurons (AVP – magenta). *(d,e)* Continued projections from the lateral Band extended into lateral hypothalamic (LA) and anterior hypothalamic (AHC) areas in eye injected GlyT2^{Cre} (d) and GlyT2^{Cre}:Ai32 mice (e). **(d-h)** GlyT2^{Cre} ipRGCs innervate the supraoptic nucleus (SON) observed in eye injected GlyT2^{Cre} (d,f,g) and GlyT2^{Cre};Ai32 mice (e,h) superior to the dense AVP cell bodies of the SON (magenta). **(i,j)** Summary illustrations of *GlyT2^{Cre}* ipRGC projections (green) to the (i) SCN 'outer core' and SCN lateral band as well as projections to the (j) SON, superior to the dense AVP+ cell bodies (magenta). Anatomical distances from bregma determined from the Franklin & Paxinos Mouse Brain Coordinate Atlas. Scale bar = (a-c,i);100 µm, (d-h); 200 µm.

GlyT2^{Cre} ipRGCs innervate the 'outer core' of the SCN

To determine the central axon projection sites of GlyT2^{Cre}-positive ipRGCs we performed intravitreal eye injections of *Cre*-dependent AAV (Fig 1, Fig. 8). Cholera toxin B (CTB), was later injected to co-label retinorecipient axon terminals (Fig. 8a). To provide anatomical reference, these regions were also compared with the CTB labeled projections of all RGCs (Fig. 12a,d,g,j) and eye injections performed in the *OPN4^{Cre}* transgenic mouse, a line which labels all ipRGCs (Fig. 12c,f,I,l). Summary central projection traces were also generated for the GlyT2^{Cre} ipRGCs (Fig. 13).

Like many other ipRGCs, *GlyT2^{Cre}*-positive ipRGCs project to the SCN, but this projection is unique for several reasons. First, their axonal projections to the SCN avoid a central 'core' region (Fig. 9a), and are concentrated at the ventral and lateral regions (Fig. 9a,b,d). Serial sections through the SCN in *GlyT2^{Cre};Ai32* mice, which express CHR2-eyfp in the axon terminals of the GlyT2^{Cre}-positive ipRGCs, illustrate that their axons did not project to the classically defined 'shell' of the SCN (Fig. 9c,e & Fig. 10), which is delineated by the anatomical

localization of neurons that express arginine vasopressin (AVP)[110-115]. Rather, they project to a subregion of the classical core, which we refer to as the 'outer core' as their axons avoid AVP neurons (Fig 9c,d,e,i). In the anterior SCN, their axon terminals were located ventrally (Fig. 9i & Fig. 10a) in a region associated with neurons expressing vasoactive intestinal peptide[110]. In more caudal regions their axons formed a peripheral shell around the SCN core, and were densest in the ventral and lateral regions (Fig. 9c, I & Fig. 10b,c). At the most caudal region of the SCN, their axon terminals formed a lateral 'band' with excursions outside of the SCN into the anterior hypothalamus and lateroanterior hypothalamus (Fig. 9d,e,i & Fig. 10d). The projections suggest that *GlyT2^Cre*-positive ipRGCs likely contribute to distinct functional light-entrainment of circadian rhythms. The functional role of their projections to the AHC and LA outside of the SCN remain unclear however these regions are thought to be involved in thermoregulation[116] and aggression control[117-119].
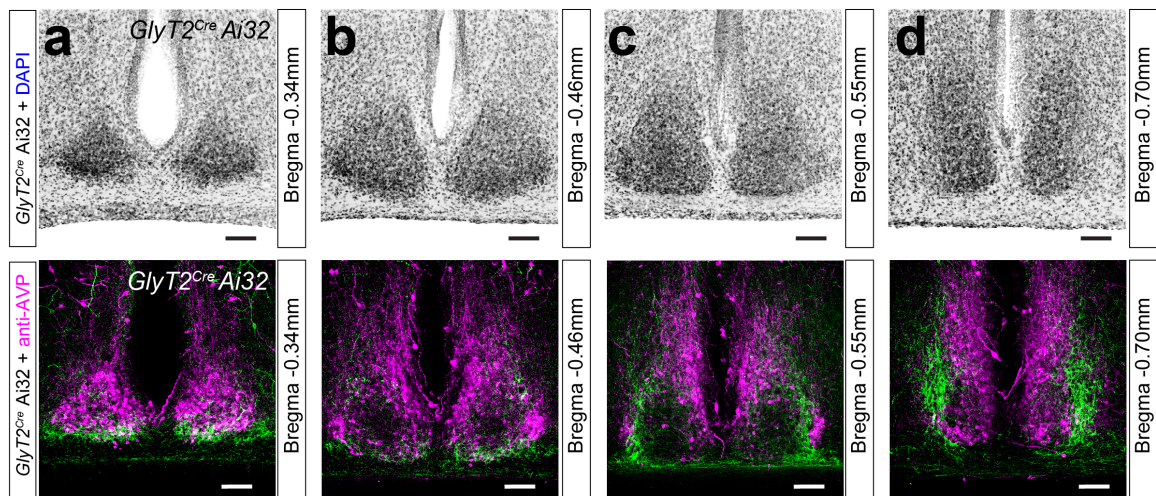
Figure 10: Distinct anatomical area of the SCN innervated by a subtype of ipRGCs

SCN brain slice in *GlyT2^Cre^;Ai32* mouse, presented anterior to posterior. *GlyT2^Cre^* ipRGCs (bottom - green) innervate a previously undescribed location of the SCN we call the SCN 'outer core' and "lateral Band," avoiding the well described anatomical SCN shell, localized by AVP staining (bottom - magenta). DAPI (top) was used from anatomical assistance. Scale bars: (a-d); 100 μm.

Outside of the SCN the *GlyT2^Cre^* ipRGCs innervated the SON, which contains neurons expressing AVP and oxytocin (Fig. 9d-i) and is thought to be involved in systemic fluid homeostasis[120], parturition[121], and appetite[122,123]. It is also thought that the innervation of this region is exclusively from Brn3b+ M1 ipRGCs [45,62,65]. *GlyT2^Cre^*-positive ipRGC axons most prominently innervated the region of the SON immediately dorsal to the optic tract and dorsomedial to the SON known as the perinuclear zone (Fig. 9d; pSON)[62,65,124]. Some of their axons did however, innervate the SON in addition to extending medially into the lateral hypothalamus (Fig. 9f-h,j & Fig. 11a). Outside of the hypothalamus, their axons formed prominent projections to the zona incerta (Fig. 11b) [65], IGL and parvocellular division of the vLGN (Fig. 12b), the lateral posterior nucleus (Fig. 12b), the ventral shell of the OPN (Fig. 12b,d,e - blue) and pretectal regions ventral to the superior colliculus (Fig. 12d,e,g,h,j,k). Many of these *GlyT2^Cre^* ipRGC projections, particularly the SON, accessory hypothalamic nuclei, and the OPN shell are regions thought to be innervated primarily by M1 ipRGCs [45].
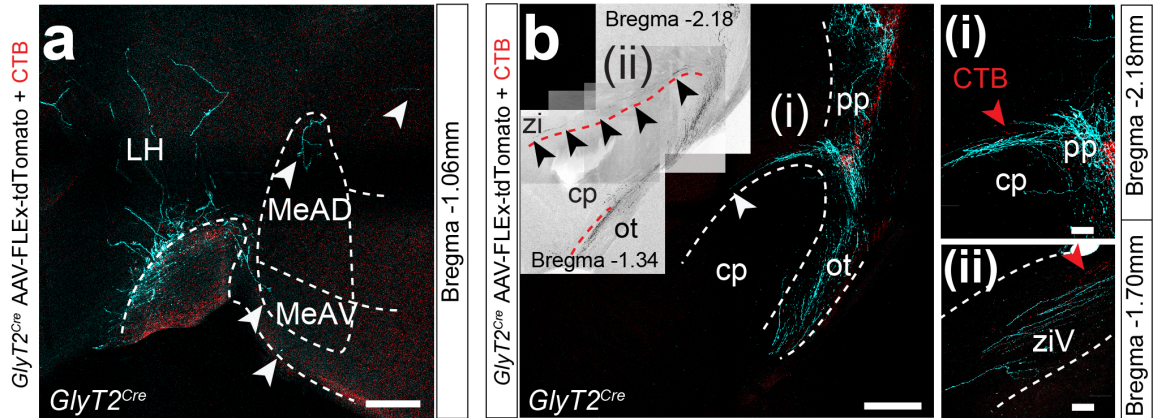
Figure 11: Other sites of hypothalamic projection
(a) Cre-dependent AAV (AAV-FLEX-tdTomato) eye injection in the *GlyT2^Cre* mouse also labeled sparse projections in the lateral hypothalamus and in the anteroventral and anterodorsal edges of the medial amygdalar nucleus (MeAD & MeAV). (b) At the level the rostral ventral lateral geniculate nucleus (vLGN), before entering the geniculate complex, *GlyT2^Cre* ipRGCs emerge from the optic tract and split at the peripeduncular nucleus (pp) (n(i)). A moderate number of ventromedial axons wrap around the cerebral peduncle (cp) and project nearly 1mm caudally along the ventral length of the zona incerta (ziV) (i,ii = inlay from n) (red arrow denotes presence of CTB). The function of the zona incerta is unknown. Scale bars: (a,b); 200 µm, (i,ii); 50 µm.
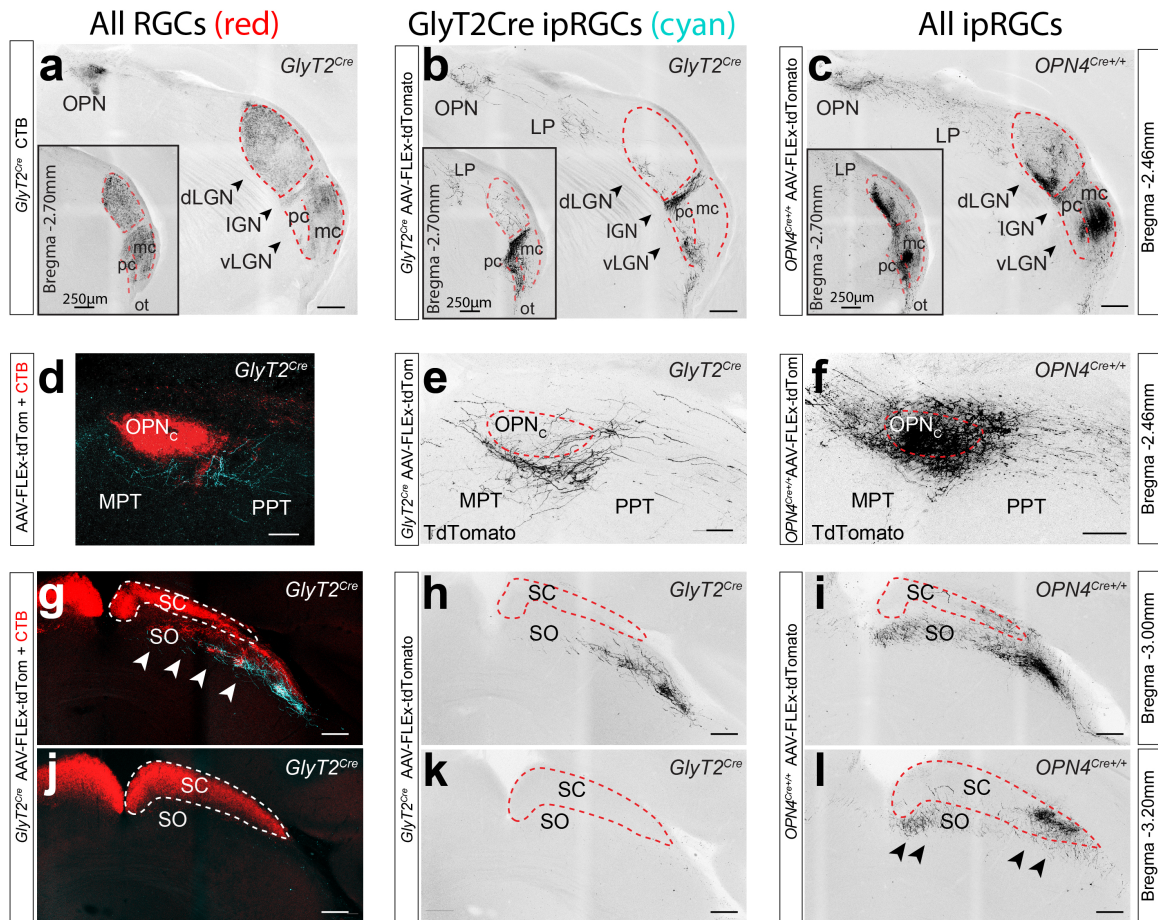
Figure 12: Thalamic, pretectal, and collicular ipRGC projections
Anterograde tracing of central projections in *GlyT2^Cre* and *OPN4^Cre* mouse lines following intravitreal eye injections with Cre-dependent AAV (AAV-FLEX-tdTomato). Cholera toxin subunit B (CTB), which labels all RGC axons, was used for anatomical assistance (a,d,j – red). **(a-c)** Confocal images of coronal brain slice reveal that ipRGCs labeled in the *GlyT2^Cre* innervate the parvocellular (pc) division of the ventrolateral geniculate complex (vLGN) and the intergeniculate leaflet (IGL) (b) IpRGCs labeled in the *OPN4^Cre* more broadly innervate the parvocellular (pc) and magnocellular (mc) divisions of the vLGN, IGL, and focal portions of the dorsolateral geniculate complex (dLGN) (c) *GlyT2^Cre* ipRGCs also form a plexus of terminals in the lateral posterior nucleus (LP). **(d-f)** Confocal images of the olivary pretectal nucleus (OPN) identify that *GlyT2^Cre* ipRGCs innervate the ventral cup of the OPN shell, where ipRGCs labeled in the *OPN4^Cre* project to both core and shell regions, similar to that observed by CTB labeling (d – red). Sparse innervation to neighboring pretectal structures such as medial pretectal (MPT) and posterior pretectal (PPT) areas are also observed. **(g-l)** Confocal images of the superior colliculus (SC), reveal that *GlyT2^Cre* ipRGCs have some innervation to the superior colliculus (SC) (h), like many ipRGCs and RGCs (g,i,j,l). These projections are sparse and localized to the superficial layer of the stratum opticum (SO) (h), with very few projections to the central SC,

unlike those in the OPN4Cre or the CTB labeling (d –red). Scale bars: (a-c,g-l); 250 µm, (d-f); 100 µm.
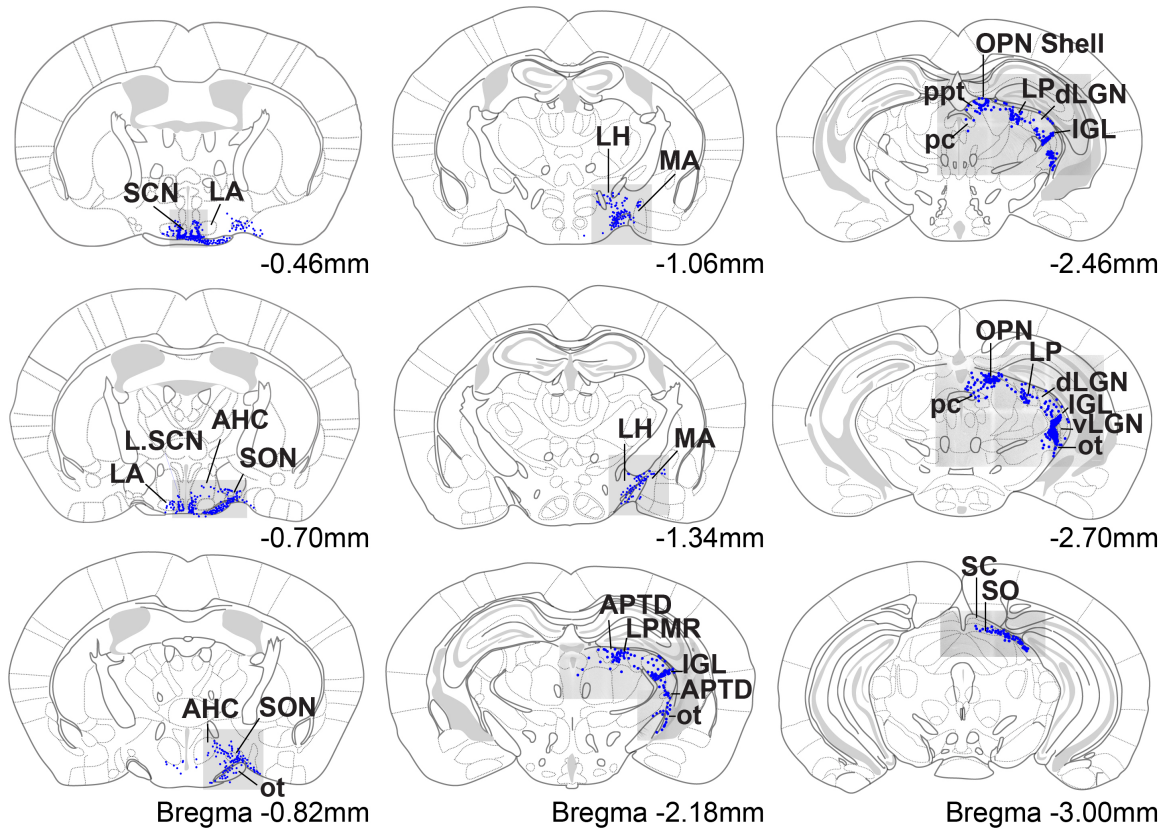
Figure 13: Summary of ipRGC central projections in the *GlyT2^Cre* mouse
Graphical atlas maps (blue: axons and terminals) drawn from the brain slices of *GlyT2^Cre* mice using the Franklin & Paxinos Mouse Brain Coordinate Atlas. suprachiasmatic nucleus (SCN) supraoptic nucleus (SON), optic tract (ot), lateral anterior hypothalamic (LA), anterior hypothalamic (AHC), lateral hypothalamus (LH), Medial amygdalar nucleus (MA) superior colliculus (SC), stratum opticum (SO), posterior pretectal area (PPT), olivery pretectal nucleus core & shell (OPN), ventrolateral geniculate complex (vLGN), intergeniculate leaflet (IGL), lateral posterior nucleus (LP), dorsolateral geniculate complex (dLGN).

SON-ipRGCs: a mosaic of ipRGCs retro-labeled from the SON

Due to the heavy innervation of the pSON and surrounding areas when compared with previous reports, we hypothesized that (1) GlyT2^Cre-positive ipRGCs may be the sole projection to this region, and (2) that only the M1 morphological 'type' of GlyT2^Cre-positive ipRGCs project to this region[7,54]. Since it

is comparatively isolated from the SCN, and the LGN, we decided to selectively target M1 GlyT2^{Cre}-positive ipRGCs using retrograde injections of Cre-dependent AAV injected into the pSON (Fig. 14a,b). These injections labeled melanopsin positive M1 ipRGCs in the retina with dendrites in the OFF layer which restricted to the dorsal hemisphere and in similar density to those identified in *GlyT2^{Cre};Ai140* (Fig. 14c,f,g; 113 ± 5.4; n = 2 mice). Next, we performed the same injections in *OPN4^{Cre}* mice, which expresses *Cre* in all ipRGCs, to determine if the dorsal location and OFF stratification of these SON-labeled ipRGCs is specific to neurons expressing *GlyT2^{Cre}* (Fig. 6d-g). Significantly, the majority of ipRGCs labeled with these injections were OFF-stratifying M1 ipRGCs (~97%) (Fig. 14d,e,f) and located in the dorsal retina in similar quantity and distribution to those labeled in *GlyT2^{Cre}* mice (n = 131 ± 16.4 OFF ipRGCs, n = 4 ± 1 ON ipRGCs, n = 3 animals) and similar in number to those quantified from our counts of GFP and melanopsin positive M1 ipRGCs in *GlyT2^{Cre};Ai140* mice (Fig. 14f & Fig. 7).
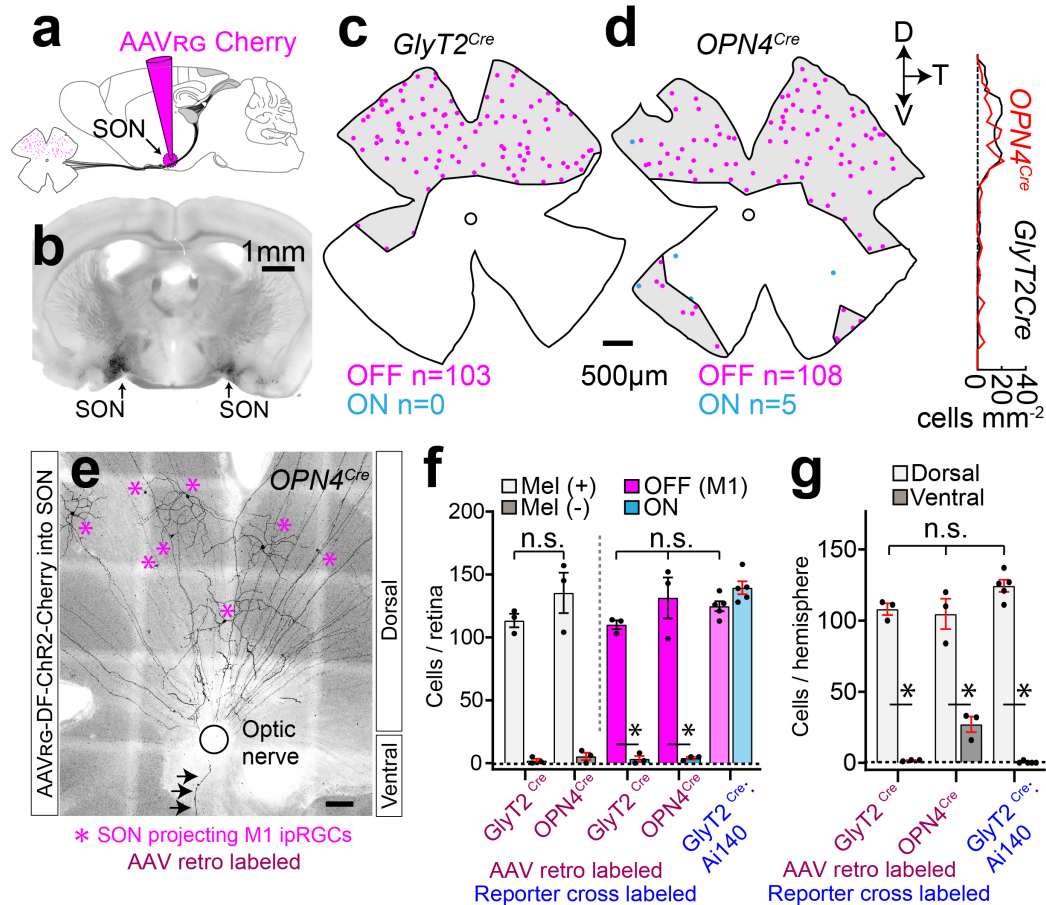
Figure 14: SON is exclusively innervated by GlyT2^{Cre} ipRGCs
(a,b) Stereotactic injections of Cre-dependent retroAAV (magenta) into the SON
(b) labels **(c,d)** a population of M1 ipRGCs (OFF stratifying; magenta) in the
GlyT2^{Cre} **(c)** and *OPN4^{cre}* **(d)** mouse lines. Density at each retinal location along
the dorso-ventral axis is plotted on the right. **(e)** Confocal image of the flat mount
retina show that retro-labeled M1 ipRGCs in the *OPN4^{Cre}* localize to the dorsal
retina, black arrow points out rare ventral axon. **(f)** Bar graphs of ipRGCs per
retina that are melanopsin positive (white) or negative (gray) (left) and either OFF
(M1, magenta) or ON (turquoise) stratifying ipRGCs (right) in SON injected
GlyT2^{Cre} and *OPN4^{Cre}* mice retinas (AAV retro labeled; maroon). *GlyT2^{Cre};Ai140*
retinas quantified for comparison (I - far right, Reporter cross labeled; blue). **(g)**
Bar graphs of population of cells per hemisphere in the SON injected *GlyT2^{Cre}*
and *OPN4^{Cre}* mouse retinas. *GlyT2^{Cre};Ai140* retinas quantified for comparison (g -
far right). Values are mean±SEM. Statistical significance assessed using one-
way Anova with Bonferroni correction for comparisons between multiple groups
(*$p \leq 0.01$) Scale bar = (a); 1mm, (c,d); 500 µm,(e);100 µm.

We observed a small number of ventral OFF ipRGCs labeled by AAV injections

into the SON in *OPN4^{Cre}* mice, in addition to a small number of ON ipRGCs (Fig.

14d,f; n = 27 ± 5.5 ipRGCs). As these ipRGCs were (1) rarely labeled, (2) restricted to small regions, and (3) the ON ipRGCs were also predominantly in the ventral retina, we conclude that this is most likely due to spillover of AAV into the optic tract which lies immediately ventral to the SON. We also noticed some non-ipRGCs, which appeared to be amacrine cells labeled in the retina (*GlyT2^Cre* 2 ± SD 2.6 neurons from 3 mice; *OPN4^Cre* 5.3 ± SD 5 neurons from 3 mice). We conclude that their labeling likely arose from trans-synaptic labelling, or viral spillover from ipRGCs in the retina. Together these data suggests that the dorsal *GlyT2^Cre* ipRGCs represent the sole retinorecipient projection to the SON, and further strengthens our conclusions from anatomical mapping data illustrating these ipRGCs represent a distinct subtype that is located solely in the dorsal retina. Because these ipRGCs represent the exclusive projection to the SON, we now refer to them as SON-ipRGCs.
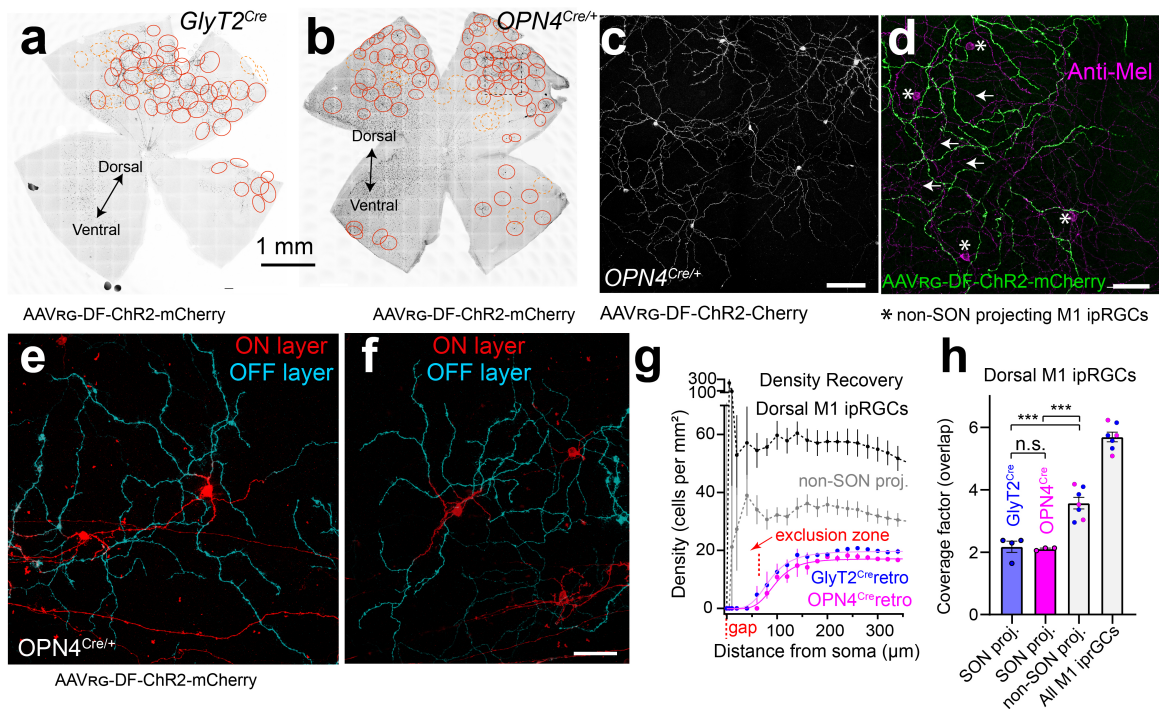
Figure 15: SON ipRGCs form a tiling mosaic that minimizes dendritic overlap

Whole retina images of tiling SON M1 ipRGCs retro-labeled in the $GlyT2^{Cre}$ **(a)** and $OPN4^{Cre}$ **(b)** with dendritic arbor circled in red. (c) Confocal images of mosaic spacing in SON M1 ipRGCs labeled in the $OPN4^{Cre}$. **(d)** Higher magnification confocal image of OFF stratifying INL with dendrites (d - green) overlapping with surrounding M1 ipRGCs dendrites (magenta = melanopsin OFF stratifying), cell bodies (arrow) and displaced cell bodies (* - white) not labeled in the SON injection. **(e,f)** Dendritic morphology of SON M1 ipRGCs with 3-4 short dendritic segments in the ON layer (red) that dive into their terminal dendrites in the OFF layer (cyan). **(g)** Density recovery profile displaying density of cell bodies at distances (μm) from each soma. Gap (red) minimizes the overlap of SON ipRGCs in the SON injected $GlyT2^{Cre}$ and $OPN4^{Cre}$ retina. **(h)** Coverage factor or the proportion of dendritic overlap calculated from the average diameter of M1 ipRGCs, measured from Neurobiotin fills. Non-SON proj. M1s (gray) = M1 ipRGCs not labeled in the central injection. Dorsal M1s = Non-SON proj. M1s + SON proj. M1s = All M1s. Statistical significance assessed using one-way Anova with Bonferroni correction for comparisons between multiple groups (***$p \leq 0.001$) Scale bar = (a,b); 1mm, (c); 100 μm,(d-f); 50 μm.

We noticed that SON-ipRGCs were evenly spaced in our anatomical mapping experiments and uniform mosaic distribution of RGCs is one of the defining characteristics of a unique functional subtype. Our retro-labelling of SON ipRGCs with brain injections into $GlyT2^{Cre}$ and $OPN4^{Cre}$ mice were even more striking. The dendrites of SON-ipRGCs in the dorsal retina formed non-overlapping territorial mosaics, reminiscent of other territorial RGC subtypes (Fig. 15a-c)[100,101]. Upon close examination using confocal microscopy, the dendrites of SON-ipRGCs overlapped with the dendrites of other OFF stratifying ipRGCs in sublamina-a of the IPL stained with anti-melanopsin, and displaced M1 ipRGCs somata (Fig. 15d). SON ipRGCs have a uniform and unique dendritic morphology with 3-4 short dendritic segments that project through the ON layer and extend their terminal dendrites in the OFF layer (Fig. 15e,f). To provide a quantitative framework of analysis of the mosaic distribution of SON ipRGCs, we

quantified (1) the density recovery profile [125,126], a measurement of cell density at increasing distances from the soma (Fig. 15g & Fig. 16a,b,d), and (2) the coverage factor, which is a quantitative measurement of dendritic overlap in mosaic distributions (Fig. 15h & Fig. 16c). Our density recovery profile data indicated that M1 ipRGCs and non-SON projecting M1 ipRGCs together overlapped significantly as evidenced by high values in very close proximity to the soma (< 100 μm) (Fig. 15g). SON-ipRGCs labeled with retro-injections in *GlyT2^{Cre}* and *OPN4^{Cre}* mice exhibited a clearly defined exclusion zone around the soma, which indicates their cell bodies are regularly spaced (Fig. 15g, Fig. 16). We next examined their coverage factor, which measures the average number of dendritic fields of a RGC mosaic overlapping any point in space. Most RGC subtypes that represent a functional visual channel have a coverage factor ~2 indicating there are roughly 2 dendritic fields (or receptive fields) of each specific functional visual channel at any point in the retina[77]. To calculate the coverage we used the average dendritic field diameter from morphological Neurobiotin fills (324 ± 18 μm), as the edges of the dendritic fields labeled from SON virus injections were difficult to resolve due to their overlap. Using these measurements we found that SON-ipRGCs had a coverage factor of just over 2 (2.2 ± 0.18 *GlyT2^{Cre}*; 2.1 ± 0.03 *OPN4^{Cre}*) indicating each point in the dorsal retina is covered by at least 2 ipRGCs. Non SON-projecting ipRGCs has a coverage of 3.6 ± 0.19, and all M1 ipRGCs has a coverage factor of 5.7 ± 0.16 (Fig. 15h & Fig. 16c & Table 2). This indicates that SON ipRGCs are territorial, and provide a seamless coverage of the retina with minimal overlap, similar to

61

some other highly territorial RGC subtypes[101]. These results also support the hypothesis that there are two more territorial M1 ipRGCs subtypes in the dorsal retina or an additional subtype of M1 ipRGCs with higher coverage and slightly more overlap with SON-ipRGCs. Together, these results strongly support the hypothesis that there are multiple ipRGC subtypes in the dorsal retina and that SON-ipRGCs are a unique subtype.
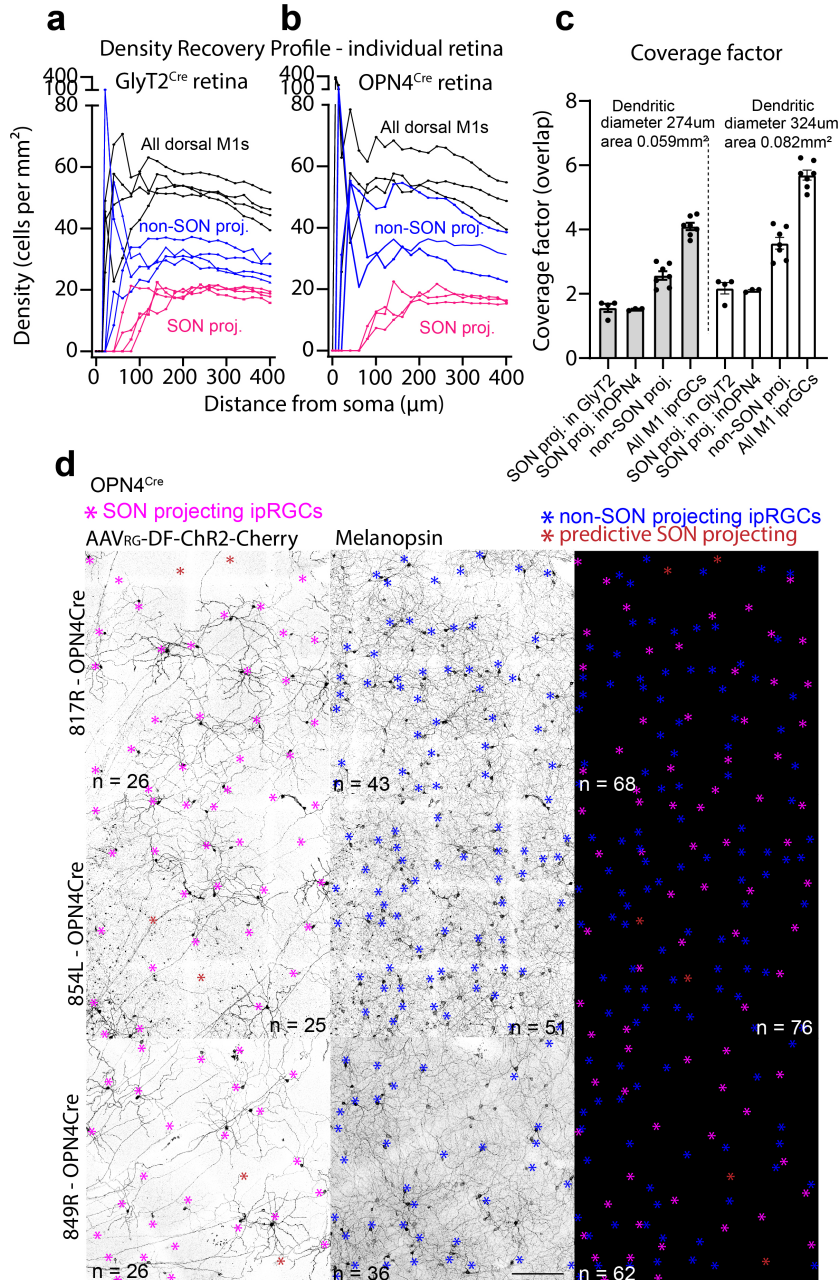
Figure 16: Stereotactic SON injection identifies M1 GlyT2 ipRGCs
(a,b) Density recovery profile (per retina) of dorsal M1 ipRGCs labeled by central injection (SON) in *GlyT2^Cre* (a) and *OPN4^Cre* (b) mice. Density recovery profiles display density of neighboring M1 ipRGC cell bodies at distances (μm) from each soma for All M1 ipRGCs (black), non-SON projecting M1 ipRGCs (blue), and SON-projection M1 ipRGCs (magenta). M1 ipRGCs were identified morphologically. SON-projecting M1 ipRGCs = labeled from retrograde injection, non-SON projecting M1 ipRGCs = M1 ipRGCs not labeled from retrograde injection, All dorsal M1 ipRGCs = SON + non-SON projecting M1 ipRGCs. (c) Coverage factor ei: the proportion of dendritic overlap calculated from the

average diameter of *GlyT2^Cre* M1 ipRGCs measured from either Neurobiotin fills (left) or calculated from the average diameter of M1 ipRGCs reported by Berson et al. 2010[69] (right). (g - Left) Dorsal retina of M1 ipRGCs labeled (TdTomato) by retrograde central injection (SON) in OPN4Cre retina (magenta * = proximal to soma). (g – middle) M1 ipRGCs not labeled by central injection (melanopsin staining) (blue * = proximal to soma). (g right) overlap of SON (magenta) and non-SON (blue) projecting M1 ipRGCs in the dorsal retina. Brown * = predicted as unlabeled SON projecting M1 ipRGC (GlyT2 ipRGC) based on mosaic spacing (still considered non-SON (blue) projecting for any calculations). N = 3 retina for each strain. Area = 1mm^2. Values are mean±SEM. Scale bars: (d); 200 µm, (i,ii); 200 µm.
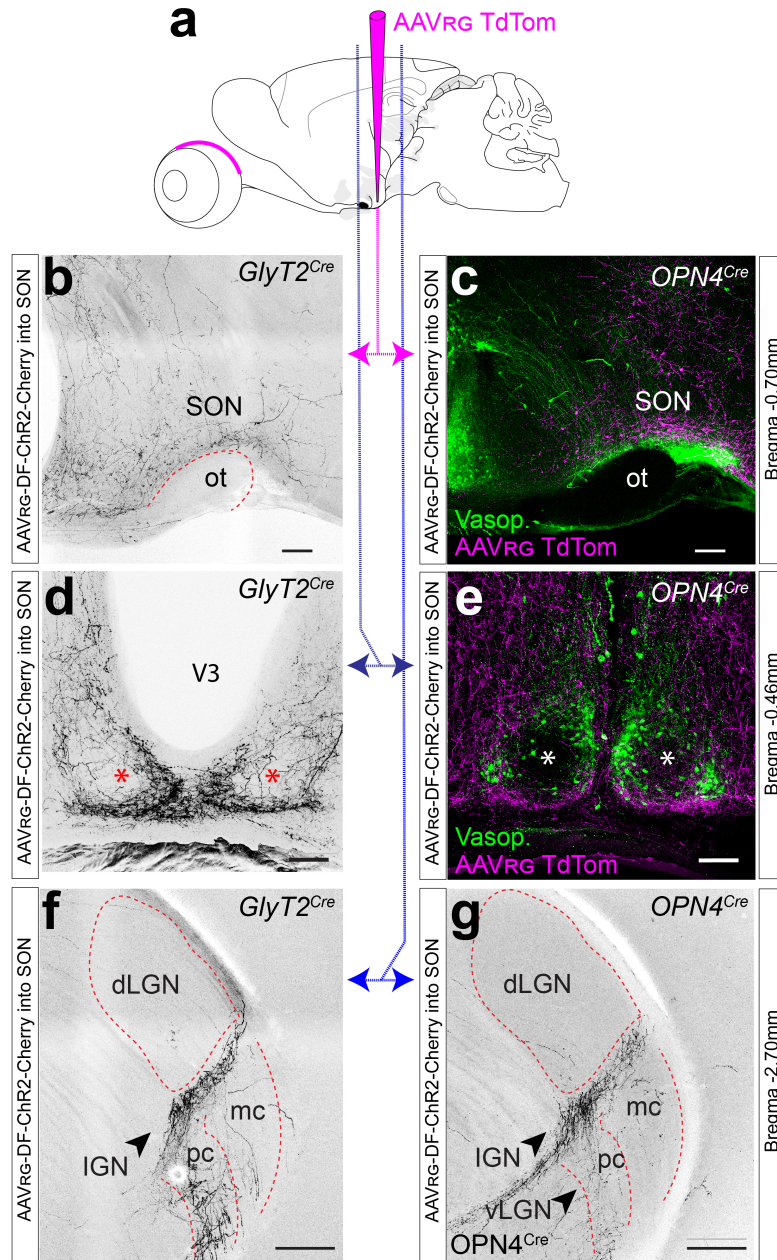
Figure 17: SON ipRGCs have unique innervation to circadian brain regions
(a-i) Focal injections of Cre-dependent retroAAV (AAVRG-DF-ChR2-mCherry) into the supraoptic nucleus (SON) of *GlyT2^Cre* (left) and *OPN4^Cre* (right) mice. In confocal images of coronal brain slice (200um) retrograde tracing is observed in SON (a,b), shell of the suprachiasmatic nucleus (SCN)(e,f), and the parvocellular division (pc) and intergeniculate leaflet (IGL) (h,i) of the geniculate complex, in a projection pattern similar that observed in brain slices from anterograde eye injections in *GlyT2^Cre* mice (Fig. 9-13). (c,f) Co-stained with vasopressin (green) to aid in anatomical visualization of the SON and SCN shell. Confocal images of brain slices from anterograde eye injection of Cholera toxin subunit B (CTB) (d,g) provided for anatomical comparison. Distance from Bregma determined

anatomically using Franklin & Paxinos Mouse Brain Atlas. Scale bar a; 1mm, b,c; 200μm, d-f; 100μm, g-i; 250μm.

Next, we examined other central projection locations following SON injections (Fig. 17). As these mice only have OFF stratifying SON-ipRGCs labeled in the retinas, this allows us to determine the projection patterns without contamination from other ON stratifying ipRGCs that are labeled using anterograde injections into the eye (Fig. 8,9 11,& 12). These results illustrate that the unique projections to the 'outer core' of the SCN are from SON-ipRGCs (Fig. 17d,e) and patterns of innervation appeared similar between $GlyT2^{Cre}$ and $OPN4^{Cre}$ animals. Projections to the IGL; a site of accessary circadian function, was also observed (Fig. 17f,g). These results suggest that the IGL, SON and 'outer core' of the SCN are co-innervated by a single dorsal subtype of ipRGCs, the SON-ipRGCs.

SON-ipRGCs release glutamate at central synapses

Having established that SON-ipRGCs represent a unique subtype of M1 ipRGCs according to their expression and distribution in the retina, we asked if their targeting in $GlyT2^{Cre}$ mice underlies unique neurotransmitter release in the brain. This is particularly important given the recent discovery that some ipRGCs, which project to the SCN, IGL, and OPN release GABA at their central synapses[73]. As SON-ipRGCs are labeled in a mouse line that selectively labels inhibitory neurons throughout the brain and retina, we asked if they released GABA or glycine using two optogenetic approaches to express channelrhodopsin in their axon terminals and to record light-evoked neurotransmitter release (Fig. 18 &

Fig. 19). We chose to record from multiple central locations to rule out the possibility SON-ipRGCs differentially release neurotransmitters at different central locations. Our recordings were focused primarily in the SCN and IGL, due to their dense innervation from SON-ipRGCs, but we also recorded from the SON to test for direct synaptic connectivity between the retina and the SON.
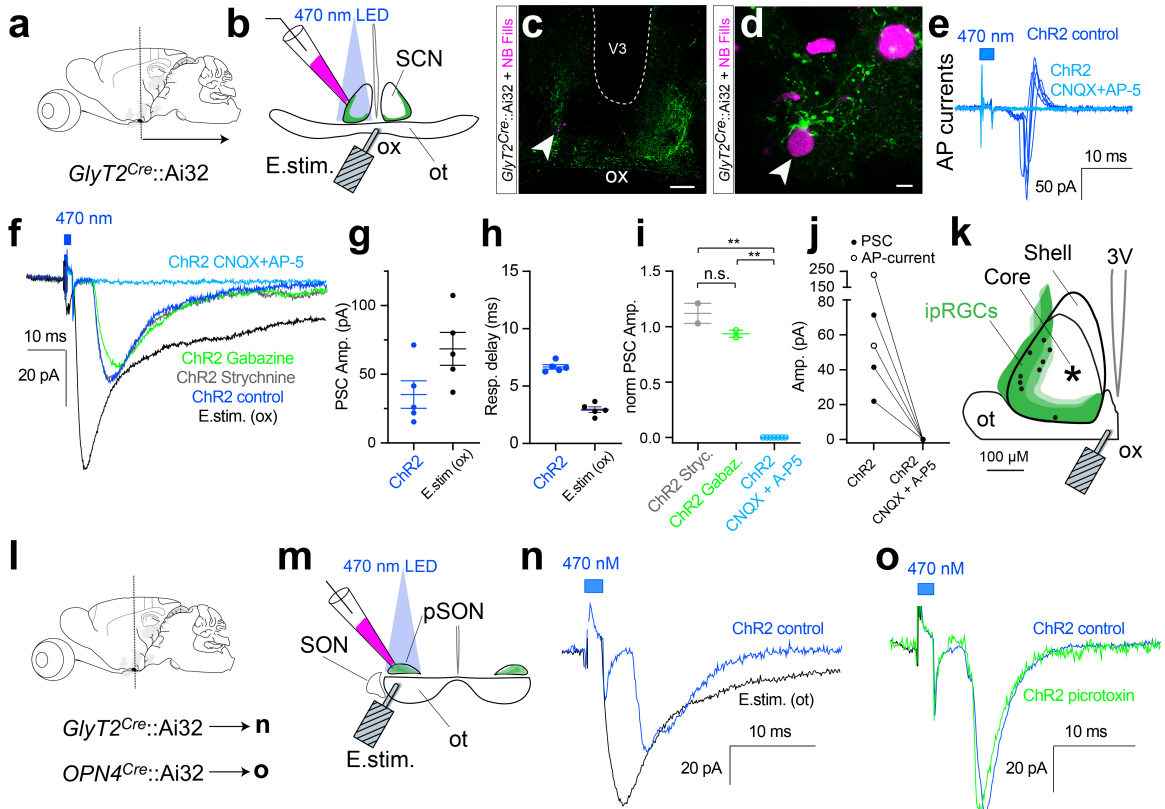
Figure 18: SON-ipRGCs release glutamate in the 'outer core' of the SCN
(a,b) Brain slice recordings in the SCN were performed in coronal sections of the *GlyT2^{Cre};Ai32* mouse. Patch electrode prefilled with Neurobiotin (magenta) and electrical stimulating electrode placed in the optic chiasm (E.stim) in order to stimulate retinal axons. **(c)** Location of the photo-responsive cells (black dots) relative to SON-ipRGC central innervation of the SCN outer core (green). **(d-e)** Confocal images of SCN slice, immunostained following recordings. Recorded cells localized with Neurobiotin in close proximity to SON-ipRGC terminals. **(f)** Photo-stimulation evoked action potential currents (dark blue) are abolished following bath application of CNQX + AP-5 (light blue). **(g)** Whole cell voltage clamp recording traces of electrical (black) and channelrhodopsin-evoked (ChR2) inward post-synaptic currents (PSCs) in control (dark blue), 1 µM strychnine (grey), 10 µM SR-95531 (green). ChR2-evoked currents were abolished with CNQX (20 µM) and AP-5 (50 µM; light blue). **(h)** Response amplitude and (**i**)

67

delay of ChR2- evoked (right) and electrical stimulation evoked (E.Stim) PSCs in the same SCN neurons. **(j)** ChR2-evoked response amplitude in strychnine (grey), SR-95531 (green), or CNQX + AP-5 (light blue) normalized to the control response amplitude. Values are mean ± SEM. **(k)** PSC amplitude before and after CNQX + AP-5. **(l, m)** Coronal brain slices were used for recordings in the SON of the *GlyT2^Cre^;Ai32* mouse and *OPN4^Cre^;Ai32* mouse. **(n)** Whole cell voltage clamp recording traces of electrical (black) and ChR2-evoked inward post-synaptic currents (PSCs) (blue) in the SON. **(o)** Voltage clamp recording traces of ChR2-evoked inward post-synaptic currents (PSCs) in the SON before (blue) and after (green) 50 µM picrotoxin. Statistical significance assessed using one-way Anova with Sidak correction for comparisons between multiple groups (*$p \leq 0.01$). Scale bar = (c); 100 µm, (d); 5 µm.

We crossed *GlyT2^Cre^* mice with a Cre-dependent *ChR2^EYFP^* reporter (Ai32; Jackson 024109), which results in the expression of ChR2 in the terminals of SON-ipRGCs (Fig. 8a-e). Lateral SCN neurons were targeted in coronal slices (Fig. 18b). In cell-attached voltage clamp mode photo-stimulation activated robust action potential currents (APC), which demonstrates that the SCN neuron was depolarized beyond its action-potential threshold by the release of an excitatory transmitter. The amplitude and latency of APCs (Fig. 18h) were robust and fast, consistent with monosynaptic excitatory synaptic connections (Fig. 18g; (mean ± SEM) 7.2 ± 0.5 ms (range 6.3 – 8.2 ms) and 193.7 ± 74.2 pA (range 53.8 – 306.3 pA), n = 3). In whole cell voltage clamp recordings detected photo-stimulation evoked inward post-synaptic currents (PSCs) at holding potentials between -60 mV and -40 mV (Fig. 18f). The PSCs latency and amplitude were 6.7 ± 0.2 ms (range 6.3 – 7.4 ms) and 35.2 ± 10.0 pA (range 15.4 – 71.3 pA), n = 5, Fig. 18g,h). Similar excitatory synaptic input to SCN neurons was demonstrated by electrical stimulation of the optic chiasm (Fig. 18b,f-h), which resulted in larger and faster PSCs (Fig. 18f,h). Pharmacological blockers were

used to identify the neurotransmitter released by SON-ipRGCs. The glycine receptor antagonist strychnine (1 µM) and the GABA$_A$ antagonist SR-95531 failed to inhibit photos-stimulation-induced PSCs (Fig. 18f,i). In contrast, PSCs were blocked by co-application of the selective AMPA and NMDA glutamate receptor antagonists CNQX (20 µM) and AP-5 (50 µM) (Fig. 18f,i,j). Similarly, in cell-attached mode, photo-stimulation-induced APCs were inhibited by co-application of CNQX and AP-5 (Fig. 18j). Together, these results are consistent with a model where SON-ipRGCs are excitatory and release glutamate onto SCN neurons.

The whole-cell patch electrodes contained Neurobiotin and the location of recorded SCN neurons and their proximity to SON-ipRGC axon terminals was reconstructed with confocal microscopy. While only a small percentage of recordings resulted in photo-stimulation evoked PSCs, the locations of connected neurons were mapped to each slice by referencing infrared microscopy images taken of the living slice with the subsequent post-fixed confocal images (Fig. 18k). The locations of synaptically connected SCN neurons were consistent with anterograde and retrograde tracing experiments showing SON-ipRGC axon terminals resided in the 'outer-core' of the SCN (Fig. 9 & Fig. 10). Similar inward PSCs with a latency of 5.72 ± 0.13 ms (range 5.56 – 5.98 ms, n = 3) and amplitude of 64.7 ± 7.1 pA (range 55.9 – 78.9 pA, n = 3) which were not blocked by picrotoxin (50 µM) were recorded in voltage clamped SON neurons (Fig. 18n,o). Electric stimulation of the optic chiasm evoked PSCs in SON neurons

confirming the retinal projection to this nucleus (latency 2.6 ± 0.2 ms, amplitude 215.8 ± 50.1 pA, n = 6).

To determine if SON-ipRGCs might differentially release neurotransmitter at separate central locations, we performed whole-cell voltage-clamp recordings in the IGL in coronal slices made from $GlyT2^{Cre};Ai32$ mice (Fig. 19a, b). We used a different approach to isolate inhibitory currents with 65 mM internal chloride, which changed the inhibitory reversal potential and allowed us to observe inward PSCs for both excitatory and inhibitory events. Photo-stimulation in the IGL resulted in mixed neurotransmitter release, with evidence for GABA, glycine, and glutamate release in our recordings (Fig. 19 c-g). Most photostimulation-evoked synaptic currents were stable in the presence of CNQX, and were strongly attenuated by strychnine, and completely abolished in CNQX, strychnine, and GABAzine (Fig. 19e-g). These results conflict with our SCN recordings and might suggests that SON-ipRGCs release inhibitory neurotransmitters in the IGL while releasing excitatory neurotransmitters in the SCN. However, the IGL receives inhibitory input from other central brain regions[127], some of which contain neurons labeled in the $GlyT2^{Cre}$ mouse line.
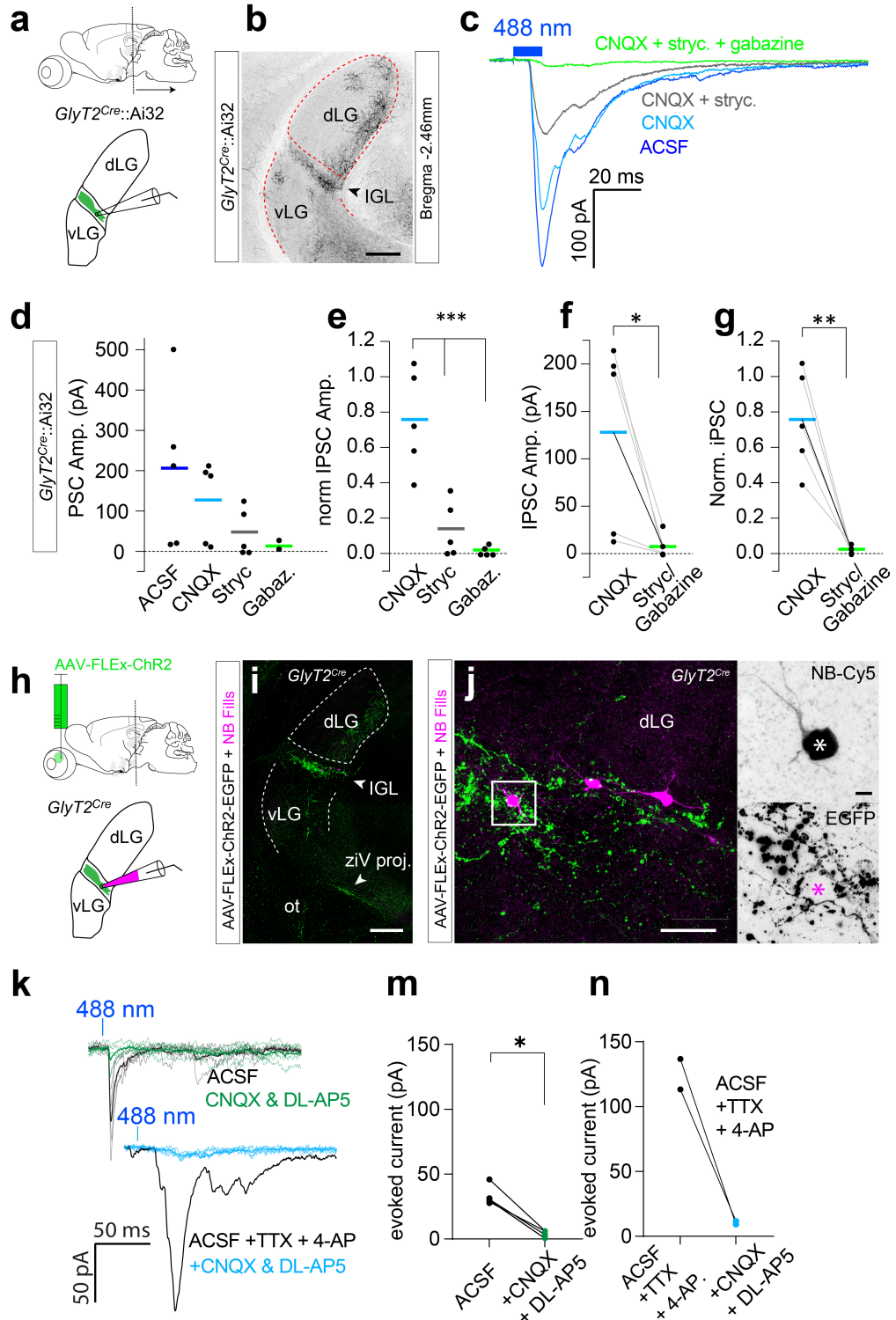
Figure 9: SON-ipRGCs release glutamate at the IGL
(a) Illustration of brain slice recordings in the IGL of the *GlyT2^Cre;Ai32* mouse. **(b)** Confocal image of the vLGN, IGL, and dLGN EGFP expression in GlyT2^Cre::Ai32 coronal brain slice. **(c)** Whole cell voltage clamp recording traces of photo-stimulation under ACSF (black), 20 μM CNQX (blue), 0.5 μM strychnine + CNQX

(red), and 3 µM gabazine + strychnine + CNQX (green). **(d,e)** Photo-response amplitude (d) and normalized photo-response amplitude (e) of PSC under blocker conditions. **(f,g)** Photo-response amplitude (f) and normalized photo-response amplitude (g) in CNQX before and after the addition of gabazine + strychnine. **(h)** Illustration of brain slice recordings in the IGL of the $GlyT2^{Cre}$ mouse 3wks following Cre-dependent ChR2 expression in the eye. **(i-j)** Confocal images of EGFP expression in the IGL brain slice, fixed after recording. Biocytin filled IGL neuron (magenta) surrounded by SON-ipRGC terminals (green). **(k)** (k - top) Photo-stimulation evoked inward PSCs (black) that were blocked by excitatory neurotransmitters CNQX and DL-AP5 (green). (k – bottom) Photo-stimulation evoked inward PSCs (black) in tetrodotoxin and 4-aminopyridine were blocked with co-application of CNQX and DL-AP5 (blue). **(m,n)** Amplitude of photo-induced PSC in ACSF before and after CNQX and DL-AP5. Statistical significance assessed using one-way Anova with Holm-Sidaks correction for multiple comparisons (***$p \leq 0.001$). Scale bar = (a,i); 250 µm, (j); 50 µm.

To determine whether photo-stimulation-evoked inhibitory PSCs in the IGL arise from non-retinal neurons, we restricted ChR2-expression to the retina with eye injections of Cre-dependent ChR2 in $GlyT2^{Cre}$ mice (Fig. 19h). After allowing 2 – 3 weeks for the ChR2 to express, we recorded from the IGL, which was targeted in coronal slices with brief epi-fluorescent illumination to identify eGFP-expressing axon terminals, which form a dense band in the IGL (Fig. 19i - green). IGL neurons were filled with biocytin and recovered for confocal microscopy (Fig. 9j). Photo-stimulation evoked inward PSCs that were completely abolished with the bath application of the AMPAR antagonists CNQX and NBQX (Fig. 19k). These excitatory PSCs were on average smaller than evoked in recordings from $GlyT2^{Cre};Ai32^{ChR2:EYFP}$ mice, which may be due to viral expression of ChR2 being lower than expression driven by the *Ai32* line. To augment photostimulation-induced PSCs and rule out the possibility that inhibitory synaptic terminals need greater depolarization to reach the threshold required to activate transmitter release, we included tetrodotoxin (TTX) and 4-aminopyridine (4-AP) in the ACSF.

Despite 4-AP substantially increasing the light-evoked currents they were completely abolished by the co-application of CNQX (Fig. 19k). Thus, when we expressed ChR2 in the axon terminals of ipRGCs, we found no evidence for inhibitory synaptic release. This suggests that inhibitory inputs to the IGL in GlyT2Cre::Ai32 mice likely arise from central regions, and that SON-ipRGCs only release glutamate, but not GABA or glycine.

3.4 - Discussion

Mosaic tiling and distribution

In most retinal ganglion cell subtypes the fundamental organizing feature of retinal output is a 'mosaic', where the receptive field and corresponding dendritic fields of individual cells of the same subtype are arranged in territorial, regularly spaced grids[78,128,129]. Such arrangement leads to uniform coding of the visual scene across each retinal 'channel'. This has remained unclear for ipRGCs, which overlap considerably, about 4-fold in the retina for the M1 ipRGCs[69]. As M1 ipRGCs participate primarily in non-image forming vision it is possible that spatial organization is deemphasized in favor of maximizing photon capture[44]. Our results show that M1 ipRGCs can be further subdivided and comprise independent subtypes that tile retinal space, like many of the well-described conventional RGC subtypes[101,129-131]. Indeed the coverage factor of SON-ipRGCs is similar to the average coverage factor of most RGCs, identified from their functional receptive fields[77]. This indicates SON-ipRGCs are territorial and their dendrites overlap minimally. The functional significance of this arrangement

remains unclear, but it suggests retinotopy might be important for circadian biology [132], and other non-image forming functions mediated by the SON.

Our mapping data illustrates that the increased density of ipRGCs in the dorsal retina[5,109] arises from an additional population of ipRGCs found only in this region. There are two pieces of evidence supporting this conclusion; (1) when SON-ipRGCs are subtracted from retinal density maps, the dorso-ventral density gradient disappears and the number of M1 ipRGCs is equivalent in both hemispheres. (2) Retrograde labelling of SON-ipRGCs in *OPN4^{Cre}* mice labels the same dorsal M1 ipRGCs as those localized in the *GlyT2^{Cre}* mouse. These results suggest that there are at least 2 independent populations of M1 ipRGCs in the dorsal retina, each with their own appropriate coverage factors. We estimate that SON-ipRGCs overlap ~twice, whereas the total population of M1 ipRGCs in the dorsal retina overlap ~5.5-fold. These values were calculated using the average dendritic diameter of Neurobiotin filled M1 ipRGCs in the *GlyT2^{Cre}* mouse (d = 324 µm) and are slightly larger than the dendritic diameter of M1 ipRGCs previously described (d = 274 µm)[69], resulting in slightly different coverage values (Fig. 16c). Though these differences are likely due to labeling technique, we cannot exclude the possibility that SON-ipRGCs have a different dendritic structure than neighboring M1 non-SON-ipRGCs). Currently it remains unclear if the ventral M1 ipRGCs belong to the same subtype of ipRGCs as those in the dorsal retina that overlap with the SON-ipRGCs. If the overlapping M1 ipRGCs follow the same spacing and distributions as the SON-ipRGCs, then

there may be two distinct subtypes of M1 ipRGCs in the rodent retina; one that is distributed across the entire retina and one that tiles the dorsal retina.

Localized vision and photoreceptor organization

The dorsal-only location of SON-ipRGCs suggests retinotopy at the level of the dorso-ventral axis is fundamental for non-image forming vision. For the rodent, the horizon divides the visual scene into two distinct areas, consisting of differences in color, contrast, and behavioral relevance[107]. Accordingly, this is reflected in the asymmetric organization of cone photoreceptors across the dorso-ventral axis of rodent retina[107,108]. The higher density of UV-sensitive cones in the ventral retina enhances the dynamic range of photoreceptors for encoding the darker contrasts, which dominate the upper visual field and is likely important for predator detection[78,107]. Similarly, the dynamic range of the green cones that are in abundance in the dorsal retina is matched to encode the more even distribution of both light and dark contrasts found in the ventral visual field, likely aiding in navigation through foliage or burrows.

While rodent RGCs can form non-uniform topographic variations across the retina[133], SON-ipRGCs are the first example of a RGC subtype restricted to a sub-region of retina. Strikingly, their location is almost identical to the region of dorsal retina that is low in UV-sensitive cones, suggesting ipRGCs and cone photoreceptors may have adapted similarly to encode information that is asymmetrically distributed in visual space. Non-image forming vision might also

be adapted to encode the more uniform distribution of bright and dark contrasts, like cone photoreceptors. Alternatively, as the visual system of the rodent is optimized for nocturnal vision, they might require additional processing power in night or daylight environment. Luminance reflected off the ground is likely to predominate in nocturnal environments and reflected luminance might contain more useful information to drive the suppression of SON-mediated behaviors such as activity or feeding[134,135].

Central projections and behavioral relevance

There are currently six known 'types' of ipRGCs (M1–M6), primarily distinguished by their morphology [45,96]. However, recent evidence suggests additional functional subtypes likely exist within this current organization [62,64,71-73,88,106]. How do these additional ipRGC subtypes fit with our current understanding of M1 ipRGCs? Some ipRGCs do not express the transcription factor Brn3b and this small number of ipRGCs projects to the SCN and IGL only, avoiding other brain regions[64]. Our results suggest that a separate tiling subpopulation of M1 ipRGCs co-innervate the SON, the outer core of the SCN and the IGL, likely performing distinct behavioral functions.

The SON is a collection of secretory cells that participate in the hypothalamic-pituitary-adrenal axis by producing antidiuretic hormone (ADH) and oxytocin. ADH is responsible for regulating water reabsorption in the kidneys [136] and oxytocin plays a critical role in lactation and parturition [137]. The significance of

visual input to this area via the SON-ipRGCs is unclear but circadian changes in urine volume and concentration [138,139], as well as patterns of lactation [140,141] are well established in humans and animal models. Like the influence of ipRGCs on entrainment of the SCN, bright light might act as a Zeitgeber in the SON, keeping the daily release of AVP well-timed or to aid in adjusting fluid balance to altered light cycles, such as when changing time zones. Alternatively, ipRGCs that innervate the SON might be involved in more direct effects of light on the release of AVP or oxytocin by SON neurons. It is also possible that SON-ipRGCs regulate the release of oxytocin, AVP, or other neuropeptides such as cholecystokinin, or CART, throughout the brain, rather than in the pituitary, where SON ipRGCs might be important for regulating direct light-activated influence on maternal behaviors, or feeding.

Separate ipRGC populations influence both the circadian and direct effect of light on body temperature [72]. It's possible that innervation to the SON functions similarly, acting as a synchronizer of different SON-mediated behaviors over shorter timescales than those governed by the SCN.

The peptide pituitary adenylate cyclase-activating polypeptide (PACAP) is present in a dorsal population of ipRGCs in the rat[109] and both PACAP and the PACAP receptor PAC_1 are expressed in the SON[142,143]. Additionally, PACAP positive retinal hypothalamic tract terminals are localized to a SCN region that resembles the 'outer-core' projections of SON ipRGCs. Thus SON ipRGCs are likely the PACAP-containing ipRGCs described in rat retina but further studies are required to specifically determine this.

The unique innervation of SON-ipRGCs to known circadian structures (SCN and IGL) is also of significant interest. Oscillatory activity in the SCN functions as a circadian timing circuit, predicting physiological and behavioral needs throughout the day and night[144]. The SCN is divided into two distinct subdivisions, designated as 'core' and 'shell' based primarily on localized peptidergic expression, innervation, and projection [21]. The 'core' is the site of direct visual input from ipRGCs, indirect visual input from IGL, and is localized by the expression of vasoactive intestinal polypeptide (VIP) and gastrin releasing peptide (GRP) [110]. Alternatively, the SCN 'shell' contains a large number of AVP neurons and receives innervation from other CNS nuclei [110,145]. Our results show that SON-ipRGCs innervate a localized region of the SCN we call the 'outer core', avoiding the central 'core' of primary ipRGC input and the AVP neurons that comprise the SCN 'shell'. As SON-ipRGCs represent a distinct subtype of ipRGC it suggests that the SCN receives at least two types of direct retinal input, segregated to at least two localized areas of the SCN. The behavioral relevance of this organization is unclear but given the localized distribution of SON-ipRGCs in the retina, and their overlap with other M1 ipRGCs, it suggests that subtypes may be encoding different aspects of environmental light. Given their broad projections to the SCN, IGL, SON and other regions, and the limited knowledge of their specific connectivity within the SON, behavioral analysis of the specific functional role of this unique subtype would require surveying many behaviors that might rely on subtle inputs from SON-ipRGCs.

Neurotransmitter release

Why are there ipRGCs labeled in the *GlyT2*[Cre] line, which, other than ipRGCs, labels predominantly glycinergic inhibitory neurons in the retina? This question is particularly prescient given the recent discovery of GABAergic ipRGCs that project to the SCN, IGL and OPN [73]. Our results, however, indicate that SON-ipRGCs do not release GABA or glycine, and thus must form a separate population from GABAergic ipRGCs. It remains unclear if they express the *GlyT2* transporter in their axon terminals, and if they do, what functional role the transporter might play in modulating central synapses. It is possible that SON-ipRGCs release glycine to modulate the glycine binding site on post-synaptic NMDA receptors. Alternatively their labelling in *GlyT2*[Cre] mice may be some other function of the bacterial artificial chromosome (BAC) insertion in this particular transgenic line. Indeed, other BAC lines, like the *HB9*[GFP] line that labels ON-OFF direction selective ganglion cells (ooDSGCs), reflect the genomic insertion site of the BAC[146].The BAC maps to chromosome 12 rather than the endogenous location of chromosome 7. Regardless, our anatomical mapping data predicts there are likely only two subtypes of ipRGCs in the dorsal retina, if other ipRGCs follow similar mosaic spacing rules as SON-ipRGCs. While we do not know if GABAergic ipRGCs are M1 ipRGCs, their projections to the SCN strongly suggest some of them are, whereas their projections to the shell of the LGN might indicate some are not ipRGCs[73]. Given they are more numerous in the dorsal retina, it remains unclear if they are the other subtype we predict to lie in

the dorsal retina or, instead, they might be part of multiple subtypes of ipRGCs that do not form complete mosaics throughout the retina. Future studies of both retrograde tracing of these populations and functional recording from ipRGCs in the retina are required to resolve these questions.

Contributions

M.H.B, M.M, M.A.M, T.G, O.C, E.W., B.S designed and performed experiments and analyzed data, with input from C.A, H.vG, & K.W. Confocal microscopy and analysis was performed by M.H.B and B.S., retina patch clamp recordings and dye filling and eye injections were performed by M.H.B, brain injections were performed by O.C., brain slice recordings and optogenetics were performed by M.M, M.A.M, and T.G with help from M.H.B. M.H.B and B.S. wrote the manuscript with input from all authors.

Acknowledgments

CHAPTER 4: FUNCTIONAL SUBTYPES OF INTRSINSICALLY PHOTORECEPTIVE RETINAL GANGLION CELLS IN THE RODENT RETINA

The contents of this chapter are in preparation for publication

Michael H. Berry[1,2], Benjamin Sivyer[1,2,#]

1. Department of Ophthalmology, Casey Eye Institute
2. Department of Chemical Physiology and Biochemistry
Oregon Health & Science University, Portland, OR, 97239

4.1 – Abstract

Intrinsically photosensitive retinal ganglion cells (ipRGCs) are specialized retinal ganglion cell (RGC) photoreceptors, which contain their own photopigment, melanopsin, influencing image and non-image forming behaviors. IpRGCs comprise multiple 'types' (M1-M6), which differ in their melanopsin expression and central projections. However, evidence of physiological variability within type suggests that our current organization of ipRGCs is incomplete. Using multi-electrode array (MEA) recordings and unbiased cluster analysis, we identify 8 functional subtypes of ipRGCs, each with distinct photosensitivity and response timing. Two of these functional clusters correspond to highly sensitive ipRGCs but differ in their responses to illumination across several orders of magnitude. We developed a technique to 'OptoTag' channelrhodopsin-expressing ipRGCs and used it to localize photoresponses from a unique subtype of ipRGCs in the dorsal retina that projects to the supraoptic nucleus (SON) of the hypothalamus. We find that photoresponses from SON-ipRGCs are highly uniform and represent one of the sensitive ipRGC subtypes. SON-ipRGCs also have the most sustained photoresponses, encoding constant light levels under conditions that activate melanopsin. The photoresponses from the other highly sensitive ipRGC subtypes are instead transient, and suppressed at illuminations that activate the melonpsin protein. Our results support a framework where there are at least two functional subtypes of M1 ipRGCs, each encoding luminance with distinct spike outputs.

4.2 – Introduction

Intrinsically photosensitive retinal ganglion cells (ipRGCs) are a rare, non-canonical population of photoreceptors primarily involved in reporting environmental lighting conditions to non-image forming brain regions. IpRGCs directly innervate the suprachiasmatic nucleus (SCN) and the olivary pretectal nucleus (OPN), influencing the circadian pacemaking behavior and pupillary constriction, respectively. ipRGCs also project to numerous additional locations within the hypothalamus, such as the supraoptic nucleus, though retinal input to these areas remains undetermined[7,8]. Although initially considered to be a single type[10], ipRGCs are a diverse family of photoreceptors currently organized into six 'types' (M1-M6) primarily defined by their dendritic morphology and amount of melanopsin expression[45,96]. The most studied of these, the M1 ipRGCs, have simple dendritic structures, occupying the OFF strata of the inner plexiform layer (IPL) and expressing the largest amount of melanopsin, resulting in the highest intrinsic photo-sensitivity[45,46]. Non-M1 ipRGCs (M2-M6) have their own distinct morphologies including more complex dendritic arbors and stratification in either the ON layer (M2, M4, M5) or bi-stratify in both the ON and OFF layers (M3, M6) of the IPL[6,45,105]. Non-M1 ipRGCs also express far less melanopsin, resulting in weaker intrinsic photoresponses but, in turn, receive stronger synaptic input from upstream rod and cone photoreceptors.

Despite the clearly defined morphology of M1-M6 ipRGCs, recent evidence suggests different functional roles within types. M1 ipRGCs can be separated by

their expression of the transcription factor Brn3b (Pou4f2)[64], exhibiting alternative patterns of central innervation to the SCN and OPN,[62] resulting in separate behavioral control over photo-entrainment and the pupillary light reflex. Additionally, biophysical studies of M1 ipRGCs report extensive variability in the membrane properties, synaptic input, and photo-responses[71]. Finally, unlike conventional RGC subtypes that are commonly arranged in evenly spaced mosaics with minimal dendritic overlap, the dendrites of the M1 ipRGC type overlap considerably across the retina. Together, these results illustrate that our current model of ipRGC organization is incomplete. We hypothesize that morphologically similar 'types' of ipRGCs comprise multiple, functionally distinct subtypes. However, the characteristics of these proposed subtypes remain unclear and require new investigative tools and approaches.

Recently, a unique subtype of M1 ipRGCs was described in the dorsal region of the rodent retina. These cells display patterns of central innervation distinct from other ipRGCs, representing the exclusive hypothalamic projection to the supraoptic nucleus (SON-ipRGCs), a region involved in systemic fluid homeostasis, maternal behavior, and appetite (Chapter 3). SON ipRGCs also form a mosaic distribution across the dorsal retina, overlapping with other morphologically similar M1 ipRGCs projecting elsewhere in the brain (non-SON ipRGCs). With their unique pattern of distribution and central innervation, we hypothesize this subtype of ipRGCs may extract different aspects of illumination

from the visual space, exhibiting different photoresponse properties from neighboring ipRGCs.

Comparing ipRGC photoresponses can be challenging using traditional single cell recording techniques due to the diversity of ipRGCs, their sensitivity to illumination history[147], and activation by single and 2 photon fluorescent light excitation. Even brief and dim illumination leads to melanopsin stimulation[44] and retinal adaptation,[148] altering their physiological properties. To address these sensitivity issues required that we characterize ipRGC photoresponses acquired simultaneously at the population level. Here we perform Multi-electrode Array (MEA) recordings on dark-adapted retina combined with an 'OptoTagging' strategy implemented at the end of the experiment in order to localize SON ipRGCs from the surrounding ipRGCs. By performing unbiased clustering based on their intrinsic photosensitivity rather than their morphological structure, we identify 8 functional groups of ipRGCs. The photoresponses between SON ipRGCs are highly uniform, as would be expected of a 'true' subtype, and correspond to one of the eight functionally distinct groups of ipRGCs. We demonstrate that this functional group is the most sensitive and sustained of all ipRGCs and responds over a wide range of light intensities, from starlight to bright daylight. As SON ipRGCs are localized to the dorsal retina, these findings might underlie the increased reliance on reflected luminance in nocturnal environments.

4.3 – Results
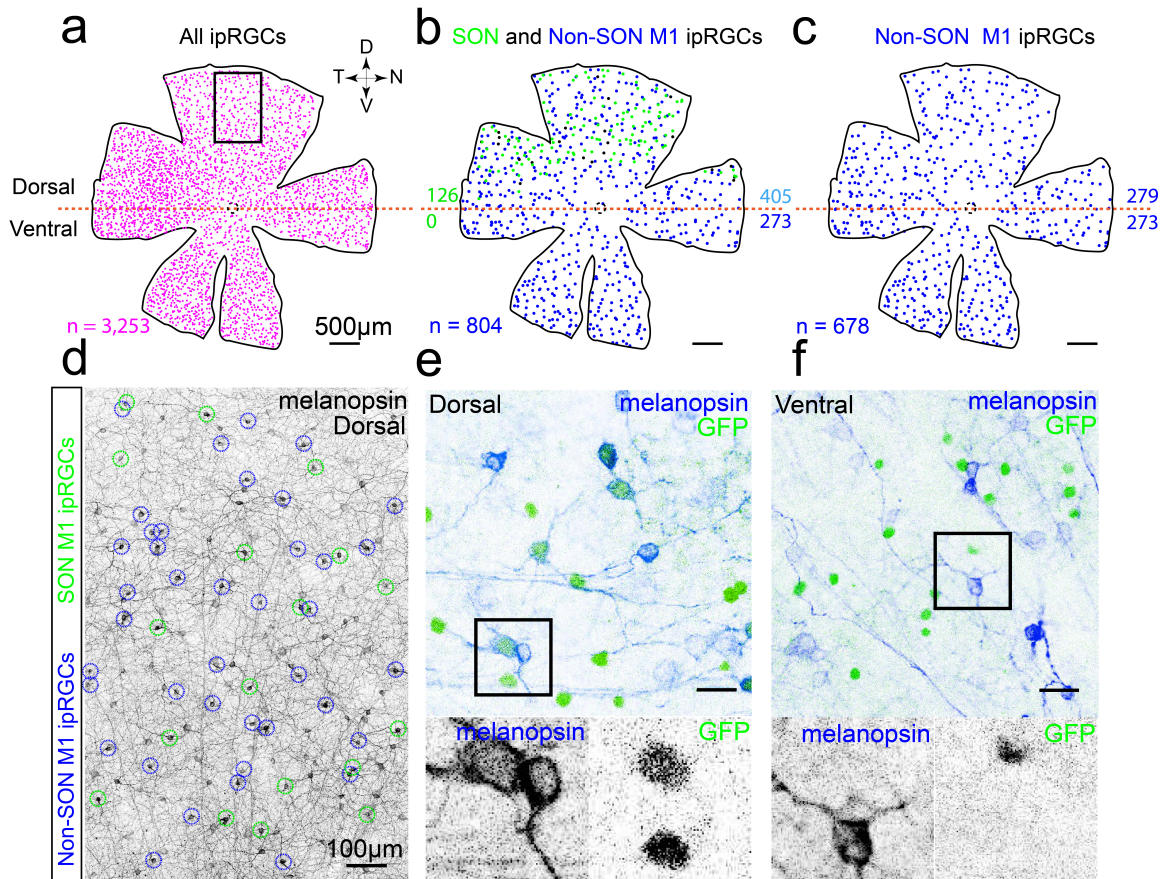
Figure 20: A subtype of M1 ipRGCs in dorsal retina
(a-c) Distribution maps of (a) all ipRGCs (melanopsin+), (b) M1 ipRGCs, and (c) transgenicly labeled M1 SON ipRGCs (EGFP+ & melanopsin+) within the GlyT2^{Cre}::TIGRE^{EGFP} retina. (d) Confocal image of ipRGCs (melanopsin+) with SON M1 ipRGCs (EGFP+) circled in green and neighboring M1 ipRGCs (Non-SON M1 ipRGCs) circled in blue. (e,f) SON ipRGCs are identified by co-localization of melanopsin+ and TdTomato+ in the (e) dorsal but not the ventral retina (f) of *GlyT2^{Cre};Ai9* mice. Displaced amacrine cells (TdTomato+) are observed in both the dorsal and ventral retina.

IpRGC diversity in the dorsal retina

There are ~3,000 ipRGCs in the mouse retina (Figure 20a), comprised of at least

6 morphological types. By staining whole mount retina for melanopsin, the M1

ipRGC type can be easily identified under microscopy by their dendritic

stratification in OFF layer of the IPL and by their abundant melanopsin expression. The mouse retina has ~800 M1 ipRGCs but they are asymmetrically distributed, with an additional ~20% of cells localized to the dorsal retina (Figure 20b). This imbalance is due to a distinct subtype of M1 ipRGCs that tile the dorsal retina and innervate the supraoptic nucleus of hypothalamus (SON-ipRGCs) (Figure 20c) (Chapter 3). We can transgenically localize SON-ipRGCs using the *slc6a5* mouse line (Figure 20d-f & Chapter 3) where Cre expression is selectively driven by a BAC encoding the inhibitory transporter GlyT2 (*GlyT2^Cre*)[104] (Figure 20d-f). SON-ipRGCs overlap with other ipRGCs in the dorsal retina, including other M1 ipRGCs (Non-SON ipRGCs) (Fig. 1d), sampling the same visual space.
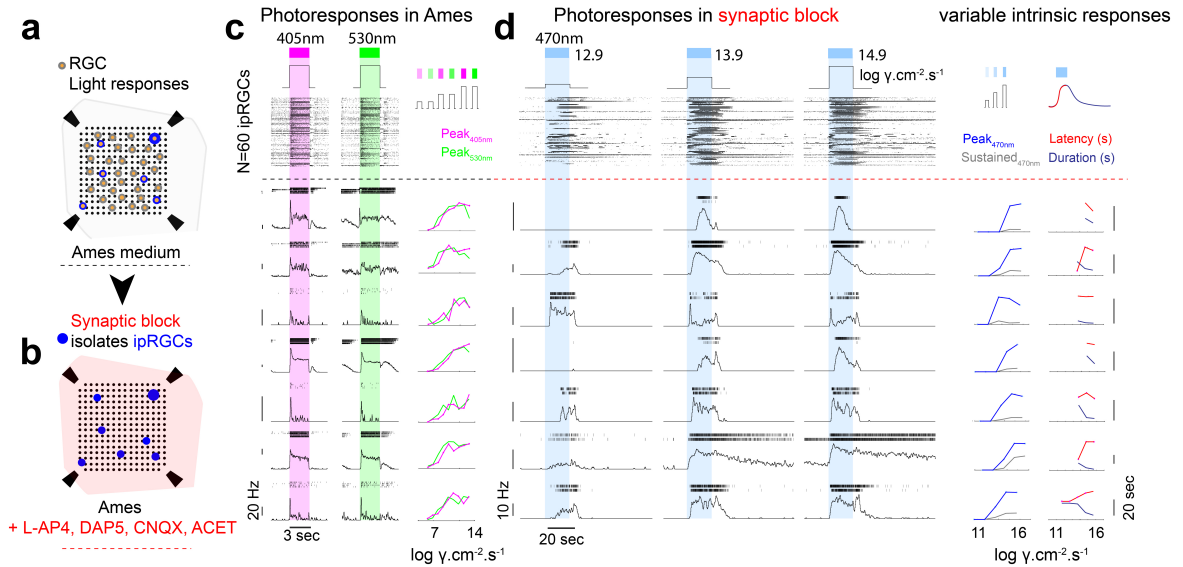
Figure 21: ipRGC response diversity in the dorsal retina
(a,b) Schematic of Multi-electrode array (MEA) recording from all RGCs (a) and isolated ipRGCs (b), following the addition of synaptic blockers. IpRGCs are identified by their intrinsic photosensitivity under pharmacological isolation. (c-d) Representative examples of photoresponses in the same 7 ipRGCs in Ames (c) and in synaptic blockers (d). Individual cells exhibit variability in rod and cone driven responses to UV (left) and green (right) light (c) and variability in intrinsic sensitivity (left and middle), latency and duration of responses (right) to blue light under synaptic blockers.

In addition to intrinsic melanopsin signaling, ipRGCs also integrate photoreceptor-mediated input[149,150]. These two light signaling pathways drive ipRGC spike outputs and is variable across ipRGC types[46,59]. To observe this variability we recorded extracellular spiking activity from ipRGCs of the dorsal retina using a multi-electrode array (Figure 21a). Photoresponses to full-field UV (405nm) and green (530nm) light were recorded for all RGCs under dark-adapted conditions. Synaptic blockers were then added to the recording solution and ipRGCs were identified by their intrinsic photosensitivity to blue (470nm) light (Figure 21b). In response to 20 sec incremental illuminations (~13-15 log photons^{-2} s^{-1}), single units, each representing individual ipRGCs, displayed substantial diversity in their light induced spiking output (Figure 21d). Cells exhibited stark differences in photosensitivity, peak and sustained firing rates (blue and gray), as well as the latency (red) and duration (navy) of their response to light (Figure 21d; right). These observations suggest a substantial amount of ipRGC diversity is reflected in their intrinsic photoresponses and functional differences of neighboring ipRGCs can be captured simultaneously using multi-electrode array recording techniques.

SON-ipRGC response properties at the population level

To target SON-ipRGCs while also recording from all ipRGCs as a population, we combined MEA recordings with an 'opto'Tagging strategy. Using *GlyT2^{Cre};Ai32* mice we restricted ChR2 expression to the SON-ipRGCs in the dorsal retina

(Figure 22a). In dark-adapted retinas, we recorded light responses to a wide range of visual stimuli (Figure 22b,e-g; Step 1). Once these data were acquired, a cocktail of synaptic blockers (40μM L-AP4, 50μM DAP5, 50μM CNQX, 2μM ACET) was used to pharmacologically isolate ipRGCs. Intrinsic photoresponses were then isolated using 20 sec light stimuli at increasing intensities (Figure 22c,h-j; Step 2). Finally, we partially blocked melanopsin responses with an opsinomide[86,151] and presented high-frequency (18Hz) and high intensity blue light stimuli to activate ChR2-expressing ipRGCs (Figure 3d,k-o; Step 3), identifying them from the other cells on the MEA.
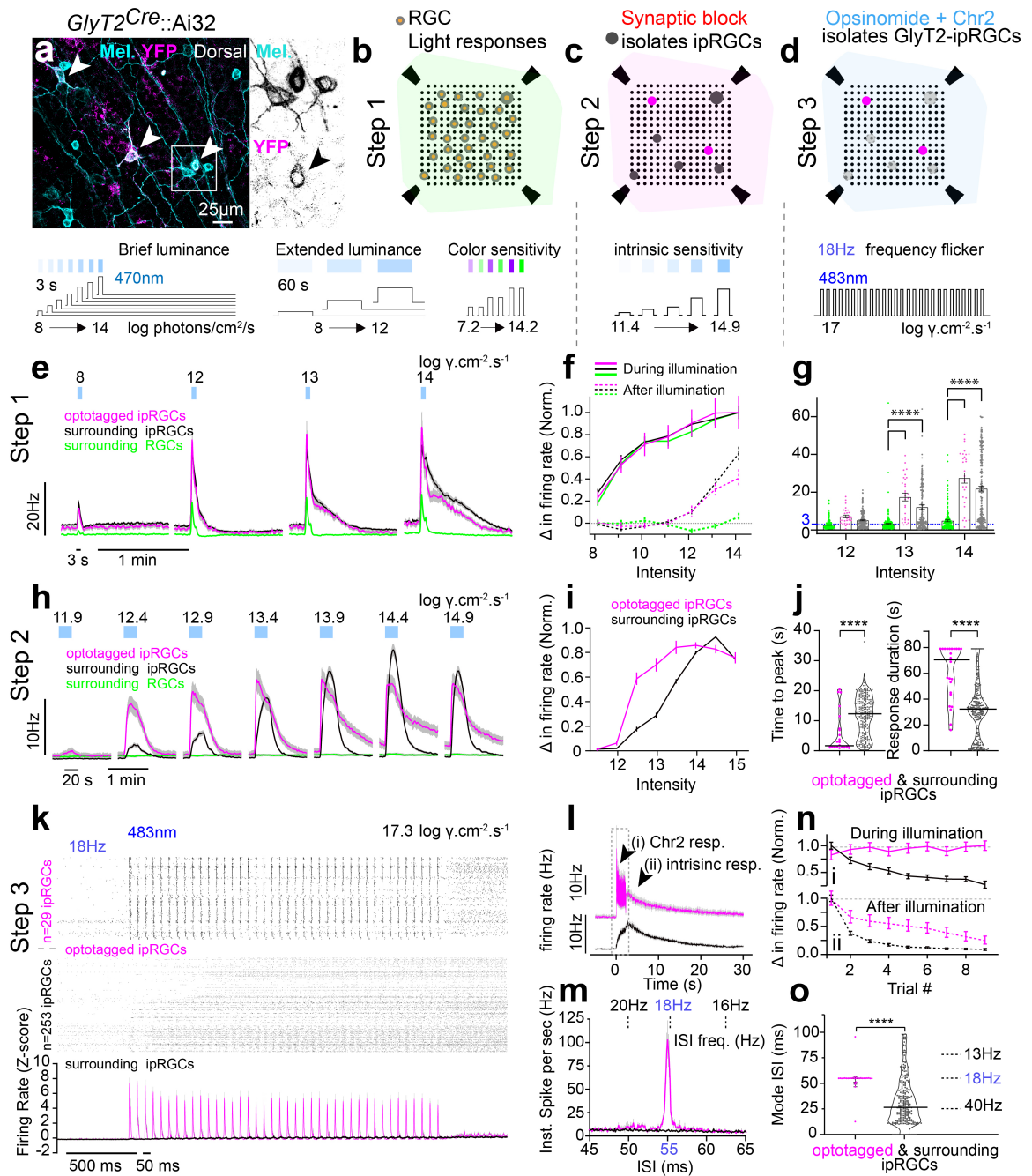
Figure 22: OptoTagging of ipRGCs on the MEA using channelrhodopsin
(a) Confocal image of GlyT2 ipRGCs co-expressing (white arrows) melanopsin (cyan) and ChR2 (magenta) in the GlyT2Cre::Ai32 dorsal retina. **(b-d)** Illustration of strategy for recording dark-adapted light responses from ipRGCs on the MEA. (b) Photoreceptor responses are recorded blindly across all RGCs (Step 1), (c) intrinsic sensitivity under synaptic blockers identify ipRGCs (Step 2), and (d) high frequency flicker under synaptic block and a melanopsin inhibitor (optoTagging) then identifies ipRGCs that express ChR2 ie. GlyT2 ipRGCs (Step 3). Further

analysis allows dark-adapted photoresponses from localized cells (units) to be retroactively examined, see methods for expanded description. (e-f) Dark-adapted photoresponse of OptoTagged ipRGCs (magenta), surrounding ipRGCs (black), and ON RGCs (green) to brief illuminations (3 sec) of blue (470nm) light. Averaged responses (e), normalized change in firing rate (f) and duration of light responses following brief illumination (bar graphs depict mean) at scotopic, meisopic and photopic light intensities. Sustained spiking (beyond the illumination period (e, f- dotted, g – blue dotted) in ipRGCs (magenta & black), compared to ON RGCs (green), emphasizes the role of melanopsin in ipRGC photoresponses. (h-j) Intrinsic photoresponses (under synaptic block) from 20 sec blue (470nm) illuminations in OptoTagged ipRGCs (magenta) and surrounding ipRGCs (black). Averaged responses (h) and normalized change in firing rate (i) at meisopic to photopic light intensities. (j) Violin plots (line depicts median) of time from illumination onset to peak photoresponse (left) and duration of photoresponse (right), measured at 13.9 log photons cm^{-2} s^{-1}, highlights the difference in OptoTagged ipRGCs (magenta) compared to surrounding ipRGCs (black). (k-o) Photoresponses of ipRGCs to OptoTagging high frequency stimulation (18Hz) at 17.3 log photons cm^{-2} s^{-1} under synaptic block and opsinamide AA92593 (melanopsin inhibitor [85,86]). (k) Peri-stimulus time histogram of ipRGCs with (n=29) (magenta; OptoTagged ipRGCs) and without (n=253) (black; surrounding ipRGCs) time locked ChR2 responses (N= 4 retina). Raster (top) displays individual spiking responses, histogram displays average change in firing rate to 18Hz flicker normalized by z-score. (l) Averaged response of OptoTagged (magenta) and surrounding ipRGCs (black) with arrows (i,ii) identifying a transient ChR2 dependent component (i) (doted box is k) and slow sustained intrinsic (melanopsin dependent) component. (n) Tracking of normalized change in firing rate for ChR2 response (i) and intrinsic response (ii) across repeated trials of flicker stimuli (9 trials). (m,o) Average inter-spike interval (ISI) histogram (m) and ISI occurrence (mode) (o) in response to the OptoTagging stimulation. Inter-spike interval frequency equivalents (m- top, o-right) are provided for ease of comparison with stimulation frequency (18Hz). (e-i & k-m) Values are mean+SEM, (j,o) violin plot bar is median. Statistical significance assessed using Mann-Whitney test for comparisons between two groups or one-way Anova with Sidaks correction for multiple comparisons (****$p \leq 0.0001$). N= 282 ipRGCs, N = 4 retina.

These OptoTag stimuli isolated a small population of ipRGCs (13%±4.6% of ipRGCs n=4 retina) that had time locked spike responses (Figure 22k - top) with an inter-spike interval equivalent to the stimulation frequency (18Hz) (Figure 22m,o). Observing these photoresponses on a larger time scale, all ipRGCs clearly exhibited a slow sustained response (Figure 22l), which resembled

melanopsin activation that is not completely blocked by the application of the opsinomide. However, OptoTagged cells could be easily separated by an additional fast component paired with high frequency stimulation. (Figure 22l; ChR2 resp.). Upon repeated trials, the light induced change in spiking activity of the slow component declined while the ChR2 component remained intact (Figure 22n). These results are consistent with the resistance of ChR2 to photo-bleaching over repeated trials and melanopsin's capacity for adaptation under bright illumination[147,152].

Once separated into OptoTagged and surrounding (non-OptoToaged) ipRGC populations (Figure 22k-o), light responses to visual stimuli acquired prior to synaptic blockade and OptoTagging were retroactively tracked for further analysis (Chapter 2). IpRGCs respond to scotopic, meisopic and photopic light stimuli with fast rod and cone mediated drive over a similar time course as other ON RGCs (Figure 22e-g), yet had very sustained spike responses to luminance levels that activated melanopsin (Figure 22e,f). Indeed, ipRGCs often spiked for 30 seconds or more following the offset of a 3 second light pulse (Figure 22g), a well established characteristic of the melanopsin protein[4,105]. Under synaptic blockade (Figure 22h-j), OptoTagged ipRGCs exhibited enhanced sensitivity (Figure 22i), a shorter response latency, and longer response duration (Figure 22j) when compared to other ipRGCs, suggesting their responses are homogeneous and primarily driven by melanopsin, rather than synaptic input from photoreceptors.

Functional organization of ipRGCs

Intrinsic photoresponses of ipRGCs differ considerably in the dorsal retina (Figure 21), yet SON ipRGCs (OptoTagged) appear homogeneous in their response latency and duration (Figure 22j) (minimal variability). To further differentiate OptoTagged ipRGCs from other ipRGCs, we performed unsupervised cluster analysis[77,89] on ipRGC intrinsic photoresponses (Figure 23a,b). Our unbiased approach ignores morphological and molecular criteria, and classifies ipRGCs based on their light responses (Chapter 2).
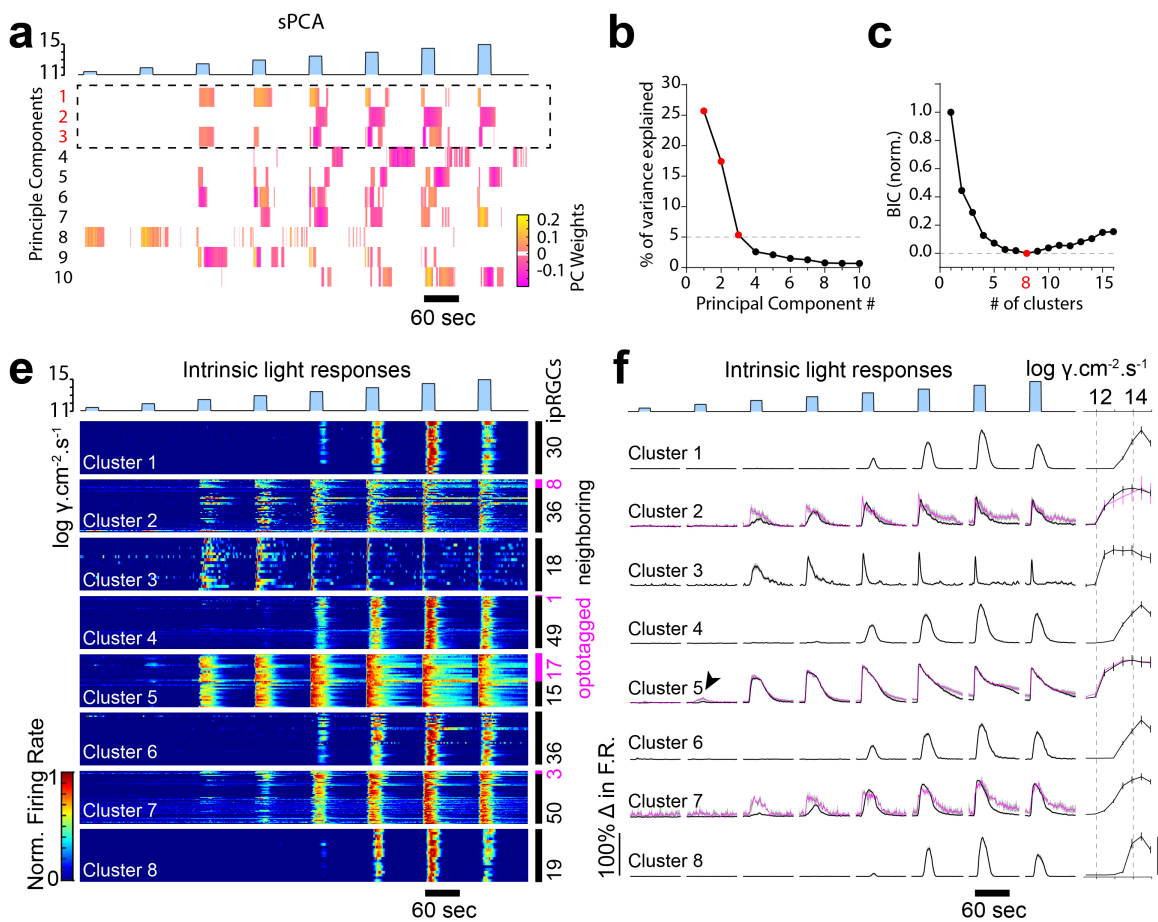
Figure 23: Unbiased clustering identifies eight functional groups of ipRGCs
(a) Heat map of the first 10 weighted sparse principal-components generated from the intrinsic ipRGC photoresponses to increasing irradiances of 20 sec

duration (above). (b) Percentage of variance in ipRGC responses explained by each sparse principal component. Components that explained more than 5% of the variance were used for subsequent analysis (dotted box in a). (c) Normalized bayesian (Schwarz) Information Criterion (BIC) value plotted as a function of each potential gaussian mixture model with a red data point (8 clusters) denoting the model chosen. BIC values serve as a balanced correlate of likelihood for the number of clusters by rewarding complexity but penalizing overfitting. The lower the BIC value, the closer the fit of the gausian mixture model to the data. BIC values for ipRGCs responses decline until reaching a model with 8 clustered groups (red dot), before increasing from 9 though 16. (e,f) Unbiased clustering of intrinsic ipRGC responses identifies 8 functionally distinct clusters. Individual cell heatmaps (e) and averaged histogram (f) of normalized intrinsic responses to increased irradiance. (e – right) Number of OptoTagged ipRGCs (magenta) versus surrounding ipRGCs (black) per cluster. (f – right). N= 282 ipRGCs, N = 4 retina.

We identified 8 distinct functional groups (Figure 23e,f), which differed in their sensitivity, response onset and duration (Fig. 24a-d). The two groups with the highest photosensitivity, Clusters 3 and 5, stood out from the others (orange & turquoise). Both exhibited identical photosensitivity, peak firing rate (Figure 24a), and a short latency (Figure 24c) in their responses. However, both groups differed dramatically in their sustained firing rate during illumination (Figure 24b) and in their response duration (Figure 24d), forming opposing extremes among the 8 functional groups of ipRGCs. But what functional groups are represented by the OptoTagged SON ipRGCs?
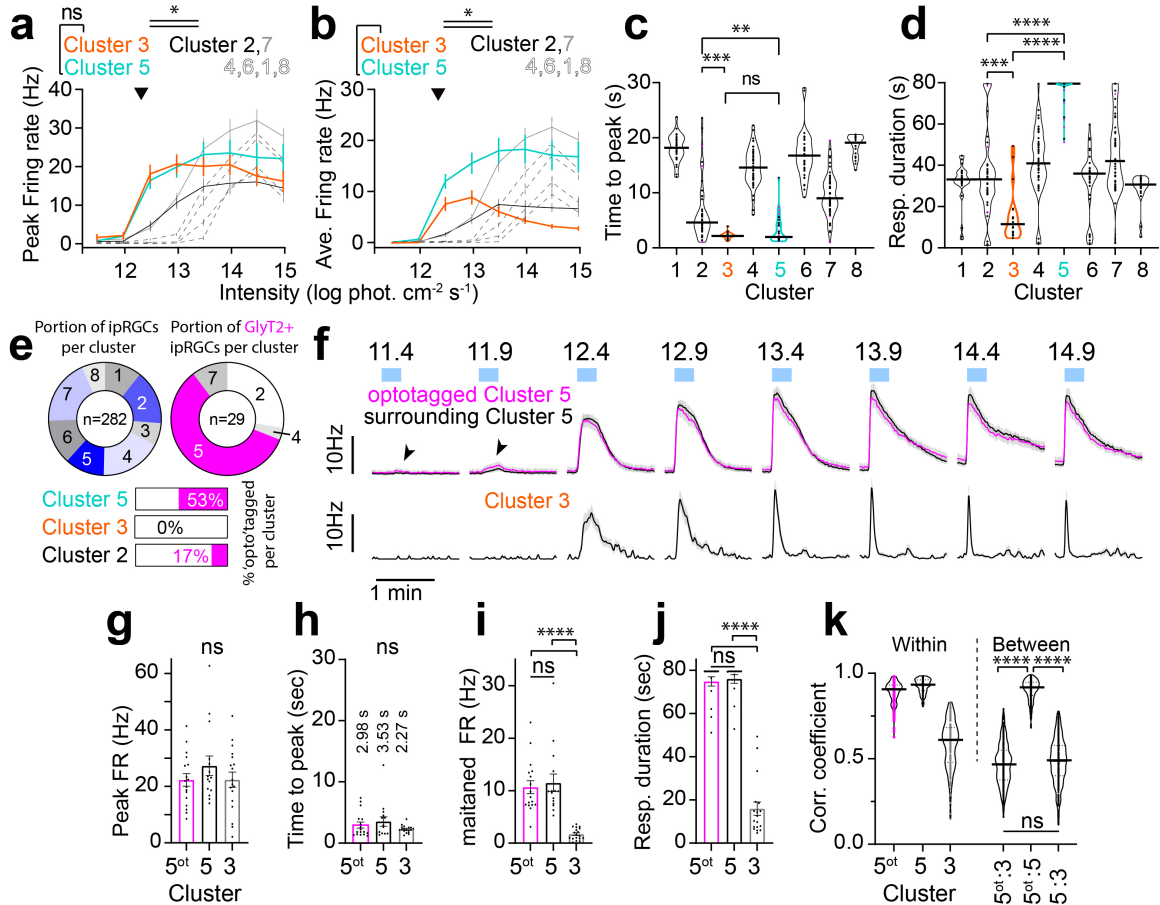
Figure 24: SON ipRGCs are part of a functionally distinct and highly sensitive subtype

(a,b) sensitivity curves of peak firing rate (a) and average firing rate (b) per cluster across increasing light intensity. Violin plots of time from light onset to peak (c) and duration of response (d) per cluster. Cluster 3 (orange) and Cluster 5 (turquoise) highlighted as the most intrinsically photosensitive. (e) Portion of ipRGCs per cluster (left) and portion of SON ipRGCs (OptoTagged) per cluster (right) with % displayed for relevant clusters (bottom). (f) Intrinsic photoresponses of Cluster 5 and 3 under synaptic block, consisting of 20 sec of blue (470nm) light exposure at mesopic to photopic intensities. (g-j) Quantitative characteristics: Peak firing rate (g), time to peak (h), maintain firing rate (i), and response duration (j) for Clusters 5 and 3 under 13.9 log photons cm^{-2} s^{-1}. (k) Cross correlation coefficients for cells compared within (right) and between clusters. Values are mean+SEM, (j,o) violin plot bar is median. Statistical significance assessed using Mann-Whitney test for comparisons between two groups or one-way Anova with Sidaks correction for multiple comparisons (*$p \leq 0.05$)

We find the majority of 'Opto'Tagged ipRGCs fell into cluster 5 (Figure 24e), but

none in the equally sensitive cluster 3. Examining the photoresponses of the two

groups across all light intensities (Figure 24f), we find that Cluster 3 responds to light transiently (Figure 24i), representing the shortest response duration (Figure 24d,j). Cluster 5 instead exhibits an extended photoresponse (Figure 24i), lasting more than a minute after the end of illumination (Figure 24j), representing the longest response duration of all functional groups (Figure 24d). The correlation values (Figure 24k) within (left) and between (right) clusters identify that the 'Opto'Tagged ipRGCs ('Opto'Tagged Cluster 5) are homogeneous in their response to light, despite sharing some properties with Cluster 3. Because of their high sensitivity and low response latency, these clusters share features of M1 ipRGCs (M1-like), which contain the highest melanopsin concentration and have the largest intrinsic photoresponses[45,58,105]. This is further functional evidence for distinct ipRGC subtypes in the dorsal retina and confirms previous morphological studies on the distribution of M1 ipRGCs (Chapter 3).
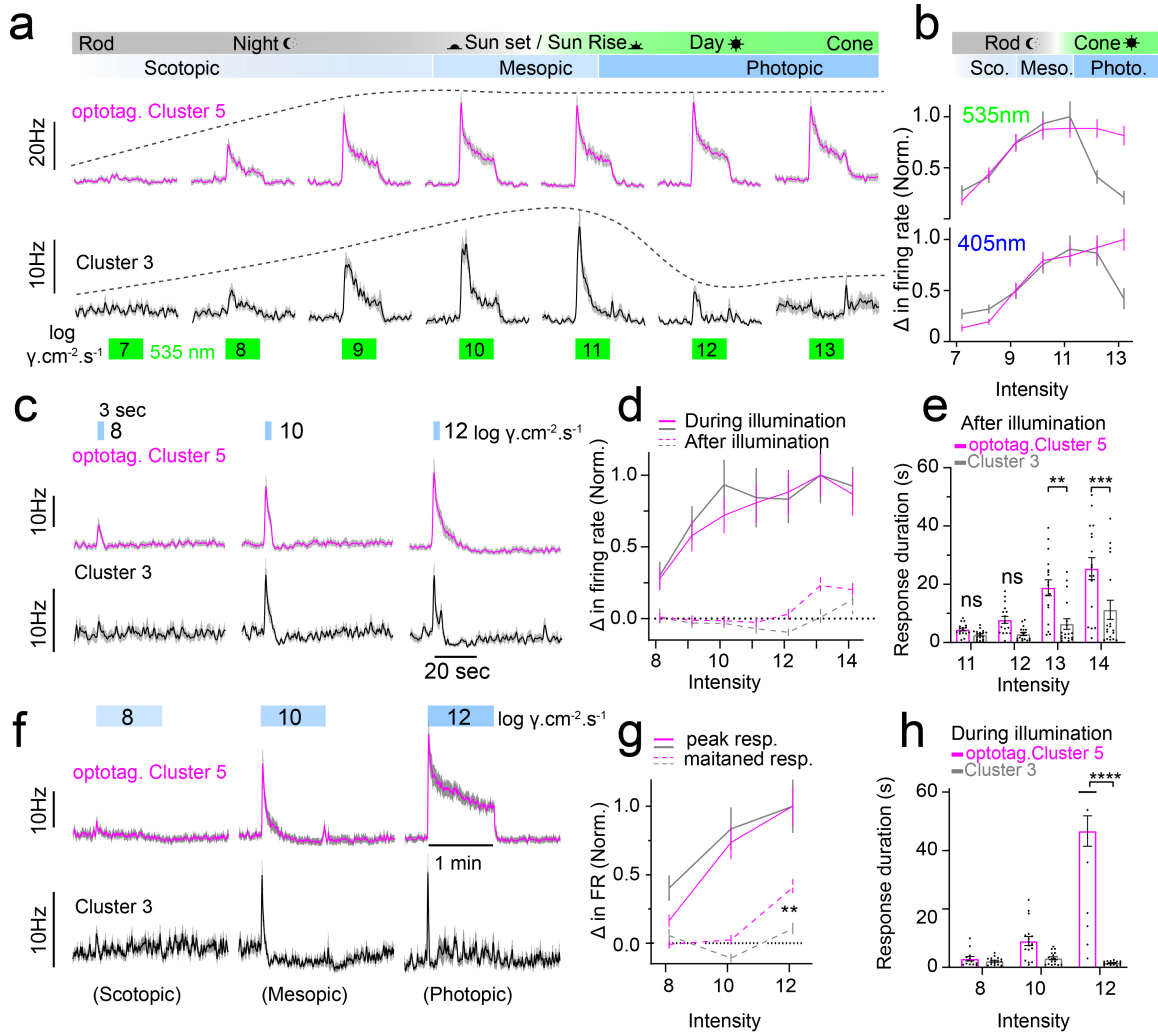
Figure 25: SON ipRGCs encode sustained luminance from starlight to bright day

(a-i) Dark adapted photoresponses of 'Opto'Tagged Cluster 5 (magenta - top) and Cluster 3 (gray – bottom). (a) Average photoresponses to green (535nm) illumination from dim moonlight (left) to bright sunlight (right). (b) Normalized change in firing rate across UV (blue - 405nm) and green (green - 535nm) light intensity ranges for 'Opto'Tagged Cluster 5 (top) and Cluster 3 (bottom). (c) Average dark-adapted photoresponse to brief luminance (3 sec). (d) Normalized change in firing rate during (solid) and after brief (3 sec) illumination (dotted) from starlight (scotopic) to daylight photopic. (e) Bar graphs of response duration following brief illumination under mesopic to photopic light intensities. (f) Average dark-adapted photoresponse to extended luminance (60 sec) to scotopic and mesopic light intensities. (g) Normalized change in firing rate during (solid) and after (dotted) extended (60 sec) illumination from starlight (scotopic) to daylight (mesopic). (h) Bar graphs of response duration during extended illumination under mesopic to photopic light intensities. Values are mean+SEM. Statistical significance assessed using Mann-Whitney test for comparisons between two

98

groups or one-way Anova with Sidaks correction for multiple comparisons (**$p≤0.01$, ***$p≤0.001$, ****$p≤0.0001$)

SON-ipRGCs encode sustained luminance between scotopic and photopic light intensities

Our data illustrates that, under synaptic blockade, the two most photosensitive clusters of ipRGCs respond differently to prolonged illumination, suggesting they encode different aspects of environmental light. Next, we examined their photoresponses prior to synaptic blockade to determine how they encode irradiance from nocturnal to day lighting conditions (Figure 25). 'Opto'Tagged SON-ipRGCs (Cluster 5: sustained ipRGCs) encode very dim scotopic light intensities starting at ~7 log photons cm^{-2} s^{-1} (535 nm) and were sustained at all light intensities (Figure 25a). Transient ipRGCs (Cluster 3) responded well to photoreceptor mediated input (scotopic to mesopic) but were suppressed under daylight conditions (photopic), presumably because they undergo depolarization block[99]. This dichotomy in luminance signaling occurred under both green and UV wavelengths across similar irradiance levels (Figure 25b). Short presentations of blue light matching the peak for melanopsin (470nm), produced similar responses in both clusters until the luminance reached daylight conditions (>11 log) (Figure 25c-e). Long duration visual stimuli that lasted one minute also produced pronounced differences in spike output between each cluster (Figure 25f-h). Like the short duration stimuli, these differences were produced by melanopsin-dependent depolarization at photopic light intensities (Figure 25h,i), rather than photoreceptor inputs. Together these results demonstrate M1-like

ipRGCs can share the same rod, cone and intrinsic photosensitivity, but can differ in their encoded components of luminance. These differential responses are due to inherent factors effecting their melanopsin-dependent depolarization and result in separate functional subtypes.

4.4 – Discussion

Here, we performed Multi-electrode Array (MEA) recordings on dark-adapted retina and used 'Opto'Tagging to selectively identify a unique *Cre*-expressing subtype of ipRGCs (SON-ipRGCs) with known morphology and central innervation. We find their photoresponses are highly sensitive, sustained and homogeneous, encoding luminance from scotopic to photopic light intensities. Though the behavioral relevance of visual input to the SON is unknown, our results suggest that a broad range of environmental light is continually encoded and conveyed to this central region.

Our MEA approach provides several advantages over traditional single cell recordings of ipRGCs and was chosen for several reasons. First, the melanopsin protein can be directly activated by single and 2 photon light excitation, meaning that fluorescent targeting strategies can alter the physiological properties of ipRGCs[44,148]. A MEA approach allowed us to avoid unnecessary light exposure in dark-adapted retina. Second, the slow sustained response properties of ipRGCs are critical to their functional encoding of environmental light levels, temporal characteristics that necessitate long stable recordings. A MEA approach allowed

us to acquire scotopic, mesopic, photopic and intrinsic photoresponses from the same ipRGCs over an extended time course (3hrs). Third, lpRGCs are a diverse population that are particularly sensitive to illumination history, adapting to environmental luminance at the level of the cell (photoreceptor adaptation) and circuit (network adaptation)[147]. This makes comparisons of photoresponses in neighboring ipRGCs, using sequential single cell targeted recordings quite challenging to interpret. Our approach allowed us to record from numerous neighboring ipRGCs simultaneously responding to the same visual stimuli.

A disadvantage of the MEA technique in retina is the inability to confirm the identity of recorded cells. To address this we developed a strategy for localizing cells of interest using the optogenetic marker channelrhodopsin (ChR2), stimulated at the end of the recording under synaptic blockers ('Opto'Tagging). Similar approaches have been used to identify ChR2-expressing neurons *in vivo*[153,154]. This approach allowed physiologically relevant photoresponses to be acquired in individual ipRGCs before exposing the retina to synaptic blockers and the ChR2 'Opto'Tagging stimuli that was used to confirm their identity. We applied this paradigm to a recently described (Chapter 3) subpopulation of ipRGCs labeled in the *GlyT2^Cre* mouse line, that tile the dorsal retina, overlap with other morphologically similar ipRGCs and uniquely innervate the SON of the hypothalamus (SON-ipRGCs). With known morphology, retinal distribution, and central innervation, but unknown photo-responsive properties and functional characteristics, SON-ipRGCs in the *GlyT2^Cre* mouse were appealing targets for

101

'Opto'Tagging on the MEA. We chose to use ChR2 for 'Opto'Tagging because of its fast and repeatable response kinetics, initiating spiking at the millisecond timescale[87,155]. Conversely, the intrinsic responses mediated by melanopsin are slower, on the order of seconds, allowing 'Opto'Tagged cells to be temporally localized.

IpRGCs were identified on the MEA by their intrinsic photoresponses under synaptic blockade. Some ipRGCs are electrically connected to wide-field amacrine cells, which signal over long ranges in the retina through their spiking axons. Therefore, it's possible that melanopsin-mediated responses are passed through gap-junctions, inducing spiking of some displaced amacrine cells, and leading us to falsely identify them in MEA recordings as ipRGCs. However, these types of responses are heavily attenuated, more likely in degenerative retina[156], and are rarely encountered in other studies[157].

To organize our ipRGCs into functional groups, we performed sparse principle component analysis (sPCA) and unsupervised clustering[77,89] using intrinsic photoresponses. We fitted each potential clustering paradigm with Gaussian Mixture Models with expectation maximization (EM), and selected appropriate groupings using Bayesian information-theoretic criteria (BIC). This approach identified 8 functional subtypes of ipRGCs each with distinct differences in their sensitivity, response onset and duration of response, highlighting the diversity observed among the many established ipRGCs types. 'Opto'Tagged cells (SON-

ipRGCs) were primarily clustered into a single highly uniform group as expected of a true subtype.

Of the eight functional clusters of ipRGCs in the dorsal retina, our results indicate there are at least two distinct functional subtypes of highly sensitive ipRGCs. We presume these are M1 ipRGCs as they share M1-like features[46], including high intrinsic photosensitivity (half max response $\sim$ 12.2 log photons cm^{-2} s^{-1}) and short response latency ($\sim$ 2 sec), both signs of high melanopsin expression[58]. IpRGCs of Cluster 5 (SON-ipRGCs) responded with sustained photoresponses; Cluster 3 responded similarly until reaching daylight conditions (>11 log photons cm^{-2} s^{-1}), where responses become transient. The functional characteristics of these two groups appear to closely correspond to the unimodal and monotonic responses recorded from individual M1 ipRGCs[99]. M1 ipRGCs with unimodal spike responses increase their firing rates until they enter depolarization block such that increases in illumination beyond this point fail to elicit spikes. Conversely, monotonic M1 ipRGCs increase their spike rates to all increases in illumination. These two groups are similar to photosensitive Cluster 3 and Cluster 5 identified in our MEA recordings. Similarly, our results suggest that in the dorsal retina, SON-ipRGCs are monotonic and do not enter depolarization block, encoding luminance over all ranges from scotopic to photopic light intensities. Cluster 3, however, becomes quickly inactivated by light-mediated depolarization and is silent at brighter light intensities, suggesting these ipRGCs likely signal transitions in illumination, rather than illumination level.

The remaining clusters identified in our MEA recordings (Cluster 1,2,4,6,7,8) are likely associated with the non-M1 ipRGCs (M2-M6). After M1 ipRGCs, ON stratifying M2 and bistratified M3 ipRGCs have the second highest concentration of melanopsin, exhibiting intrinsic responses with gradual graded changes in firing rate and latency at increasing light intensities[46,48,58]. In our recordings, these types likely correspond to Clusters 2 and 7, as they share the next highest photosensitivity (response half max ~ 13 log photons cm^{-2} s^{-1}), and display a response delay (~5 sec & ~9 sec) and duration (~20 sec beyond illumination) similar to values reported from individual M2 and M3 ipRGC recordings[46,48,58]. Additionally, Cre-expressing ipRGCs with M2 and M3 morphology have been identified in the GlyT2Cre mouse through targeted Neurobiotin fills (Chapter 3). As some portion of 'Opto'Tagged cells recorded in the GlyT2Cre::Ai32 were associated with Cluster 2 (27%) and Cluster 7 (10%), it provides further evidence that these clusters are associated with M2 and M3 ipRGCs. Clusters 2 and 7 primarily differ in their firing during light exposure. Although it is possible that these two clusters reflect the morphological distinction established between M2 and M3 ipRGCs[6,59], targeted studies suggest M3 ipRGCs are rare, share many physiological characteristics of M2 ipRGCs, and probably represent an intermediary or partially differentiated M2 ipRGCs rather a separate subtype[48]. It is more likely that Clusters 2 and 7 represent two functionally distinct subtypes of M2 ipRGCs. This is consistent with studies that describe variability in the biophysical properties of M2 ipRGCs despite a shared morphology[71]. Indeed, our

Neurobiotin fills illustrate M2 ipRGCs are similar to SON-ipRGCs and form territorial mosaics (data not shown). Given the density of ON Cre-expressing ipRGCs in the dorsal retina, it suggests their coverage may exceed the coverage estimates for a single type, thus it is likely M2 ipRGCs also consist of multiple subtypes, like M1 ipRGCs.

M4, M5, and M6 ipRGCs express the lowest amount of melanopsin, requiring higher levels of light intensity at more extended durations to initiate photoresponses[45,46,56,58]. These types primarily rely on synaptic drive from rod and cone photoreceptors and project to image forming brain regions, similar to traditional RGCs[8,54,55,66]. The functional contribution of melanopsin signaling is believed to adjust excitability and contrast sensitivity in these image-forming types[45,158] using non-canonical signaling mechanisms[36,37]. In our recordings, Clusters 1,4,6, and 8 exhibited the lowest levels of intrinsic photosensitivity (response half max >13.5 log photons cm^{-2} s^{-1}), requiring extended illumination (latency > 15 sec) to initiate spiking responses, likely representing M4-6 ipRGCs. Interestingly, these clusters displayed 'bell shaped' response profiles, with a firing rate that would climb slowly even at high light intensities, similar to those observed in targeted recordings[46,56,58]. It is currently unclear if the shared shape of these responses is due to the lower melanopsin concentration or differences in signaling transduction, but our unbiased clustering approach suggests that they can be separated into four clusters (cluster 1,4,6, and 8) based on their intrinsic photosensitivity alone. Given that there are currently three types of highly

insensitive ipRGCs (M4, M5, and M6), it suggests perhaps one of these types can be subdivided further. Alternatively, the intrinsic photoresponses of M5 and M6 cells may not be strong enough to be detected in our recordings and the different functional groups might represent subtypes of M4s or combinations of the three subtypes. Further experiments to 'Opto'Tag these groups based on unique channelrhodopsin targeting strategies will shed further insight onto these questions.

Irradiance is the principal cue for synchronizing circadian regulation and gene expression[159]. This relies on photon counting during sustained levels of illumination and transitions in illumination, the latter of which might interrupt irradiance encoding. Sustained levels of illumination occur during the day and night with the most drastic of illumination transitions occurring at sunset and sunrise. Nocturnal foraging likely increases the probability that luminance encoding arises from reflected light off the ground, which is inverted by the lens onto the dorsal retina[160]. The two clusters of likely M1 ipRGCs in the dorsal retina presumably innervate the SCN, conveying different components of visual information. As the pattern of SCN input from SON-ipRGCs (SCN 'outer core') is distinct from that of other M1 ipRGCs that innervate the anatomical 'core,' (Chapter 3) it suggests that the SCN circuitry (1) requires at least two distinct forms of light information, and (2) that computation of retinal inputs are segregated to at least two localized areas of the SCN. Perhaps input to the SCN core is critical for light transitions from dark to light. This is consistent with

evidence that minutes of even dim light exposure is sufficient for circadian entrainment in rodent models[161]. Alternatively, computation at the 'outer core' of the SCN may be important for assessing some sustained component of environmental light. For example, animals exposed to different light intensities on a similar 12 hr cycle will entrain to the brighter of the two, establishing normal circadian rhythms. As encoding luminance across 7 orders of magnitude with a linear increase in spiking is inefficient, and does not occur, it is also possible that two independent populations of ipRGCs may be required to signal the entire range of luminance. In this model, the transient ipRGCs will signal a 'mode' of light intensity from scotopic, where they are functional to photopic, where they are inactivated. SON ipRGCs would then signal intensity gradients within each of these modes, allowing downstream areas to gather information about changes in luminance at specific times of the day.

'Opto'Tagged ipRGCs (Cluster 5) also represent the exclusive input to the SON (Chapter 3), which is a neuroendocrine control region where peptidergic neurons regulate a variety of physiological functions, such as parturition, lactation, osmotic balance, and satiety[162] through release of oxytocin and vasopressin from their axons in the posterior pituitary, and throughout the brain. Although SON neurons receive synaptic inputs from the retina[163], the functional role of this projection remains untested. Our results demonstrate that SON projecting ipRGCs deliver sustained environmental light information to SON neurons under most lighting conditions. This innervation might influence the functional release of

peptides in the pituitary, but might also influence oxytocin or vasopressin release directly. Therefore, SON-ipRGCs may underlie mechanisms of self-preservation, altering satiety, urination, and lactation behaviors upon exposure to changes in luminance.

4.5 – Future directions

In Chapter 3 I described a subpopulation of M1 ipRGCs that exhibit a mosaic distributed across the dorsal retina and innervate the SON. Mosaic distributions are a well-established feature of RGC subtypes but SON-ipRGCs represent the first example of a tiling distribution of ipRGCs (Chapter 3). SON-ipRGCs overlap with other M1 ipRGCs that presumably project to other central locations. These results suggest that the previously described overlap[5,69] of other ipRGCs may represent multiple subtypes yet to be separated. Future directions could address this by establishing distribution maps of cells organized by site of central projection. Retrograde AAVs driving fluorescent reporters injected into localized retinorecipient nuclei could be used to retro-label ipRGCs in the retina. Retinal maps, density recovery profiles and coverage analysis could be employed to identify the distribution of cells with shared innervation.

These approaches are particularly tractable for the study of the M2 ipRGCs. M2 ipRGCs are an ON-stratifying population, which express a moderate levels of melanopsin, suggesting that intrinsic photosensitivity is highly relevant to their function[6,45]. However, their central innervation and behavioral role in image or

non-image forming vision remains unclear. Targeted brain injections and mapping analysis of retrolabeled M2 ipRGCs in the retina would aid in establishing their organization. An increased density of M2 ipRGCs has also been observed in the dorsal retina[70], suggesting that M2 ipRGCs may also contain a localized subtype, similar to SON-ipRGCs. As evidence suggests that M2 ipRGCs may project to the superior colliculus (SC), olivary pretectal nucleus (OPN), and dorso-lateral geniculate nucleus (dLGN)[45], these locations might serve as appropriate sites for initial tracing experiments.

In Chapter 4 we identified that ipRGCs can be functionally organized by their intrinsic photoresponses and that a localized subtype of ipRGCs innervating the SON share similar light encoding capacity. However, ipRGCs innervate more than 17 distinct areas in the brain[7,8] and the light encoding capacity of ipRGCs that project to these other regions remain unknown. Future directions using the OptoTagging strategy on the MEA could be expanded to study other ipRGC subtypes with distinct patterns of central innervation. These experiments could be executed by performing retrograde AAV-ChR2 central injections at an ipRGC recipient nuclei of interest. Photoresponses of ipRGCs with a shared site of projection could then be localized on the MEA using the OptoTagging strategy described in this chapter. A functional description of ipRGC light encoding organized by their sites of central innervation would provide insight into how ipRGCs influence specific photo-dependent behavioral functions.

There are currently 6 morphologically distinct types of ipRGCs described in the rodent retina[45]. We identify 8 functionally distinct subtypes of ipRGCs based on unbiased clustering of their intrinsic photoresponses. Future experiments could determine how functional organization relates to the previously established ipRGC types (M1-6). This could be addressed by performing targeted single cell recordings under synaptic blockers with concurrent dye fills. Photoresponses to a small number of visual stimuli from ipRGCs with known morphology could then be compared to the organized clusters previously obtained on the MEA. One pertinent question is whether ipRGCs with very little melanopsin expression (M5 and M6) elicit an intrinsic photoresponse and can be identified in our MEA recordings.

CHAPTER 5: CLINICAL SIGNIFICANCE OF ipRGCs AND NON-IMAGE
FORMING VISION

*An extended discussion

5.1 – Chapter preface

Many aspects of biology are rhythmic and display daily oscillations in physiology and behavior. Light responses generated in the ipRGCs serve as the body's main biochemical synchronizer, entraining the body's hormonal and neuronal modulators to a 24hr day night cycle. IpRGCs are therefore important in health maintenance and interruptions to these signals can cause dysregulation in the timekeeping of many biological processes. Unfortunately, industrial and technological changes to modern society have led to an overexposure of artificial lighting, underexposure to natural sunlight, and a chronic disconnect in circadian day-night cycles in both adults and children[164]. This can lead to imbalances in sleep and hormonal control, resulting in an increased risk of certain types of cancer, immunosuppression, metabolic disease, and both psychiatric and behavioral disorders[165-168]. Additionally, eye diseases associated with retinal degeneration can directly alter light sensation, leading to similar downstream sequelae. This chapter will serve as a broader discussion of ipRGC function and their clinical significance; tying together experimental animal studies, ecological reports, and public health outcomes. It will begin with the physiological relevance of light in non-image forming vision (5.2), then discuss the health implications of modern light exposure (5.3), ending with a description of ipRGC dysfunction during retinal disease (5.4).

5.2 - The significance of light

Daylight is emitted from the sun as electromagnetic radiation and is altered significantly on its journey to the eye. The atmosphere reflects, filters, and polarizes the light. Weather and geographic location additionally alter the spectrum and irradiance, producing changes in color, brightness and direction of these emitted waves[169]. This diverse energy is captured by the rod and cone photoreceptor cells of the retina and converted to electrical signals that encode our visual world. Additionally, light is also captured by intrinsically photosensitive retinal ganglion cells (ipRGCs), the small population of melanopsin expressing[5] luminance detectors that primarily project to non-image forming brain regions[45,65,94], influencing many subconscious biological processes[4,9,10,72,95].

One direct site of ipRGC innervation is the suprachiasmatic nucleus (SCN) of the hypothalamus, the body's main circadian clock[164]. Oscillatory activity in the SCN functions as a timing circuit, predicting physiological and behavioral needs throughout the day and night[144]. This biological metronome is electrically silent at night but begins cycling near dawn, establishing a steady pace throughout the day[170]. Light encoded by ipRGCs entrains the SCN to the day-night cycle, altering the phase of clock genes and readjusting biological patterns to the external environment. Photo-entrained rhythms are then communicated from the SCN to other central brain areas and peripheral organ systems[171] using a variety of direct and indirect mechanisms[41]. This hierarchical structure allows ipRGCs to influence the oscillators active in nearly every cell in the body. To narrow the

scope, this discussion will center round a few interesting physiological examples that emphasize the diverse effects of light exposure.

Desynchronizing effects of light exposure – jet lag

Although the SCN projects to many diverse areas throughout the brain, ipRGCs are the only form of light input for the circadian system[8]. In laboratory animals, ablation of all ipRGCs has minimal effects on image forming vision but results in the inability to shift circadian rhythms to changing environmental light[172]. This phenotype is called 'free running', as the activity levels, without encoded luminance cues, no longer adhere to a 24hr period but reflect the endogenous period of the circadian clock. Alternatively, an over abundance of luminance cues can also alter circadian function. Even brief exposure to periods of light during the night ('skeleton photo period') is enough to shift wild-type mice to an altered pattern of sleep and activity[173]. Modern humans artificially achieve similar results during travel across time zones. Since the expansion of air travel, the experience of jet lag, also called desynchronosis[174] is a common occurrence but can have sinister consequences[175].

The feeling of fatigue, irritability, and anxiety that occurs when crossing time zones is primarily attributed to an acute disconnect between the body's internal clock and one's environmental expectations[176-178]. Additionally, the host of secondary clocks that rely on coordinated SCN signaling are desynchronized from each other, resulting in irregular and inappropriately timed activity[179].

Thankfully, this is typically transient and alleviated over a couple of days with light-dependent realignment of our circadian rhythm. Evidence suggest that it takes ~1 day of recovering per time zone crossed,[180] but this can exceed a week following international travel. Treatments for jetlag often focus on addressing the symptoms, such as insomnia or daytime sleepiness, rather than the underlying misalignment. Inducing sleep with medication or arousal using caffeine are frequent "tricks" that are often timed incorrectly, worsening symptoms in the recovering traveler[179]. Interestingly, patients often describe going to bed early or late (following western or eastern travel) in order to ameliorate jet lag. Reducing sleep debt is no doubt beneficial, but the success of this behavior is more likely due to the limited physical activity and light exposure of the sleep process, rather than a resetting of the circadian clock[179]. Its likely that similar results could be achieved by sitting quietly in a dark room, though this phenomenon has yet to be assessed. Indeed, studies show that the most effective treatment for jet lag is to re-entrain the sleep-wake cycle prior to traveling, using gradual and appropriately timed bright light exposure, activating the ipRGCs of the retino-hypothalamic tract (RHT).

But what happens in individuals under chronic misalignment? Studies of flight attendants, cabin crews, and frequent international business travelers with frequent jet lag report changes in sleep-wake, long-term deficits in cognitive function and irregularities in circadian related hormones such as cortisol and melatonin[176,181-184]. One study published before the discovery of ipRGCs found

that frequent flyers had higher rates of insurance claims for psychological issues, with the quantity of claims being correlated with the number of flights[185]. Observational reports such as these were convincing enough for the Federal Aviation Administration (FFA) to limit the number of international flights, back-to-back shifts, and time zone crossings per week for American flight attendants beginning in the 90s[186]. However, professionals, at least before the COVID pandemic, have continued to cross time zones frequently, with 30% of corporate travelers flying once per month and 5% flying 20-40 times per year[187]. The biological effects of these career long readjustments are still being addressed, but, unsurprisingly, laboratory animals with chronic asynchrony have numerous cognitive impairments[188,189] and associated brain atrophy[190]. These findings together emphasize the need for more practical methods of circadian realignment as well as a reassessment of healthy travel practices.

Central effects of light exposure – melatonin

As discussed above, photo-entrained rhythms extend beyond the SCN, communicated to other central and peripheral systems via neuronal or hormonal signaling[191]. The literature on secondary sites of photic influence is vast, but one area of particular importance is the light mediated control of melatonin production in the pineal gland[192].

SCN activity stimulates the continued production of melatonin, which builds up in the bloodstream during the afternoon and evening, inducing sleep onset when

appropriate thresholds are reached (sleep gating)[193,194]. Interestingly, light exposure reduces the circulating levels of melatonin (and its synthesis) and is strongly associated with ipRGC function[195,196]. Indeed, melatonin suppression is especially sensitive to the short wavelength range of the color spectrum[195], equivalent to the sensitivity range of the melanopsin protein. Although the biochemical mechanisms remains unclear, light mediated melatonin suppression is partially responsible for sleep disturbances following late night light exposure[197] and is the impetus behind the avoidance of blue emitting LED computer and phone screens before bed. Recently, the avoidance of these wavelengths has reached public awareness, due to the advertising campaigns and commercial success of "blue blocking" glasses. Although an appreciated service announcement and profitable industry, there is little scientific evidence that these products reduce eye fatigue, improve sleep patterns, or impact any vision related metric[198].

The synaptic pathway from retina to SCN to pineal gland is often called the photo-neuro-endocrine system. This broad nomenclature is appropriate as melatonin not only acts peripherally as an endogenous hormone but also acts as a surrogate agent, indirectly communicating environmental light levels to other neuroendocrine structures, including the hypothalamic pituitary axis (HP-axis)[199]. Studies have emphasized this relationship by showing that light exposure in mice activates the adrenal cortex, stimulating gene transcription and glucocorticoid release[191,200]. All animal species, including humans, have diurnal and nocturnal

fluctuations in HP axis-related signaling molecules such as cortisol, testosterone, estradiol, and thyroid stimulating hormone[201]. As these hormones are critical for the predictable timing of arousal, hunger, sex and reproductive efforts, the light mediated titration of melatonin concentrations entrains the neuroendocrine circuits, catering to the precise time dependent needs of these behaviors[202-206]. For instance, the well-timed circadian rise of circulating cortisol levels in the early mornings activates a waking response, increasing blood pressure in preparation for rising from bed[207]. Anyone who has experienced dizziness and nausea upon rising uncharacteristically early can appreciate the importance of these anticipatory mechanisms and our reliance on the photo-entrainment of autonomic functions.

Peripheral effects of light exposure – metabolism

Unsurprisingly, oscillatory changes in systemic hormones can have effects on peripheral organ systems. Given the obesity epidemic, circadian regulation of metabolic function has been an area of exceptional research effort. Clocks regulate rhythmic feeding, which synchronizes circadian and metabolic utilities[208]. Digestive hormones such as ghrelin, insulin, and glucagon, exhibit predictable secretions in line with environmental light levels and in anticipation of food consumption[209,210]. The SCN also increases insulin sensitivity and glucose storage in muscle,[211,212] preparing the body for athletic activities such as hunting. Similarly, the liver has "dusk and dawn peaks" in gene transcription where glucose transporters, glucagon receptors, and enzymes that regulate the

metabolism of complex sugars, are elevated in response to central pacemaker activity[213]; a process of energy management necessary for fasting periods in-between meals. Although feeding behavior is considered an additional environmental stimulus for entrainment, these effects have been well segregated and it remains clear that light is still the dominant external source required for appropriate metabolic alignment[212,214].

As chronic metabolic dysfunction is the cause of many medical disorders, such as diabetes, the influence of irregular light exposure on energy regulation has also been extensively examined. Unsurprisingly, constant long-term light exposure in laboratory animals identified overt changes in metabolism[215], no doubt confounded by sleep deprivation and stress. However, a more relevant follow-up found that slightly prolonged daily light exposure (16 hrs rather than 12 hrs) led to increased fat mass without a change in food consumption or exercise[215]. Additionally, animals exposed to dim light at night (12hrs day light: 12 hrs dim light), compared to control animals on a normal light-dark schedule (12hrs Light: 12 hrs Dark), consumed similar amounts of food but had increased weight gain, glucose intolerance, and epididymal fat[216] (a metabolically active fat deposit around the testis of males used to study adiposity). These and other studies highlight the importance of light exposure on metabolism and drew global attention from health, ecological, and occupational experts regarding the rise in artificial lighting.

Seasonal effects of light exposure – psychological disorders

Though ipRGCs can sense the presence or absence of light, their interaction with circadian systems is far from binary and extends beyond the 24hr cycle. The variability in spectrum, intensity, and timing of the light input, although not thoroughly worked out, provides important ecological information, triggering changes in seasonal behaviors and preparing the body for the environmental transitions critical for survival. For example, many species have seasonal alterations in both feeding[217-219] and reproductive activities[220], the annual molting of bird feathers is tied to the gradual changes in length of day light[221], and photo-exposure can influence the sleep of patterns hibernating mammals[222]. It appears that the rate of light change during light transitions at dusk can be especially important for many of these seasonal effects[169]. As ipRGCs receive cone input driven by short, medium, and long wavelength opsins, in addition to their intrinsic photosensitivity (~480nm)[223], its likely that color differences are integral to the circadian response[159,223-225]. Indeed, some types of ipRGCs encode differences in opposing colors[55] and information mediated exclusively by cone photoreceptors is sufficient to stimulate the SCN in mice[226,227]. These results together suggest that light sensation is an important regulator of both long and short-term behavioral function, on both daily and annual time scales. The seasonal effects of light on humans are understudied, but aspects of climate change and urbanization has resulted in an increase in time spent indoors, away from natural light sources. The consequences of these changes contribute to the

continued rise in season related psychological disorders among metropolitan communities[228-230].

Light information to the circadian system is strongly associated with many cognitive functions in both animals and humans[175], and intimately involved in many mental disorders[231]. However, exciting recent studies have shown that in addition to the SCN-dependent effects on learning and memory, ipRGCs have direct SCN-independent, light mediated alterations on mood[95]. IpRGCs project to areas of the perihabenular nucleus (PHb), a location closely associated with monoamine synthesis, such as serotonin, and involved in mood, motivation, and stress. Elegant work in animal models with developmental loss of the PHb projecting ipRGCs (Brn3b+) but retained ipRGC input to the SCN (Brn3b-), exhibited normal circadian rhythms, but suppressed motivation and enhanced depression like symptoms[95]. Although behavioral measures of mood in animals are difficult to extrapolate, fMRI studies have shown that the human habenula is also responsive to changes in environmental luminance[232,233], suggesting either direct or indirect visual input.

These experimental findings are also consistent with the mood-enhancing effects of light in human disease. The daily presence of natural sunlight in patient rooms is correlated with reduced lengths of hospital stays among those admitted for depression[234] or bipolar disorder[235]. Furthermore, seasonal effective disorder (SAD), a common mood disorder preferentially affecting individuals in northern

latitudes during the darker winder season, are frequently treated with specifically timed light exposure[236]. 'Bright light therapy' mitigates symptoms within a few days and is now considered first line treatment for SAD[237]. Phototherapy is also a common clinical intervention for both refractive depression and gender-related mood disorders, and is easily combined with pharmaceutical therapies[233]. In patients treated for SAD, blue shifted light provided superior results over red-shifted light, consistent with the spectral sensitivity of the melanopsin protein[238] and strengthening the evidence for direct ipRGC influence over aspects of psychological wellbeing.

Concluding thoughts

The light dependence of jet lag, melatonin suppression, metabolism, and mood discussed above, represent only a fraction of physiological changes performed by our circadian oscillators. Still, they highlight the tremendous progress made in our understating of (both direct and indirect) ipRGC influence over homeostasis. The discovery that the molecular timekeeping of SCN neurons are also found in many tissues throughout the body has drastically revised the importance of photoentrainmnet[171]. The broad integration of SCN output allows light signals encoded by ipRGCs to be distributed throughout the body, expanding the role of vision far beyond that of image forming. Additionally, discoveries of ipRGCs influencing other behaviors via SCN-independent mechanisms, such as those associated with mood, predict that these retinal cells are more than a circadian accessary. Given the substantial number of other central projections with

unknown visual significance (Chapter 3), it suggests that our understanding of ipRGC function is only just beginning.

5.3 – Light in the modern era

Clearly, light exposure is important for health maintenance and interruptions can cause dysregulation of the body's delicate homeostasis. Unfortunately, industrial and technological changes to modern society has lead to a chronic disconnect between circadian and perceived day-night cycles in a large portion of the population[239,240]. These changes poise our planet for a medical and ecological disaster. Three areas of particular importance, discussed below, are outdoor light exposure, indoor light exposure, and irregular work schedules.

Outdoor light exposure

With expansive urbanization, construction, and transportation comes the reliance on artificial lighting. Anyone who has unknowingly driven on the freeway with a broken headlight or easily navigated the city streets after sunset can appreciate the abundant sources of light that radiate from our homes, roadways, restaurants and shops. Most of these lighting sources are on all night, contributing to a growing level of light pollution and general brightening of the evening sky[241]. In the United States more than ¾ of the population experience artificial lighting at night that is brighter than the light from a full moon[166,241]. As the moon waxes once a month, this means that many individuals don't experience full darkness and are, instead, chronically light exposed. Since 2001, a light pollution

awareness group has provided a database for measuring the worlds artificial brightening using satellite data[241]. A shocking calculation from these mappings determined that ~15% of the world's population and ~40% of the United States experience levels so bright that they no longer use/need their rod derived "night vision", but instead rely on cone derived "day vision," even when observing the night sky. As a result, only a portion of the US population can still appreciate the constellation of stars that make up our solar system[242]. Though the experience of chronic light exposure has been trivialized, the health consequences remain apparent. Increased rates of certain cancers, metabolic and psychiatric disorders, immune complications and heart disease in both humans and laboratory animals[243] are consistently and irrefutably associated with living on a perpetually illuminated planet.

Indoor light exposure

Artificial lighting has also found its way into the home, with bedrooms, appliances, and communal indoor spaces being lit by incandescent sources. This not only directly increases environmental light levels but can also disturb sleep, leading to waking events and further nightly exposure[244]. Light effects can also be heightened among vulnerable populations. For instance, the perpetual night lighting in hospital settings and intensive care units, measured at levels equivalent to overcast day light, means that ill patients receive very few natural circadian cues, likely jeopardizing their recovery[245]. The most common in-patient complaint is difficulty sleeping[246] and the well established abnormalities in sleep

architecture among hospitalized patients predict additional comorbidity[247]. Given the circadian involvement in mood regulation[248], it is possible that lighting conditions contribute to the increased episodes of psychosis[249], nocturnal delirium[250], and depression[251] in hospitalized patients.

Another contributing issue is the rise of electronic devices used for work, communication, and entertainment. The bright glow of cell phones, tablets, computers and wall-sized televisions is inescapable and their perpetual use, day and night, drives us to spend more time indoors, away from natural light sources. One highly referenced study found that reading a book off an E-reader before bed had alterations in almost every measurement of sleep architecture, including the suppression of the sleep inducing and neuroendocrine regulating hormone, melatonin (Chapter 5.2)[240]. The concerning wide spread use of portable electronic devices among children, adolescents, and even toddlers has also resulted in sleep disturbances. Though controlled research in this demographic is difficult to achieve, the rise in developmental issues, rates of obesity, anxiety, depression and poorer performance in school, has been linked to these changes in sleep[252]. As an additional point, early smart device exposure is also associated with increased rates of pediatric myopia[253], a progressive issue of the developing eye. Although, the mechanisms are unclear, the retina dopamine levels responsible for regulating pediatric eye growth are photosensitive[254] and likely controlled by ipRGC intra-retinal communication with dopaminergic amacrine

cells[255,256]. Surprisingly, natural light exposure achieved through daily play outside reduced myopia in children;[257] proof that not all light sources are equal.

The photometric qualities of artificial lighting are indeed radically different from the broad diverse irradiance emitted or reflected from natural sources. Modern, high efficiency, low cost, and easily fabricated lamps and diodes used in modern electronics and photo-emitting devices generate extremely bright light with narrow irradiance spectrum, exposing our eyes to more illumination, by any measure, than any other time in history. Worse, the limited spectrum of artificial light is shifted towards the blue wavelengths, overlapping with the excitation of the photosensitive melanopsin protein in ipRGCs. These effects are well documented by examining the levels of melatonin in the blood stream after various light exposures. Even indoor light levels can inhibit melatonin and theoretical models on sleep induction predict that it takes 40 min of incandescent light from a modern bulb to reduce circulating melatonin levels by half but only 13 min of LED exposure from an electronic screen at an equivalent light intensity[258]. These common exposures drive a further disconnect between the environmental and circadian day night cycles, representing one of many assaults to our biological timekeeping.

Work schedules

In addition to increased light exposure from modern technology and atmospheric glow from excessive light pollution, capitalism has ushered in a change in

societal work standards across the globe. Each year a greater proportion of employees are required to participate in 'shift work' or to work during non-standard hours (outside 9am-5pm). This is motivated by increased demand for 24hr services, fast delivery, and market competition. Goods shortages, limited employees, and substantial industry profits maintain these practices. Between 15-30% of full time personnel work alternative shifts, night shifts, or early morning shifts[259-262]. Ignoring the abundant evidence concerning the occupational safety and productivity of night shift workers[263], these practices also lead to a discrepancy between biological and environment time keeping[166]. Insomnia and increased rates of cardiovascular disease, breast cancer and prostate cancer are highly prevalent[264]. Shift work is also inconsistent in its scheduling, often requiring some standard and non-standard shifts throughout the week, placing extra pressure on the body's circadian system to constantly re-localize to an ever-changing day.

Individuals with "shift work disorder" represent a cautionary predictor of what wide spread nightly light exposure can lead to. As a result, research efforts have justifiably focused on the health consequences of these overtly extreme practices. However, a far larger portion of the population participates in another, more voluntary, and seemingly benign form of circadian shifting called "social jet lag". Unlike the time zone crossing of travel related jet lag, social jet lag describes the drastic shift in sleep wake patterns seen on unregimented days throughout the week[175]. Indeed, obligations of daycare, school, and work

practices typically maintain a predictable schedule during week days[265], no doubt enforced by alarm clocks. However, recreational or social events on weekends can cause drastic changes in the duration and timing of sleep. Sleep studies on teenagers reported receiving an average of ~2 hours less sleep per day[265], during a developmental period when they need it most. Additionally a large-scale epidemiological study found that the frequent disparity between internal and social clocks leads to metabolic changes (increased BMI), contributing to the current obesity epidemic[266]. Obviously, studies on the circadian disruptions of social jet lag are challenging given its ubiquity. Diversity in individual's personal timing preferences for sleep and activity (called Chronotype)[267] also complicates these discussions. At the very least, the relevance of daylight savings, early school schedules, pre-dawn athletics practices, and rigid timing of work programs should be readdressed.

Concluding thoughts

Together, the information discussed in this section underlines the importance of light exposure within modern society and contextualizes the relevance of chronobiology research in medicine and public health. Findings like those presented above can be used to make necessary health centric changes in ecological policy, technological development, and occupational practices. For instance, the disrupting effects of light exposure at night has inspired the design of new smart light sources with wavelength emission and dimming capacities that are adaptive to time of day, reducing light pollution and its circadian

consequences[268]. Studies of the acute effects of light exposure in health care settings are being acted upon hastily by hospital systems that are passionate about improving patient outcomes[269]. And lastly, the consequences of chronic night shift work are debilitating, but emerging research under long-term follow up suggests that some systemic changes are time dependent and reversible[270], placing extra incentive on advocacy for work place reform. Many of the health related consequences of irregular light exposure are mediated by sleep and endocrine disruption. Future research should focus on the crosstalk between circadian entrainment and hormone regulation under physiologically relevant lighting conditions. The benefits of artificial lighting as a therapeutic intervention for depression management are well established. A more thorough understanding of these mechanisms may be employed in the future to combat a wider variety of disorders using timed, spectrally, and intensity appropriate light exposure.

5.4 – Retinal degeneration and non-image forming vision

IpRGCs are an integral part of maintaining appropriate circadian and homeostatic functions. As discussed above, changes in light exposure captured by ipRGCs can alter physical and mental health (Chapter 5.2 & 5.3). However, damage of the nervous system can also affect the ability of ipRGCs to encode surrounding light, preventing proper entrainment, sleep and endocrine control. For instance, derangements in circadian rhythms have been observed in aging, retinal degeneration, and brain disease[271]. These associations can be difficult to

exclusively attribute to the retina as many degenerative pathologies are syndromic, and have comorbidities that exhibit complex interconnected symptoms. Still, the damage or loss of RGCs, ipRGCs, or the other cells of the retinal circuit, in both age-related and inherited retinal diseases, can contribute to a patient's aggregate health problems. In the visually impaired, reduced image forming vision is already a sizable burden, but alterations in non-image forming vision can further erode their quality of life. Thankfully, new areas of study are now focusing on morphological, physiological, and behavioral changes to ipRGCs in the setting of retinal degeneration. This exciting but still emerging field has focused on the effects of aging as well as inner and out retinal diseases. In the next decade, this field will change how clinicians manage and treat the resulting systemic effects of long-term retinal disease.
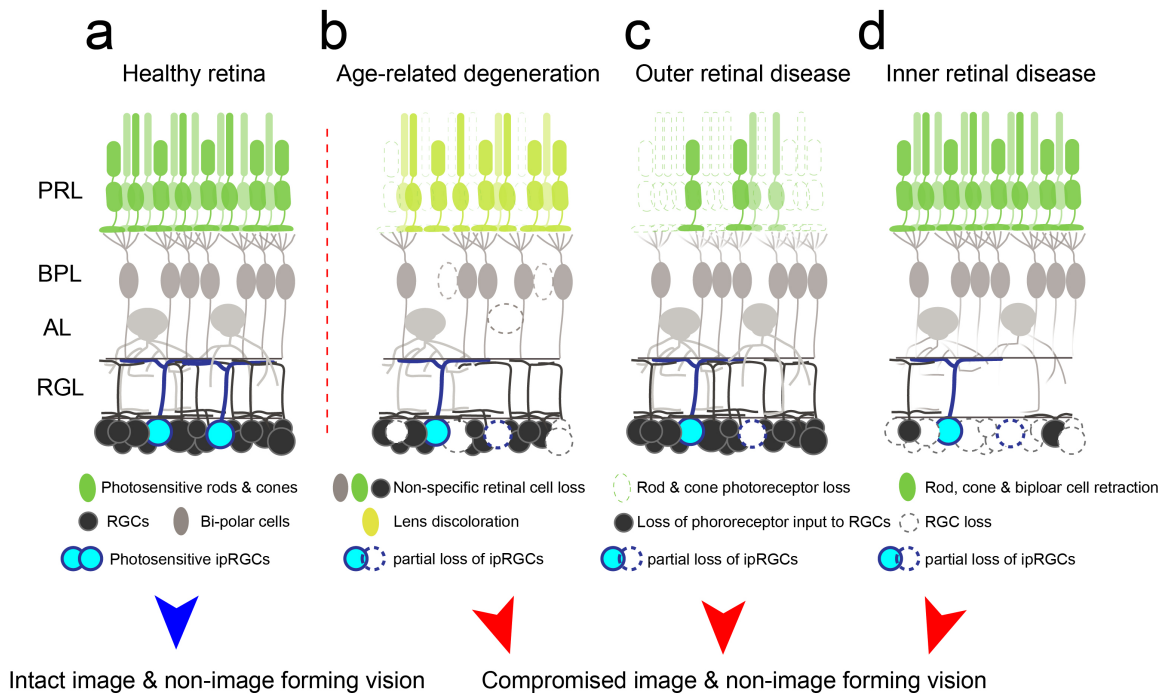
Figure 26: Illustration of retinal circuitry during degeneration

Diagram of the healthy retina (a) and degenerative retina caused by aging (b), outer retinal disease (c) and inner retinal disease. Retinal diseases lead to non-specific or specific retinal cell death, compromising image and non-image forming vision. Retinal layers denoted as Photoreceptor layer (PRL), Bipolar layer (BPL), Amacrine cell layer (AL) & retinal ganglion layer (RGL)

Aging effects on ipRGCs

During the normal aging process, neurons experience oxidative stress, acquire DNA damage, and develop energy imbalances[272]. Like all cells, neurons vary in the extent of protection employed against these age-related forms of assault. Therefore, vulnerability can alter the response properties, synaptic strength and overall survival of damaged neurons. The nervous system is a series of complex networks, and cells that are lost can compromise this circuitry (Figure 26b), leading to pathological consequences. In the retina, RGCs are lost with age[273,274], resulting in progressive deterioration of vision. Patients over 75 years report greater difficulty reading, driving at night, and matching wardrobe colors visual changes mitigated by the employment of brighter light, higher contrast and more frequent trips to their ophthalmologist. In humans, neuronal deterioration from aging can be separated from other age-related eye changes (cataracts, presbyopia, dry eyes, etc) using clinical exam findings. However, the distinction between aging of the retina and age related retinal diseases (Age related macular degeneration) are so intertwined that discriminating between them is often arbitrary, and will not be made for this discussion.

Longitudinal studies in otherwise healthy rodents show gradual loss of photosensitivity, eletroretinogram (ERG) responses[275,276], and visual acuity[277]

with age. Though non-imaging forming vision has rarely been the field's primary focus, changes in melanopsin positive ipRGCs have been studied along side general retinal cell loss. Interestingly, ipRGC density in rats remains stable until 1.5 years of age, then experiences a precipitous decline, with ~50% loss of melanopsin positive cells at 2 years of age[271,278]. Correlating with these findings, animals also experience an age-dependent decrease in activity, body temperature, and circadian rhythm[278]; all elements associated with ipRGC regulation. Additionally, aged rats (2+ years) subjected to phase advancing conditions, where the light cycles are shifted by 6 hours to mimic jet lag, experienced increased insulin insensitivity and higher mortality than younger animals[279]. These results predict that even partial loss of ipRGCs may be behaviorally and pathologically relevant.

Similar to rodents, ipRGC density in human retina remains relatively stable until the age of 70, then drops significantly (loss of ~35-50% of ipRGCs) by 81 years of age[271,280]. Careful morphological study of human ipRGCs has also demonstrated that the dendritic complexity and synaptic input of individual cells recedes in advanced age[280], suggesting that even the remaining ipRGCs may not be functioning properly. At the population level, these changes result in a greatly sparsified mesh of ipRGCs with minimal dendritic overlap and large areas of retinal space devoid of melanopsin expressing dendrites[280]; a quantity and distribution that is concerning for adequate photon capture.

Logically, reduced sensitivity to environmental light can alter light dependent behaviors. Indeed, circadian related changes in the aging population are a well-established phenomenon[281]. A study of light transmittance in the ageing eye calculated that a 75-year-old requires six times more light exposure than a 10 year old to achieve a similar circadian effect[282]. Reported impairment in the regulation of rhythmic and oscillatory strength in older adults (60+) also results in less sleep, impaired ability to accommodate ('phase shift') to changes in light and dark, and increased episodes of insomnia compared to younger adults[283-285]. The stereotypic notion that grandparents are "early birds" also carries scientific merit. Changes in sleep architecture results in the elderly falling asleep earlier, waking up earlier, and experiencing a morning shift in performance on learning and memory tasks[286]. The time dependent improvements in cognitive performance (a component of Chronotype) is a pattern younger adults typically experience later in the day, aided by the wakeful exposure of brighter daylight[281].

The contribution of retinal degeneration in these age related behavioral changes is unclear. Its likely that central circuitry at the level of the SCN also undergoes age-related alterations. Unfortunately, direct experimental evidence of light's involvement is minimal and has come from studies where transcription of specific photo-induced SCN genes are reduced in aged animal models[287]. Even this example, identifies two hypotheses; either an age dependent reduction in ipRGC signals that reach the SCN (ie: fewer functional ipRGCs), or the SCN experiences an age-dependent change in sensitivity to light input from the

retina[281]. There is evidence for both, but little is know about how ipRGC signals are integrated in the brain, even in healthy models, making these lines of investigation challenging. Excitingly, the recent development of implantable devices with high-density electrodes is poised to make *in vivo* recordings of natural behaviors more tractable[288], and will likely be appealing methods for addressing the relay of encoded sensory information (such as light) to recipient regions.

Given our current tools, the multifactorial relationship between aging, the eye, and circadian change is complicated to isolate and interrogate. Given the importance of photo-entrainment on proper central and peripheral synchrony, additional eye-related factors unrelated to retina health could be contributory in elderly patients. One factor worth considering is the transmission of light before it reaches the retina. Light entering the eye is refracted through the lens, aiding in fine image focus and filtering of the sun's harmful UV energy. The extended exposure during the aging process causes lens crystallins to interact with neighboring UV sensitive compounds[289], results in a yellowing of the lens and slow development of a cataract (Figure 26b - yellow). These changes selectively block short wavelength light (blue-shifted), preferentially reducing the irradiance spectrum absorbed by the melanopsin protein in ipRGCs. The degree of lens discoloration and opacity is correlated with increased sleep disturbances[290] and interestingly, melatonin, the sleep induction hormone, appears to be protective against the initial cataract formation[291]. However, clinical studies on surgery

candidates following cataract removal and replacement with neutral intraocular lenses (IOLs) have shown mixed circadian and sleep-related improvement[292], predicting that other factors are at play. Another age-related consideration is the difference in natural light exposure. Adults of advanced age are, on average, more sedentary[293,294] and can be bed ridden or confined to assisted living homes. This can limit the amount of total outdoor light exposure in comparison to younger, autonomous, and active adults. Though this is a logical argument, I can find no scientific evidence of older adults receiving less light exposure. Still, given the extremely high rate of vitamin D deficiency among the frail and hospitalized elderly,[295,296] we can safely assume that the health benefits of natural light exposure in aging adults is worth prioritizing.

Outer retinal disease and effects on ipRGCs

Retinal diseases can be genetically inherited, spontaneously acquired, or be secondary sequelae of central (Huntington's disease) or peripheral disease (diabetic retinopathy). Outer retinal degenerations (Figure 26c) are a family of diseases including retinitis pigmentosa (RP), which are characterized by a progressive loss of rod and cone photoreceptors. RP effects close to 1 million individuals world wide and is associated with severe visual loss, beginning as early as childhood (testing signs seen at age 6), and can be caused by more than 45 distinct gene mutations[297]. Though the mechanisms of these diseases differ, the loss of photoreceptors in the outer retina leads to subsequent degeneration of the inner retina, including RGCs[298]. These secondary changes

can be caused by synaptic reorganization, a decrease in coherent signaling input, and strangulation of axons from displaced vessels[298]. IpRGCs are also compromised, with a declining number of melanopsin positive cells in late stages of RP models correlating with changes in circadian rhythm[271,278]. Surprisingly, the deterioration of ipRGCs during RP progression is protracted relative to other neighboring retinal cells. Though the mechanism is unclear (and discussed later), injury resistance of ipRGCs in outer retinal disease prompts two important considerations. (1) During disease progression, there is a sizable window of opportunity for clinical treatment, maintenance, and neuro-protection of remaining ipRGCs. Therefore, research development should prioritize these avenues. Many gene therapies, photochemicals and ocular prosthetics are currently in development with the aim of restoring vision in patients with early or late RP [299]. It remains unknown if these approaches may have a stabilizing effect on ipRGCs or are compatible with non-image forming vision, but present interesting research areas that are worth exploring. Injury resistance also suggests (2) that even in late stages of photoreceptor loss, where patients are functionally blind, ipRGCs and their biological influence still persists. This emphasizes the importance of continued eye care, symptom management and retina treatment, long after blindness, insuring that the photo-entraining features of circadian regulation are maintained as long as possible.

Most ipRGCs also receive sizable synaptic input from rod and cone photoreceptors, in addition to their intrinsic photosensitivity[59]. Presumably, in

diseases of the outer retina, this synaptic input is preferentially lost, leaving ipRGCs to rely exclusively on their melanopsin driven responses. The functional relevance of rod/cone and melanopsin photoresponse integration in ipRGCs of either healthy or diseased retina is an unknown feature. However, their individual contributions have been explored in the context of one non-image forming behavior, the pupillary light reflex (PLR).

Light mediated constriction of the pupil is controlled by a relay circuit beginning at the olivary pretectal nucleus (OPN), a site of direct ipRGC and RGC input[8]. Experiments in rod-less, cone-less mice (*rd/rd*) observed slow and incomplete constriction of the pupil upon light exposure[300]. On the other hand, melanopsin knockout mice with intact outer retinal photoreceptors exhibited fast constriction that waned at bright light intensities[63], consistent with the sensitivity and kinetics of the melanopsin protein. Since initial discoveries, confirmatory studies of the individual photoreceptive components of the PLR have also been isolated in the human retina using the unique spectral and temporal properties of the opsins[159,301,302]. In 2017, a study of patients with severe photoreceptor blindness (Leber Congenital Amaurosis) reported no pupillary light reflex under brief light exposures, but a respectable constriction in most patients (18/21 patients) during extended light exposures (~3 sec delay, normal = ~100ms)[303]. These results suggest that the melanopsin component of remaining ipRGCs in patients with outer retinal disease is likely sufficient for controlling some non-image forming functions under bright outdoor light. It also suggests that the pupillary light reflex

137

under specific lighting conditions could be used as a "surrogate marker" to access early presence of disease or to determine the remaining function of ipRGCs in progressing patients[303]. It may even be a clinical measurement helpful in determining if circadian entrainment should be managed pharmacologically[304].

Inner retinal disease and effects on ipRGCs

Disease of the inner retina primarily consists of glaucoma as well as more global forms of neurodegenerative disease. Glaucoma is a family of optic neuropathies characterized by a progressive loss of RGCs and effects ~70 million individuals worldwide, 10% of who are bilaterally blind[305,306]. Clinically, this degeneration results in distinct changes in the appearance of the optic disc (nerve head) under exam, accompanied by corresponding visual field defects and is typically associated with elevated intraocular pressures (IOP). Unfortunately, the damage acquired by RGCs is irreversible, making lifelong disease management a considerable burden for patients. The only treatments for glaucoma are to delay progression of disease by lowering the intraocular pressure either through pharmacological agents, surgical means, or a combination of both. The classical pattern of RGC damage begins in the periphery, often outside the typical sphere of daily perception. Unfortunately, this means that for many, clinical symptoms only become visually intrusive enough to seek medical attention after significant damage has already been caused. My clinical mentor, Dr. Beth Edmunds, often describes its process to patients as a speeding train; therapeutic intervention has

put the breaks on but there's momentum, disease progression will continue and the distance left to travel is often difficult to predict.

The initial mechanism of glaucoma is unclear but appears to be multifactorial with anatomical variability, genetic predisposition and RGC vulnerability playing contributory roles. Proposed theories center round a chronic lack of appropriate fluid drainage from the eye (elevated IOP) and/or blood flow to the optic nerve, preferentially damaging the ~1 million RGC axons carrying visual information to the brain[307]. As a subpopulation of RGCs, the ipRGC are presumably exposed to similar injury. Unlike the high density of light sensitive cone photoreceptors that make up central vision, a large portion of ipRGCs are located in the periphery of the retina[280], where classical forms of glaucomatous cell loss initially occurs. Consequently, patients even at early stages of disease can have afferent pupillary defects[308,309] followed by sleep changes at more severe disease stages[306,310]. Abnormalities in pupillary constriction are most pronounced under bright blue light exposure and correlate with glaucoma severity, pointing to ipRGCs involvement[311].

An interesting clinical correlate is the high rate of nightly apneic breathing episodes in glaucoma patients[312]. Obstructive sleep apnea is particularly concerning in the context of glaucoma, as abnormal breathing can limit the blood supply to an already fragile optic nerve (hypoxia, vascular dysregulation) accelerating disease progression. For this reason, glaucoma patients are often

assessed for breathing and sleep disorders upon diagnosis. However, sleep apnea is also associated with circadian misregulation[313,314], with the body performing inappropriately timed breathing episodes. It is therefore possible that the breathing-related sleep issues in glaucoma patients is both a 'contributor to' and a 'result of' ipRGC loss. Further research and proactive clinical studies will be required to investigate this relationship.

Given the reliance on ipRGCs for sleep regulation, entrainment, and the pupillary light reflex, the assumption would be that these glaucoma related behavioral changes should by accompanied by significant anatomical loss of ipRGCs in the retina. However, the results thus far appear divisive. Some quantification studies of ipRGCs in glaucomatous human[315] and rodent models[316] identify a decrease (~50%) in ipRGCs, consistent with the clinical manifestations, but many other studies find ipRGCs have significant resistance to injury compared to conventional RGCs[271,317,318]. What are the reasons for these discrepancies? A potential explanation could be variability in disease severity/progression among patients and in the lack of analogous glaucoma models for laboratory study. An alternative explanation might be a misattributed relevance to the anatomical survival of ipRGCs in histological studies. Presence does not equal function, and researchers have yet to show that remaining ipRGCs are in a functional state late in disease. In fact, given the unique response properties of ipRGCs, a quiescent state of non-function is highly possible.

Some ipRGCs (particularly the M1 type) can enter a state of depolarization block, where the membrane potential of individual cells is so elevated that voltage gated sodium channels are stuck in an inactivate state, preventing the cell from repolarizing[42]. This transiently prevents the cell from initiating action potentials and effectively silences all output under bright lighting conditions (Chapter 4). The proposed function of this is thought to limit the range of light intensities encoded through sensitivity-dependent synaptic drive[42], however, neuro-protection is also possible. Cell survival is reduced with increased metabolic activity[319] and a well-known feature of retinal degeneration is the increased levels of spontaneous activity in RGCs[320,321] (likely due in part to synaptic reorganization and reduced synaptic input to RGCs). In a disease of direct cell damage, such as glaucoma, some ipRGCs may enter a state of electrical inactively, prolonging the degeneration process, preserving ipRGC morphology in the retina (explaining melanopsin staining) but contributing little to non-image forming functions.

Concluding thoughts

Due to the importance of human sight, clinical management of retinal diseases have primarily focused on conscious image-forming functions. However, a growing body of research, discussed above, now suggests that subconscious vision is also compromised during the degeneration process. Reported alterations in the quantity, morphology, and distribution of ipRGCs in age-related and inherited forms of retinal disease likely contribute to central and peripheral

comorbidities. As a result, the clinical management of visually impaired patients should consider more integrative medical approaches, including the assessment of light exposure and its relationship to sleep quality, metabolic function, and mental health. Indeed, a thorough understanding of these associations could lead to alternative diagnostic markers of disease progression. For example, the extent of changes in the pupillary light reflex of glaucoma patients is associated with disease progression and could be used as intermediate measure in remote settings where the visual field and optic nerve examination are not frequently accessible. However, reported discrepancies in the sensitivity of ipRGCs to disease-related damage, as well as differences in behavioral measures predict a more complicated relationship between ipRGC function and degeneration state. In healthy retina, the light information encoded by ipRGCs is still being explored (Chapter 4) and the relevance of many ipRGC brain projections are currently unknown (Chapter 3 & 5.2). In this regard, interpreting the outcome of retinal disease on non-image forming function is challenging and perhaps premature. Future experimental studies should focus on establishing the functional changes that occur in damaged ipRGCs using electrophysiological methods. This should provide context for any behavioral perturbation observed in follow up work. As a further complication, many retinal diseases with shared clinical outcomes have substantially different mechanisms of degeneration, severity, and progression. Future clinical studies within this new field should establish well-defined disease criteria and focus on clear repeatable assessment time points, allowing changes

in non-image forming vision to become a diagnostic component of retinal disease, rather than a subjective footnote.

REFERENCES

1.   Provencio, I., Jiang, G., De Grip, W.J., Hayes, W.P. & Rollag, M.D. Melanopsin: An opsin in melanophores, brain, and eye. *Proc Natl Acad Sci U S A* **95**, 340-345 (1998).

2.   Freedman, M.S.*, et al.* Regulation of mammalian circadian behavior by non-rod, non-cone, ocular photoreceptors. *Science* **284**, 502-504 (1999).

3.   Lucas, R.J., Freedman, M.S., Muñoz, M., Garcia-Fernández, J.M. & Foster, R.G. Regulation of the mammalian pineal by non-rod, non-cone, ocular photoreceptors. *Science* **284**, 505-507 (1999).

4.   Berson, D.M., Dunn, F.A. & Takao, M. Phototransduction by retinal ganglion cells that set the circadian clock. *Science* **295**, 1070-1073 (2002).

5.   Hattar, S., Liao, H.W., Takao, M., Berson, D.M. & Yau, K.W. Melanopsin-containing retinal ganglion cells: architecture, projections, and intrinsic photosensitivity. *Science* **295**, 1065-1070 (2002).

6.   Schmidt, T.M., Chen, S.K. & Hattar, S. Intrinsically photosensitive retinal ganglion cells: many subtypes, diverse functions. *Trends Neurosci* **34**, 572-580 (2011).

7.   Hattar, S.*, et al.* Central projections of melanopsin-expressing retinal ganglion cells in the mouse. *The Journal of comparative neurology* **497**, 326-349 (2006).

8. Beier, C., Zhang, Z., Yurgel, M. & Hattar, S. Projections of ipRGCs and conventional RGCs to retinorecipient brain nuclei. *The Journal of comparative neurology* **529**, 1863-1875 (2021).

9. Panda, S*., et al.* Melanopsin (Opn4) requirement for normal light-induced circadian phase shifting. *Science* **298**, 2213-2216 (2002).

10. Hattar, S*., et al.* Melanopsin and rod-cone photoreceptive systems account for all major accessory visual functions in mice. *Nature* **424**, 76-81 (2003).

11. Albert, D.M. Clyde E. Keeler: The Rodless Mouse and the Early Days of Retinal Genetic Research. *Ophthalmol Retina* **3**, 716-723 (2019).

12. McLaughlin, M.E., Sandberg, M.A., Berson, E.L. & Dryja, T.P. Recessive mutations in the gene encoding the beta-subunit of rod phosphodiesterase in patients with retinitis pigmentosa. *Nat Genet* **4**, 130-134 (1993).

13. Keeler, C.E. The Inheritance of a Retinal Abnormality in White Mice. *Proceedings of the National Academy of Sciences of the United States of America* **10**, 329-333 (1924).

14. Keeler, C.E. IRIS MOVEMENTS IN BLIND MICE. *American Journal of Physiology-Legacy Content* **81**, 107-112 (1927).

15. Klein, T*., et al.* Circadian Sleep Regulation in the Absence of Light Perception: Chronic Non-24-Hour Circadian Rhythm Sleep Disorder in a Blind Man With a Regular 24-Hour Sleep—Wake Schedule. *Sleep* **16**, 333-343 (1993).

16.   Martens, H., Endlich, H., Hildebrandt, G. & Moog, R. Sleep/wake distribution in blind subjects with and without sleep complaints. *Sleep Res* **19**, 398 (1990).

17.   Sack, R.L., Lewy, A.J., Blood, M.L., Keith, L.D. & Nakagawa, H. Circadian rhythm abnormalities in totally blind people: incidence and clinical significance. *The Journal of Clinical Endocrinology & Metabolism* **75**, 127-134 (1992).

18.   Czeisler, C.A.*, et al.* Suppression of melatonin secretion in some blind patients by exposure to bright light. *The New England journal of medicine* **332**, 6-11 (1995).

19.   Provencio, I.*, et al.* A novel human opsin in the inner retina. *J Neurosci* **20**, 600-605 (2000).

20.   Provencio, I., Cooper, H.M. & Foster, R.G. Retinal projections in mice with inherited retinal degeneration: implications for circadian photoentrainment. *The Journal of comparative neurology* **395**, 417-439 (1998).

21.   Moore, R.Y. Chapter 8 Entrainment pathways and the functional organization of the circadian system. in *Progress in Brain Research*, Vol. 111 (eds. Buijs, R.M., Kalsbeek, A., Romijn, H.J., Pennartz, C.M.A. & Mirmiran, M.) 103-119 (Elsevier, 1996).

22.   Brown, T.M.*, et al.* Melanopsin contributions to irradiance coding in the thalamo-cortical visual system. *PLoS biology* **8**, e1000558-e1000558 (2010).

23. Badia, P., Myers, B., Boecker, M., Culpepper, J. & Harsh, J.R. Bright light effects on body temperature, alertness, EEG and behavior. *Physiol Behav* **50**, 583-588 (1991).

24. Güler, A.D.*, et al.* Melanopsin cells are the principal conduits for rod-cone input to non-image-forming vision. *Nature* **453**, 102-105 (2008).

25. Dacey, D.M.*, et al.* Melanopsin-expressing ganglion cells in primate retina signal colour and irradiance and project to the LGN. *Nature* **433**, 749-754 (2005).

26. Menaker, M., Moreira, L.F. & Tosini, G. Evolution of circadian organization in vertebrates. *Braz J Med Biol Res* **30**, 305-313 (1997).

27. Peirson, S.N., Halford, S. & Foster, R.G. The evolution of irradiance detection: melanopsin and the non-visual opsins. *Philos Trans R Soc Lond B Biol Sci* **364**, 2849-2865 (2009).

28. Nilsson, D.E. Photoreceptor Evolution: Ancient Siblings Serve Different Tasks. *Current Biology* **15**, R94-R96 (2005).

29. Walker, M.T., Brown, R.L., Cronin, T.W. & Robinson, P.R. Photochemistry of retinal chromophore in mouse melanopsin. *Proc Natl Acad Sci U S A* **105**, 8861-8865 (2008).

30. Panda, S.*, et al.* Illumination of the melanopsin signaling pathway. *Science* **307**, 600-604 (2005).

31. Sonoda, T. & Lee, S.K. A novel role for the visual retinoid cycle in melanopsin chromophore regeneration. *Journal of Neuroscience* **36**, 9016-9018 (2016).

32. Zhao, X., Pack, W., Khan, N.W. & Wong, K.Y. Prolonged inner retinal photoreception depends on the visual retinoid cycle. *Journal of Neuroscience* **36**, 4209-4217 (2016).

33. Fu, Y. Phototransduction in Rods and Cones. in *Webvision: The Organization of the Retina and Visual System* (eds. Kolb, H., Fernandez, E. & Nelson, R.) (University of Utah Health Sciences Center

Copyright: © 2021 Webvision . Salt Lake City (UT), 1995).

34. Hughes, S., Hankins, M.W., Foster, R.G. & Peirson, S.N. Melanopsin phototransduction: slowly emerging from the dark. *Prog Brain Res* **199**, 19-40 (2012).

35. Sonoda, T., Lee, S.K., Birnbaumer, L. & Schmidt, T.M. Melanopsin Phototransduction Is Repurposed by ipRGC Subtypes to Shape the Function of Distinct Visual Circuits. *Neuron* **99**, 754-767.e754 (2018).

36. Jiang, Z., Yue, W.W.S., Chen, L., Sheng, Y. & Yau, K.W. Cyclic-Nucleotide- and HCN-Channel-Mediated Phototransduction in Intrinsically Photosensitive Retinal Ganglion Cells. *Cell* **175**, 652-664 e612 (2018).

37. Contreras, E., Nobleman, A.P., Robinson, P.R. & Schmidt, T.M. Melanopsin phototransduction: beyond canonical cascades. *J Exp Biol* **224**(2021).

38. Emanuel, A.J. & Do, M.T. Melanopsin tristability for sustained and broadband phototransduction. *Neuron* **85**, 1043-1055 (2015).

39. Somasundaram, P*., et al.* C-terminal phosphorylation regulates the kinetics of a subset of melanopsin-mediated behaviors in mice. *Proceedings of the National Academy of Sciences* **114**, 2741-2746 (2017).

40. Graham, D.M. & Wong, K.Y. Melanopsin-expressing, intrinsically photosensitive retinal ganglion cells (ipRGCs). *Webvision: The Organization of the Retina and Visual System [Internet]* (2016).

41. Mohawk, J.A., Green, C.B. & Takahashi, J.S. Central and peripheral circadian clocks in mammals. *Annu Rev Neurosci* **35**, 445-462 (2012).

42. Milner, E.S. & Do, M.T.H. A Population Representation of Absolute Light Intensity in the Mammalian Retina. *Cell* **171**, 865-876 e816 (2017).

43. Nelson, D.E. & Takahashi, J.S. Sensitivity and integration in a visual pathway for circadian entrainment in the hamster (Mesocricetus auratus). *The Journal of physiology* **439**, 115-145 (1991).

44. Do, M.T*., et al.* Photon capture and signalling by melanopsin retinal ganglion cells. *Nature* **457**, 281-287 (2009).

45. Aranda, M.L. & Schmidt, T.M. Diversity of intrinsically photosensitive retinal ganglion cells: circuits and functions. *Cell Mol Life Sci* **78**, 889-907 (2021).

46. Zhao, X., Stafford, B.K., Godin, A.L., King, W.M. & Wong, K.Y. Photoresponse diversity among the five types of intrinsically photosensitive retinal ganglion cells. *The Journal of physiology* **592**, 1619-1636 (2014).

47. Sand, A., Schmidt, T.M. & Kofuji, P. Diverse types of ganglion cell photoreceptors in the mammalian retina. *Progress in Retinal and Eye Research* **31**, 287-302 (2012).

48. Schmidt, T.M. & Kofuji, P. Structure and function of bistratified intrinsically photosensitive retinal ganglion cells in the mouse. *The Journal of comparative neurology* **519**, 1492-1504 (2011).

49. Kong, J.H., Fish, D.R., Rockhill, R.L. & Masland, R.H. Diversity of ganglion cells in the mouse retina: unsupervised morphological classification and its limits. *The Journal of comparative neurology* **489**, 293-310 (2005).

50. Coombs, J., van der List, D., Wang, G.Y. & Chalupa, L.M. Morphological properties of mouse retinal ganglion cells. *Neuroscience* **140**, 123-136 (2006).

51. Schmidt, T.M.*, et al.* A role for melanopsin in alpha retinal ganglion cells and contrast detection. *Neuron* **82**, 781-788 (2014).

52. Viney, T.J.*, et al.* Local retinal circuits of melanopsin-containing ganglion cells identified by transsynaptic viral tracing. *Current biology : CB* **17**, 981-988 (2007).

53. Sonoda, T., Okabe, Y. & Schmidt, T.M. Overlapping morphological and functional properties between M4 and M5 intrinsically photosensitive retinal ganglion cells. *The Journal of comparative neurology* **528**, 1028-1040 (2020).

54. Ecker, J.L., *et al.* Melanopsin-expressing retinal ganglion-cell photoreceptors: cellular diversity and role in pattern vision. *Neuron* **67**, 49-60 (2010).

55. Stabio, M.E., *et al.* The M5 Cell: A Color-Opponent Intrinsically Photosensitive Retinal Ganglion Cell. *Neuron* **97**, 150-163.e154 (2018).

56. Quattrochi, L.E., *et al.* The M6 cell: A small-field bistratified photosensitive retinal ganglion cell. *J Comp Neurol* **527**, 297-311 (2019).

57. Levine, J.N. & Schwartz, G.W. The Olivary Pretectal Nucleus Receives Visual Input of High Spatial Resolution. *bioRxiv*, 2020.2006.2023.168054 (2020).

58. Reifler, A.N., *et al.* The rat retina has five types of ganglion-cell photoreceptors. *Exp Eye Res* **130**, 17-28 (2015).

59. Schmidt, T.M. & Kofuji, P. Differential cone pathway influence on intrinsically photosensitive retinal ganglion cell subtypes. *J Neurosci* **30**, 16262-16271 (2010).

60. Denman, D.J., Siegle, J.H., Koch, C., Reid, R.C. & Blanche, T.J. Spatial Organization of Chromatic Pathways in the Mouse Dorsal Lateral Geniculate Nucleus. *J Neurosci* **37**, 1102-1116 (2017).

61. Ebihara, S. & Tsuji, K. Entrainment of the circadian activity rhythm to the light cycle: effective light intensity for a Zeitgeber in the retinal degenerate C3H mouse and the normal C57BL mouse. *Physiol Behav* **24**, 523-527 (1980).

62. Li, J.Y. & Schmidt, T.M. Divergent projection patterns of M1 ipRGC subtypes. *The Journal of comparative neurology* **526**, 2010-2018 (2018).

63. Lucas, R.J*., et al.* Diminished pupillary light reflex at high irradiances in melanopsin-knockout mice. *Science* **299**, 245-247 (2003).

64. Chen, S.K., Badea, T.C. & Hattar, S. Photoentrainment and pupillary light reflex are mediated by distinct populations of ipRGCs. *Nature* **476**, 92-95 (2011).

65. Hattar, S*., et al.* Central projections of melanopsin-expressing retinal ganglion cells in the mouse. *The Journal of comparative neurology* **497**, 326-349 (2006).

66. Estevez, M.E*., et al.* Form and function of the M4 cell, an intrinsically photosensitive retinal ganglion cell type contributing to geniculocortical vision. *J Neurosci* **32**, 13608-13620 (2012).

67. Baver, S.B., Pickard, G.E., Sollars, P.J. & Pickard, G.E. Two types of melanopsin retinal ganglion cell differentially innervate the hypothalamic suprachiasmatic nucleus and the olivary pretectal nucleus. *Eur J Neurosci* **27**, 1763-1770 (2008).

68. Do, M.T.H. & Yau, K.-W. Intrinsically photosensitive retinal ganglion cells. *Physiol Rev* **90**, 1547-1581 (2010).

69. Berson, D.M., Castrucci, A.M. & Provencio, I. Morphology and mosaics of melanopsin-expressing retinal ganglion cell types in mice. *The Journal of comparative neurology* **518**, 2405-2422 (2010).

70. Hughes, S., Watson, Thomas S., Foster, Russell G., Peirson, Stuart N. & Hankins, Mark W. Nonuniform Distribution and Spectral Tuning of Photosensitive Retinal Ganglion Cells of the Mouse Retina. *Current Biology* **23**, 1696-1701 (2013).

71. Emanuel, A.J., Kapur, K. & Do, M.T.H. Biophysical Variation within the M1 Type of Ganglion Cell Photoreceptor. *Cell Rep* **21**, 1048-1062 (2017).

72. Rupp, A.C*., et al.* Distinct ipRGC subpopulations mediate light's acute and circadian effects on body temperature and sleep. *Elife* **8**(2019).

73. Sonoda, T*., et al.* A noncanonical inhibitory circuit dampens behavioral sensitivity to light. *Science* **368**, 527-531 (2020).

74. Zeng, H. & Sanes, J.R. Neuronal cell-type classification: challenges, opportunities and the path forward. *Nature Reviews Neuroscience* **18**, 530-546 (2017).

75. Masland, R.H. Neuronal cell types. *Current biology : CB* **14**, R497-500 (2004).

76. Abraira, V.E. & Ginty, D.D. The sensory neurons of touch. *Neuron* **79**, 618-639 (2013).

77. Baden, T*., et al.* The functional diversity of retinal ganglion cells in the mouse. *Nature* **529**, 345-350 (2016).

78. Heukamp, A.S., Warwick, R.A. & Rivlin-Etzion, M. Topographic Variations in Retinal Encoding of Visual Space. *Annu Rev Vis Sci* (2020).

79. Masland, R.H. The neuronal organization of the retina. *Neuron* **76**, 266-280 (2012).

80. Wassle, H. Parallel processing in the mammalian retina. *Nat Rev Neurosci* **5**, 747-757 (2004).

81. Roux, M.J. & Supplisson, S. Neuronal and glial glycine transporters have different stoichiometries. *Neuron* **25**, 373-383 (2000).

82. Eulenburg, V*., et al.* GlyT1 determines the glycinergic phenotype of amacrine cells in the mouse retina. *Brain Struct Funct* **223**, 3251-3266 (2018).

83. Dumitrescu, O.N., Protti, D.A., Majumdar, S., Zeilhofer, H.U. & Wassle, H. Ionotropic glutamate receptors of amacrine cells of the mouse retina. *Vis Neurosci* **23**, 79-90 (2006).

84. Arganda-Carreras, I*., et al.* Trainable Weka Segmentation: a machine learning tool for microscopy pixel classification. *Bioinformatics* **33**, 2424-2426 (2017).

85. Jones, K.A*., et al.* Small-molecule antagonists of melanopsin-mediated phototransduction. *Nature chemical biology* **9**, 630-635 (2013).

86. Mure, L.S., Vinberg, F., Hanneken, A. & Panda, S. Functional diversity of human intrinsically photosensitive retinal ganglion cells. *Science* **366**, 1251-1255 (2019).

87. Lin, J.Y. A user's guide to channelrhodopsin variants: features, limitations and future developments. *Experimental physiology* **96**, 19-25 (2011).

88. Caval-Holme, F., Zhang, Y. & Feller, M.B. Gap Junction Coupling Shapes the Encoding of Light in the Developing Retina. *Current biology : CB* **29**, 4024-4035 e4025 (2019).

89.   Sjöstrand, K., Clemmensen, L.H., Larsen, R., Einarsson, G. & Ersbøll, B. SpaSM: A MATLAB Toolbox for Sparse Statistical Modeling. *2018* **84**, 37 (2018).

90.   Moldavan, M.G. & Allen, C.N. Retinohypothalamic tract synapses in the rat suprachiasmatic nucleus demonstrate short-term synaptic plasticity. *Journal of neurophysiology* **103**, 2390-2399 (2010).

91.   Moldavan, M.G., Sollars, P.J., Lasarev, M.R., Allen, C.N. & Pickard, G.E. Circadian Behavioral Responses to Light and Optic Chiasm-Evoked Glutamatergic EPSCs in the Suprachiasmatic Nucleus of ipRGC Conditional vGlut2 Knock-Out Mice. *eNeuro* **5**, ENEURO.0411-0417.2018 (2018).

92.   Güler, A.D.*, et al.* Melanopsin cells are the principal conduits for rod–cone input to non-image-forming vision. *Nature* **453**, 102-105 (2008).

93.   Hatori, M.*, et al.* Inducible Ablation of Melanopsin-Expressing Retinal Ganglion Cells Reveals Their Central Role in Non-Image Forming Visual Responses. *PLOS ONE* **3**, e2451 (2008).

94.   Do, M.T.H. Melanopsin and the Intrinsically Photosensitive Retinal Ganglion Cells: Biophysics to Behavior. *Neuron* **104**, 205-226 (2019).

95.   Fernandez, D.C.*, et al.* Light Affects Mood and Learning through Distinct Retina-Brain Pathways. *Cell* **175**, 71-84.e18 (2018).

96.   Sondereker, K.B., Stabio, M.E. & Renna, J.M. Crosstalk: The diversity of melanopsin ganglion cell types has begun to challenge the canonical

divide between image-forming and non-image-forming vision. *J Comp Neurol* **528**, 2044-2067 (2020).

97. Keenan, W.T.*, et al.* A visual circuit uses complementary mechanisms to support transient and sustained pupil constriction. *Elife* **5**(2016).

98. Lall, G.S.*, et al.* Distinct contributions of rod, cone, and melanopsin photoreceptors to encoding irradiance. *Neuron* **66**, 417-428 (2010).

99. Milner, E.S. & Do, M.T.H. A Population Representation of Absolute Light Intensity in the Mammalian Retina. *Cell* **171**, 865-876.e816 (2017).

100. Dacey, D.M. The mosaic of midget ganglion cells in the human retina. *J Neurosci* **13**, 5334-5355 (1993).

101. Vaney, D.I. Territorial organization of direction-selective ganglion cells in rabbit retina. *J Neurosci* **14**, 6301-6316 (1994).

102. Wassle, H. & Riemann, H.J. The mosaic of nerve cells in the mammalian retina. *Proc R Soc Lond B Biol Sci* **200**, 441-461 (1978).

103. The Gene Expression Nervous System Atlas (GENSAT) Project, T.R.U.N.Y., NY). MGI download of GENSAT transgene data. *Database Download* (2005).

104. Ishihara, N., Armsen, W., Papadopoulos, T., Betz, H. & Eulenburg, V. Generation of a mouse line expressing Cre recombinase in glycinergic interneurons. *Genesis* **48**, 437-445 (2010).

105. Schmidt, T.M. & Kofuji, P. Functional and morphological differences among intrinsically photosensitive retinal ganglion cells. *J Neurosci* **29**, 476-482 (2009).

106. Schmidt, T.M. & Kofuji, P. Structure and function of bistratified intrinsically photosensitive retinal ganglion cells in the mouse. *Journal of Comparative Neurology* **519**, 1492-1504 (2011).

107. Baden, T*., et al.* A tale of two retinal domains: near-optimal sampling of achromatic contrasts in natural scenes through asymmetric photoreceptor distribution. *Neuron* **80**, 1206-1217 (2013).

108. Szel, A*., et al.* Unique topographic separation of two spectral classes of cones in the mouse retina. *Journal of Comparative Neurology* **325**, 327-342 (1992).

109. Hannibal, J., Hindersson, P., Knudsen, S.M., Georg, B. & Fahrenkrug, J. The photopigment melanopsin is exclusively present in pituitary adenylate cyclase-activating polypeptide-containing retinal ganglion cells of the retinohypothalamic tract. *J Neurosci* **22**, Rc191 (2002).

110. Abrahamson, E.E. & Moore, R.Y. Suprachiasmatic nucleus in the mouse: retinal innervation, intrinsic organization and efferent projections. *Brain Res* **916**, 172-191 (2001).

111. Moore, R.Y., Speh, J.C. & Leak, R.K. Suprachiasmatic nucleus organization. *Cell Tissue Res* **309**, 89-98 (2002).

112. Antle, M.C. & Silver, R. Orchestrating time: arrangements of the brain circadian clock. *Trends Neurosci* **28**, 145-151 (2005).

113. Yan, L*., et al.* Exploring spatiotemporal organization of SCN circuits. *Cold Spring Harb Symp Quant Biol* **72**, 527-541 (2007).

114. Varadarajan, S.*, et al.* Connectome of the Suprachiasmatic Nucleus: New Evidence of the Core-Shell Relationship. *eNeuro* **5**(2018).

115. Wen, S.*, et al.* Spatiotemporal single-cell analysis of gene expression in the mouse suprachiasmatic nucleus. *Nat Neurosci* **23**, 456-467 (2020).

116. Rothhaas, R. & Chung, S. Role of the Preoptic Area in Sleep and Thermoregulation. *Frontiers in Neuroscience* **15**(2021).

117. Delville, Y., De Vries, G.J. & Ferris, C.F. Neural connections of the anterior hypothalamus and agonistic behavior in golden hamsters. *Brain Behav Evol* **55**, 53-76 (2000).

118. Ricci, L.A., Schwartzer, J.J. & Melloni, R.H., Jr. Alterations in the anterior hypothalamic dopamine system in aggressive adolescent AAS-treated hamsters. *Horm Behav* **55**, 348-355 (2009).

119. Melloni, R.H., Jr. & Ricci, L.A. Adolescent exposure to anabolic/androgenic steroids and the neurobiology of offensive aggression: a hypothalamic neural model based on findings in pubertal Syrian hamsters. *Horm Behav* **58**, 177-191 (2010).

120. Zimmerman, C.A., Leib, D.E. & Knight, Z.A. Neural circuits underlying thirst and fluid homeostasis. *Nature reviews. Neuroscience* **18**, 459-469 (2017).

121. Biran, J., Tahor, M., Wircer, E. & Levkowitz, G. Role of developmental factors in hypothalamic function. *Front Neuroanat* **9**, 47-47 (2015).

122. Song, Z., Levin, B.E., Stevens, W. & Sladek, C.D. Supraoptic oxytocin and vasopressin neurons function as glucose and metabolic sensors. *Am J Physiol Regul Integr Comp Physiol* **306**, R447-456 (2014).

123. Sabatier, N., Leng, G. & Menzies, J. Oxytocin, feeding, and satiety. *Front Endocrinol (Lausanne)* **4**, 35-35 (2013).

124. Armstrong, W.E. & Stern, J.E. Electrophysiological and morphological characteristics of neurons in perinuclear zone of supraoptic nucleus. *Journal of neurophysiology* **78**, 2427-2437 (1997).

125. Rodieck, R.W. The density recovery profile: A method for the analysis of points in the plane applicable to retinal studies. *Visual neuroscience* **6**, 95-111 (1991).

126. Zhang, Y., Kim, I.J., Sanes, J.R. & Meister, M. The most numerous ganglion cell type of the mouse retina is a selective feature detector. *Proc Natl Acad Sci U S A* **109**, E2391-2398 (2012).

127. Monavarfeshani, A., Sabbagh, U. & Fox, M.A. Not a one-trick pony: Diverse connectivity and functions of the rodent lateral geniculate complex. *Visual neuroscience* **34**, E012 (2017).

128. Reese, B.E. & Keeley, P.W. Design principles and developmental mechanisms underlying retinal mosaics. *Biol Rev Camb Philos Soc* **90**, 854-876 (2015).

129. Wässle, H., Peichl, L. & Boycott, B.B. Dendritic territories of cat retinal ganglion cells. *Nature* **292**, 344-345 (1981).

130. Reese, B. Retinal Mosaics: Pattern Formation Driven by Local Interactions between Homotypic Neighbors. *Frontiers in Neural Circuits* **6**(2012).

131. Devries, S.H. & Baylor, D.A. Mosaic arrangement of ganglion cell receptive fields in rabbit retina. *Journal of neurophysiology* **78**, 2048-2060 (1997).

132. Fernandez, D.C., Chang, Y.-T., Hattar, S. & Chen, S.-K. Architecture of retinal projections to the central circadian pacemaker. *Proceedings of the National Academy of Sciences* **113**, 6047-6052 (2016).

133. Bleckert, A., Schwartz, G.W., Turner, M.H., Rieke, F. & Wong, R.O. Visual space is represented by nonmatching topographies of distinct mouse retinal ganglion cell types. *Current biology : CB* **24**, 310-315 (2014).

134. Wolfe, J.L. & Tan Summerlin, C. The influence of lunar light on nocturnal activity of the old-field mouse. *Animal Behaviour* **37**, 410-414 (1989).

135. Upham, N.S. & Hafner, J.C. Do nocturnal rodents in the Great Basin Desert avoid moonlight? *Journal of Mammalogy* **94**, 59-72 (2013).

136. Wilkin, L.D., Mitchell, L.D., Ganten, D. & Johnson, A.K. The supraoptic nucleus: afferents from areas involved in control of body fluid homeostasis. *Neuroscience* **28**, 573-584 (1989).

137. Brown, C.H. Magnocellular Neurons and Posterior Pituitary Function. *Compr Physiol* **6**, 1701-1741 (2016).

138. Noh, J.Y.*, et al.* Circadian rhythms in urinary functions: possible roles of circadian clocks? *Int Neurourol J* **15**, 64-73 (2011).

139. Douma, L.G. & Gumz, M.L. Circadian clock-mediated regulation of blood pressure. *Free Radic Biol Med* **119**, 108-114 (2018).

140. Bertram, R., Helena, C.V., Gonzalez-Iglesias, A.E., Tabak, J. & Freeman, M.E. A tale of two rhythms: the emerging roles of oxytocin in rhythmic prolactin release. *J Neuroendocrinol* **22**, 778-784 (2010).

141. Roizen, J., Luedke, C.E., Herzog, E.D. & Muglia, L.J. Oxytocin in the circadian timing of birth. *PloS one* **2**, e922-e922 (2007).

142. Hannibal, J*., et al.* Gene expression of pituitary adenylate cyclase activating polypeptide (PACAP) in the rat hypothalamus. *Regul Pept* **55**, 133-148 (1995).

143. Cagampang, F.R., Piggins, H.D., Sheward, W.J., Harmar, A.J. & Coen, C.W. Circadian changes in PACAP type 1 (PAC1) receptor mRNA in the rat suprachiasmatic and supraoptic nuclei. *Brain Res* **813**, 218-222 (1998).

144. Herzog, E.D. Neurons and networks in daily rhythms. *Nat Rev Neurosci* **8**, 790-802 (2007).

145. Moga, M.M. & Moore, R.Y. Organization of neural inputs to the suprachiasmatic nucleus in the rat. *Journal of Comparative Neurology* **389**, 508-534 (1997).

146. Laboulaye, M.A., Duan, X., Qiao, M., Whitney, I.E. & Sanes, J.R. Mapping Transgene Insertion Sites Reveals Complex Interactions Between Mouse Transgenes and Neighboring Endogenous Genes. *Front Mol Neurosci* **11**, 385 (2018).

147. Wong, K.Y., Dunn, F.A. & Berson, D.M. Photoreceptor adaptation in intrinsically photosensitive retinal ganglion cells. *Neuron* **48**, 1001-1010 (2005).

148. Denk, W. & Detwiler, P.B. Optical recording of light-evoked calcium signals in the functionally intact retina. *Proc Natl Acad Sci U S A* **96**, 7035-7040 (1999).

149. Fernandez, D.C.*, et al.* Retinal innervation tunes circuits that drive nonphotic entrainment to food. *Nature* **581**, 194-198 (2020).

150. Wong, K.Y., Dunn, F.A., Graham, D.M. & Berson, D.M. Synaptic influences on rat ganglion-cell photoreceptors. *The Journal of physiology* **582**, 279-296 (2007).

151. Keppler, A.*, et al.* A general method for the covalent labeling of fusion proteins with small molecules in vivo. *Nat Biotechnol* **21**, 86-89 (2003).

152. Pant, M., Zele, A.J., Feigl, B. & Adhikari, P. Light adaptation characteristics of melanopsin. *Vision Res* **188**, 126-138 (2021).

153. Madisen, L.*, et al.* A toolbox of Cre-dependent optogenetic transgenic mice for light-induced activation and silencing. *Nature neuroscience* **15**, 793-802 (2012).

154. Gale, S.D. & Murphy, G.J. Active Dendritic Properties and Local Inhibitory Input Enable Selectivity for Object Motion in Mouse Superior Colliculus Neurons. *J Neurosci* **36**, 9111-9123 (2016).

155. Deisseroth, K. & Hegemann, P. The form and function of channelrhodopsin. *Science (New York, N.Y.)* **357**, eaan5544 (2017).

156. Eleftheriou, C.G., *et al.* Melanopsin Driven Light Responses Across a Large Fraction of Retinal Ganglion Cells in a Dystrophic Retina. *Front Neurosci* **14**, 320 (2020).

157. Segev, R., Goodhouse, J., Puchalla, J. & Berry, M.J., 2nd. Recording spikes from a large fraction of the ganglion cells in a retinal patch. *Nat Neurosci* **7**, 1154-1161 (2004).

158. Sonoda, T., Lee, S.K., Birnbaumer, L. & Schmidt, T.M. Melanopsin Phototransduction Is Repurposed by ipRGC Subtypes to Shape the Function of Distinct Visual Circuits. *Neuron* **99**, 754-767 e754 (2018).

159. Lucas, R.J., *et al.* Measuring and using light in the melanopsin age. *Trends in neurosciences* **37**, 1-9 (2014).

160. Qiu, Y., *et al.* Natural environment statistics in the upper and lower visual field are reflected in mouse retinal specializations. *Current biology : CB* **31**, 3233-3247 e3236 (2021).

161. Foster, R.G., Hughes, S. & Peirson, S.N. Circadian Photoentrainment in Mice and Humans. *Biology (Basel)* **9**, 180 (2020).

162. Hume, C., Sabatier, N. & Menzies, J. High-Sugar, but Not High-Fat, Food Activates Supraoptic Nucleus Neurons in the Male Rat. *Endocrinology* **158**, 2200-2211 (2017).

163. Cui, L.-N., Jolley, C.J. & Dyball, R.E.J. Electrophysiological Evidence for Retinal Projections to the Hypothalamic Supraoptic Nucleus and its Perinuclear Zone. *J Neuroendocrinol* **9**, 347-353 (1997).

164. Cho, Y*., et al.* Effects of artificial light at night on human health: A literature review of observational and experimental studies applied to exposure assessment. *Chronobiol Int* **32**, 1294-1310 (2015).

165. Bedrosian, T.A. & Nelson, R.J. Influence of the modern light environment on mood. *Mol Psychiatry* **18**, 751-757 (2013).

166. Navara, K.J. & Nelson, R.J. The dark side of light at night: physiological, epidemiological, and ecological consequences. *J Pineal Res* **43**, 215-224 (2007).

167. Blask, D.E*., et al.* Melatonin-depleted blood from premenopausal women exposed to light at night stimulates growth of human breast cancer xenografts in nude rats. *Cancer Res* **65**, 11174-11184 (2005).

168. Fonken, L.K*., et al.* Light at night increases body mass by shifting the time of food intake. *Proc Natl Acad Sci U S A* **107**, 18664-18669 (2010).

169. Wirz-Justice, A., Skene, D.J. & Münch, M. The relevance of daylight for humans. *Biochemical Pharmacology* **191**, 114304 (2021).

170. Colwell, C.S. Linking neural activity and molecular oscillations in the SCN. *Nat Rev Neurosci* **12**, 553-569 (2011).

171. Yamazaki, S*., et al.* Resetting central and peripheral circadian oscillators in transgenic rats. *Science* **288**, 682-685 (2000).

172. Altimus, C.M*., et al.* Rods-cones and melanopsin detect light and dark to modulate sleep independent of image formation. *Proceedings of the National Academy of Sciences* **105**, 19998-20003 (2008).

173. Kennaway, D.J. Resetting the suprachiasmatic nucleus clock. *Front Biosci* **9**, 56-62 (2004).

174. Comperatore, C.A. & Krueger, G.P. Circadian rhythm desynchronosis, jet lag, shift lag, and coping strategies. *Occup Med* **5**, 323-341 (1990).

175. Walker, W.H., Walton, J.C., DeVries, A.C. & Nelson, R.J. Circadian rhythm disruption and mental health. *Translational Psychiatry* **10**, 28 (2020).

176. Cho, K., Ennaceur, A., Cole, J.C. & Suh, C.K. Chronic jet lag produces cognitive deficits. *J Neurosci* **20**, Rc66 (2000).

177. Gander, P.H., Nguyen, D., Rosekind, M.R. & Connell, L.J. Age, circadian rhythms, and sleep loss in flight crews. *Aviat Space Environ Med* **64**, 189-195 (1993).

178. Waterhouse, J., Reilly, T. & Atkinson, G. Jet-lag. *Lancet* **350**, 1611-1616 (1997).

179. Vosko, A.M., Colwell, C.S. & Avidan, A.Y. Jet lag syndrome: circadian organization, pathophysiology, and management strategies. *Nat Sci Sleep* **2**, 187-198 (2010).

180. Loat, C.E. & Rhodes, E.C. Jet-lag and human performance. *Sports Med* **8**, 226-238 (1989).

181. Klein, K. & Wegmann, H. The resynchronization of psychomotor performance circadian rhythm after transmeridian flights as a result of flight direction and mode of activity. In, Scheving, LE, Halberg, F., & Pauly, JE (Eds.), Chronobiology. *Tokyo: Igaku Shoin Ltd*, 564-570 (1974).

182. Lemmer, B., Kern, R.I., Nold, G. & Lohrer, H. Jet lag in athletes after eastward and westward time-zone transition. *Chronobiol Int* **19**, 743-764 (2002).

183. Winget, C.M., DeRoshia, C.W. & Holley, D.C. Circadian rhythms and athletic performance. *Med Sci Sports Exerc* **17**, 498-516 (1985).

184. Doane, L.D.*, et al.* Associations between jet lag and cortisol diurnal rhythms after domestic travel. *Health Psychol* **29**, 117-123 (2010).

185. Liese, B., Mundt, K.A., Dell, L.D., Nagy, L. & Demure, B. Medical insurance claims associated with international business travel. *Occup Environ Med* **54**, 499-503 (1997).

186. Federal Aviation Administration (FAA), D.o.T.D. Flight Attendant Duty Period Limitations and Rest Requirements. Vol. 2022 (Federal Aviation Administration, 2022).

187. Stefaan Ghijs, S.B. The Business Flight Travel Survey Statistics. (Fly Aeolus, 2017).

188. LeGates, T.A.*, et al.* Aberrant light directly impairs mood and learning through melanopsin-expressing neurons. *Nature* **491**, 594-598 (2012).

189. LeGates, T.A., Fernandez, D.C. & Hattar, S. Light as a central modulator of circadian rhythms, sleep and affect. *Nature Reviews Neuroscience* **15**, 443-454 (2014).

190. Cho, K. Chronic 'jet lag' produces temporal lobe atrophy and spatial cognitive deficits. *Nature Neuroscience* **4**, 567-568 (2001).

191. Dibner, C., Schibler, U. & Albrecht, U. The mammalian circadian timing system: organization and coordination of central and peripheral clocks. *Annu Rev Physiol* **72**, 517-549 (2010).

192. Wurtman, R.J., Axelrod, J. & Fischer, J.E. Melatonin synthesis in the pineal gland: effect of light mediated by the sympathetic nervous system. *Science* **143**, 1328-1330 (1964).

193. Shochat, T., Haimov, I. & Lavie, P. Melatonin--the key to the gate of sleep. *Ann Med* **30**, 109-114 (1998).

194. Lavie, P. Melatonin: role in gating nocturnal rise in sleep propensity. *J Biol Rhythms* **12**, 657-665 (1997).

195. Brainard, G.C.*, et al.* Action spectrum for melatonin regulation in humans: evidence for a novel circadian photoreceptor. *J Neurosci* **21**, 6405-6412 (2001).

196. Thapan, K., Arendt, J. & Skene, D.J. An action spectrum for melatonin suppression: evidence for a novel non-rod, non-cone photoreceptor system in humans. *The Journal of physiology* **535**, 261-267 (2001).

197. Blask, D.E. Melatonin, sleep disturbance and cancer risk. *Sleep Medicine Reviews* **13**, 257-264 (2009).

198. Lawrenson, J.G., Hull, C.C. & Downie, L.E. The effect of blue-light blocking spectacle lenses on visual performance, macular health and the sleep-wake cycle: a systematic review of the literature. *Ophthalmic Physiol Opt* **37**, 644-654 (2017).

199. Shi, L., Li, N., Bo, L. & Xu, Z. Melatonin and hypothalamic-pituitary-gonadal axis. *Curr Med Chem* **20**, 2017-2031 (2013).

200. Ishida, A*., et al.* Light activates the adrenal gland: timing of gene expression and glucocorticoid release. *Cell Metab* **2**, 297-307 (2005).

201. Gotlieb, N., Moeller, J. & Kriegsfeld, L.J. Circadian Control of Neuroendocrine Function: Implications for Health and Disease. *Curr Opin Physiol* **5**, 133-140 (2018).

202. Atkinson, H.C. & Waddell, B.J. Circadian Variation in Basal Plasma Corticosterone and Adrenocorticotropin in the Rat: Sexual Dimorphism and Changes across the Estrous Cycle*. *Endocrinology* **138**, 3842-3848 (1997).

203. Dinneen, S., Alzaid, A., Miles, J. & Rizza, R. Metabolic effects of the nocturnal rise in cortisol on carbohydrate metabolism in normal humans. *The Journal of Clinical Investigation* **92**, 2283-2290 (1993).

204. Guchhait, P. & Haldar, C. Circadian Rhythms of Melatonin and Sex Steroids in a Nocturnal Bird, Indian Spotted Owlet Athene brama During Reproductively Active and Inactive Phases. *Biological Rhythm Research* **30**, 508-516 (1999).

205. Lamba, V.J., Goswami, S.V. & Sundararaj, B.I. Circannual and circadian variations in plasma levels of steroids (cortisol, estradiol-17β estrone, and testosterone) correlated with the annual gonadal cycle in the catfish, Heteropneustes fossilis (Bloch). *General and Comparative Endocrinology* **50**, 205-225 (1983).

206. PLYMATE, S.R., TENOVER, J.S. & BREMNER, W.J. Circadian Variation in Testosterone, Sex Hormone-Binding Globulin, and Calculated Non-Sex Hormone-Binding Globulin Bound Testosterone in Healthy Young and Elderly Men. *Journal of Andrology* **10**, 366-371 (1989).

207. Hirotsu, C., Tufik, S. & Andersen, M.L. Interactions between sleep, stress, and metabolism: From physiological to pathological conditions. *Sleep Sci* **8**, 143-152 (2015).

208. Asher, G. & Schibler, U. Crosstalk between Components of Circadian and Metabolic Cycles in Mammals. *Cell Metabolism* **13**, 125-137 (2011).

209. Patton, D. & Mistlberger, R. Circadian adaptations to meal timing: neuroendocrine mechanisms. *Frontiers in Neuroscience* **7**(2013).

210. Challet, E. Keeping circadian time with hormones. *Diabetes Obes Metab* **17 Suppl 1**, 76-83 (2015).

211. Cailotto, C.*, et al.* The suprachiasmatic nucleus controls the daily variation of plasma glucose via the autonomic output to the liver: are the clock genes involved? *Eur J Neurosci* **22**, 2531-2540 (2005).

212. Plano, S.A.*, et al.* Circadian and Metabolic Effects of Light: Implications in Weight Homeostasis and Health. *Frontiers in neurology* **8**, 558-558 (2017).

213. Akhtar, R.A.*, et al.* Circadian cycling of the mouse liver transcriptome, as revealed by cDNA microarray, is driven by the suprachiasmatic nucleus. *Current biology : CB* **12**, 540-550 (2002).

214. Refinetti, R. Comparison of light, food, and temperature as environmental synchronizers of the circadian rhythm of activity in mice. *J Physiol Sci* **65**, 359-366 (2015).

215. Kooijman, S*., et al.* Prolonged daily light exposure increases body fat mass through attenuation of brown adipose tissue activity. *Proceedings of the National Academy of Sciences* **112**, 6748-6753 (2015).

216. Fonken, L.K*., et al.* Light at night increases body mass by shifting the time of food intake. *Proceedings of the National Academy of Sciences* **107**, 18664-18669 (2010).

217. Heydon, M., Sibbald, A., Milne, J., Brinklow, B. & Loudon, A. The interaction of food availability and endogenous physiological cycles on the grazing ecology of red deer hinds (Cervus elaphus). *Functional Ecology*, 216-222 (1993).

218. Arnold, W. Review: Seasonal differences in the physiology of wild northern ruminants. *Animal* **14**, s124-s132 (2020).

219. Bartness, T.J., Demas, G.E. & Song, C.K. Seasonal changes in adiposity: the roles of the photoperiod, melatonin and other hormones, and sympathetic nervous system. *Experimental biology and medicine* **227**, 363-376 (2002).

220. Karsch, F.J*., et al.* Neuroendocrine Basis of Seasonal Reproduction. in *Proceedings of the 1983 Laurentian Hormone Conference*, Vol. 40 (ed. Greep, R.O.) 185-232 (Academic Press, Boston, 1984).

221. Dawson, A., King, V.M., Bentley, G.E. & Ball, G.F. Photoperiodic control of seasonality in birds. *Journal of biological rhythms* **16**, 365-380 (2001).

222. Ruby, N.F. Hibernation: when good clocks go cold. *Journal of Biological Rhythms* **18**, 275-286 (2003).

223. Enezi, J*., et al.* A "melanopic" spectral efficiency function predicts the sensitivity of melanopsin photoreceptors to polychromatic lights. *J Biol Rhythms* **26**, 314-323 (2011).

224. Mouland, J.W., Martial, F., Watson, A., Lucas, R.J. & Brown, T.M. Cones Support Alignment to an Inconsistent World by Suppressing Mouse Circadian Responses to the Blue Colors Associated with Twilight. *Current Biology* **29**, 4260-4267.e4264 (2019).

225. Mouland, J.W., Martial, F.P., Lucas, R.J. & Brown, T.M. Modulations in irradiance directed at melanopsin, but not cone photoreceptors, reliably alter electrophysiological activity in the suprachiasmatic nucleus and circadian behaviour in mice. *Journal of Pineal Research* **70**, e12735 (2021).

226. Walmsley, L*., et al.* Colour As a Signal for Entraining the Mammalian Circadian Clock. *PLOS Biology* **13**, e1002127 (2015).

227. Dobb, R*., et al.* The impact of temporal modulations in irradiance under light adapted conditions on the mouse suprachiasmatic nuclei (SCN). *Scientific Reports* **7**, 10582 (2017).

228. Zhang, H., Khan, A., Chen, Q., Larsson, H. & Rzhetsky, A. Do psychiatric diseases follow annual cyclic seasonality? *PLOS Biology* **19**, e3001347 (2021).

229. Abbasi, H. The effect of climate change on depression in urban areas of western Iran. *BMC Research Notes* **14**, 155 (2021).

230. de Graaf, R., van Dorsselaer, S., ten Have, M., Schoemaker, C. & Vollebergh, W.A.M. Seasonal Variations in Mental Disorders in the General Population of a Country with a Maritime Climate: Findings from the Netherlands Mental Health Survey and Incidence Study. *American Journal of Epidemiology* **162**, 654-661 (2005).

231. Lamont, E.W., Legault-Coutu, D., Cermakian, N. & Boivin, D.B. The role of circadian clock genes in mental disorders. *Dialogues Clin Neurosci* **9**, 333-342 (2007).

232. Kaiser, C.*, et al.* The human habenula is responsive to changes in luminance and circadian rhythm. *Neuroimage* **189**, 581-588 (2019).

233. Blume, C., Garbazza, C. & Spitschan, M. Effects of light on human circadian rhythms, sleep and mood. *Somnologie (Berl)* **23**, 147-156 (2019).

234. Beauchemin, K.M. & Hays, P. Sunny hospital rooms expedite recovery from severe and refractory depressions. *J Affect Disord* **40**, 49-51 (1996).

235. Benedetti, F., Colombo, C., Barbini, B., Campori, E. & Smeraldi, E. Morning sunlight reduces length of hospitalization in bipolar depression. *J Affect Disord* **62**, 221-223 (2001).

236. Rosenthal, N.E.*, et al.* Seasonal affective disorder. A description of the syndrome and preliminary findings with light therapy. *Arch Gen Psychiatry* **41**, 72-80 (1984).

237. Partonen, T. & Pandi-Perumal, S. *Seasonal affective disorder: practice and research*, (Oxford University Press, 2010).

238. Strong, R.E.*, et al.* Narrow-band blue-light treatment of seasonal affective disorder in adults and the influence of additional nonseasonal symptoms. *Depress Anxiety* **26**, 273-278 (2009).

239. Costa, G., Haus, E. & Stevens, R. Shift work and cancer - considerations on rationale, mechanisms, and epidemiology. *Scand J Work Environ Health* **36**, 163-179 (2010).

240. Chang, A.M., Aeschbach, D., Duffy, J.F. & Czeisler, C.A. Evening use of light-emitting eReaders negatively affects sleep, circadian timing, and next-morning alertness. *Proc Natl Acad Sci U S A* **112**, 1232-1237 (2015).

241. Cinzano, P., Falchi, F. & Elvidge, C.D. The first World Atlas of the artificial night sky brightness. *Monthly Notices of the Royal Astronomical Society* **328**, 689-707 (2001).

242. Tracy, S. I Can't Sleep… Can you turn off the lights? in *Science In The News, Harvard University* (2020).

243. Aubrecht, T.G., Jenkins, R. & Nelson, R.J. Dim light at night increases body mass of female mice. *Chronobiol Int* **32**, 557-560 (2015).

244. Chepesiuk, R. Missing the dark: health effects of light pollution. *Environ Health Perspect* **117**, A20-A27 (2009).

245. Nelson, R.J. & DeVries, A.C. Medical hypothesis: Light at night is a factor worth considering in critical care units. *Adv Integr Med* **4**, 115-120 (2017).

246. Pisani, M. Sleep in the intensive care unit: An oft-neglected key to health restoration. *Heart Lung* **44**, 87 (2015).

247. Doğan, O., Ertekin, Ş. & Doğan, S. Sleep quality in hospitalized patients. *Journal of Clinical Nursing* **14**, 107-113 (2005).

248. Bedrosian, T.A. & Nelson, R.J. Timing of light exposure affects mood and brain circuits. *Transl Psychiatry* **7**, e1017 (2017).

249. Miyazaki, T.*, et al.* Correlation between serum melatonin circadian rhythm and intensive care unit psychosis after thoracic esophagectomy. *Surgery* **133**, 662-668 (2003).

250. Evans, L.K. Sundown syndrome in institutionalized elderly. *J Am Geriatr Soc* **35**, 101-108 (1987).

251. Chung, C.R., Yoo, H.J., Park, J. & Ryu, S. Cognitive Impairment and Psychological Distress at Discharge from Intensive Care Unit. *Psychiatry Investig* **14**, 376-379 (2017).

252. Hale, L.*, et al.* Youth Screen Media Habits and Sleep: Sleep-Friendly Screen Behavior Recommendations for Clinicians, Educators, and Parents. *Child Adolesc Psychiatr Clin N Am* **27**, 229-245 (2018).

253. Foreman, J.*, et al.* Association between digital smart device use and myopia: a systematic review and meta-analysis. *The Lancet Digital Health* **3**, e806-e818 (2021).

254. Zhou, X., Pardue, M.T., Iuvone, P.M. & Qu, J. Dopamine signaling and myopia development: What are the key challenges. *Progress in retinal and eye research* **61**, 60-71 (2017).

255. Vugler, A.A., Redgrave, P., Hewson-Stoate, N.J., Greenwood, J. & Coffey, P.J. Constant illumination causes spatially discrete dopamine depletion in the normal and degenerate retina. *J Chem Neuroanat* **33**, 9-22 (2007).

256. Dkhissi-Benyahya, O*., et al.* The absence of melanopsin alters retinal clock function and dopamine regulation by light. *Cell Mol Life Sci* **70**, 3435-3447 (2013).

257. Lingham, G., Mackey, D.A., Lucas, R. & Yazar, S. How does spending time outdoors protect against myopia? A review. *Br J Ophthalmol* **104**, 593-599 (2020).

258. Pauley, S.M. Lighting for the human circadian clock: recent research indicates that lighting has become a public health issue. *Med Hypotheses* **63**, 588-596 (2004).

259. Costa, G. The impact of shift and night work on health. *Appl Ergon* **27**, 9-16 (1996).

260. Costa, G. [Shift work and health]. *Med Lav* **90**, 739-751 (1999).

261. Shields, M. Shift work and health. *Health Rep* **13**, 11-33 (2002).

262. Rajaratnam, S.M. & Arendt, J. Health in a 24-h society. *Lancet* **358**, 999-1005 (2001).

263. Costa, G. Shift work and health: current problems and preventive actions. *Saf Health Work* **1**, 112-123 (2010).

264. Rivera, A.S., Akanbi, M., O'Dwyer, L.C. & McHugh, M. Shift work and long work hours and their association with chronic health conditions: A systematic review of systematic reviews with meta-analyses. *PLOS ONE* **15**, e0231037 (2020).

265. Foster, R.G*., et al.* Sleep and circadian rhythm disruption in social jetlag and mental illness. *Prog Mol Biol Transl Sci* **119**, 325-346 (2013).

266. Roenneberg, T., Allebrandt, Karla V., Merrow, M. & Vetter, C. Social Jetlag and Obesity. *Current Biology* **22**, 939-943 (2012).

267. Caliandro, R., Streng, A.A., van Kerkhof, L.W.M., van der Horst, G.T.J. & Chaves, I. Social Jetlag and Related Risks for Human Health: A Timely Review. *Nutrients* **13**, 4543 (2021).

268. Katsnelson, A. Lighting design for better health and well being. in *Nature outlook* (Nature, 2019).

269. Bernhofer, E.I., Higgins, P.A., Daly, B.J., Burant, C.J. & Hornick, T.R. Hospital lighting and its association with sleep, mood and pain in medical inpatients. *Journal of Advanced Nursing* **70**, 1164-1173 (2014).

270. Puttonen, S., Viitasalo, K. & Härmä, M. Effect of Shiftwork on Systemic Markers of Inflammation. *Chronobiology International* **28**, 528-535 (2011).

271. Lax, P., Ortuño-Lizarán, I., Maneu, V., Vidal-Sanz, M. & Cuenca, N. Photosensitive Melanopsin-Containing Retinal Ganglion Cells in Health and Disease: Implications for Circadian Rhythms. *Int J Mol Sci* **20**(2019).

272. Mattson, M.P. & Magnus, T. Ageing and neuronal vulnerability. *Nat Rev Neurosci* **7**, 278-294 (2006).

273. Harwerth, R.S., Wheat, J.L. & Rangaswamy, N.V. Age-related losses of retinal ganglion cells and axons. *Invest Ophthalmol Vis Sci* **49**, 4437-4443 (2008).

274. Katz, M.L. & Robison, W.G., Jr. Evidence of cell loss from the rat retina during senescence. *Exp Eye Res* **42**, 293-304 (1986).

275. Nadal-Nicolás, F.M., Vidal-Sanz, M. & Agudo-Barriuso, M. The aging rat retina: from function to anatomy. *Neurobiol Aging* **61**, 146-168 (2018).

276. Kolesnikov, A.V., Fan, J., Crouch, R.K. & Kefalov, V.J. Age-related deterioration of rod vision in mice. *J Neurosci* **30**, 11222-11231 (2010).

277. Sugita, Y., Yamamoto, H., Maeda, Y. & Furukawa, T. Influence of Aging on the Retina and Visual Motion Processing for Optokinetic Responses in Mice. *Front Neurosci* **14**, 586013 (2020).

278. Lax, P.*, et al.* Age-related changes in photosensitive melanopsin-expressing retinal ganglion cells correlate with circadian rhythm impairments in sighted and blind rats. *Chronobiol Int* **33**, 374-391 (2016).

279. Davidson, A.J.*, et al.* Chronic jet-lag increases mortality in aged mice. *Current biology : CB* **16**, R914-916 (2006).

280. Esquiva, G., Lax, P., Pérez-Santonja, J.J., García-Fernández, J.M. & Cuenca, N. Loss of Melanopsin-Expressing Ganglion Cell Subtypes and Dendritic Degeneration in the Aging Human Retina. *Frontiers in Aging Neuroscience* **9**(2017).

281. Hood, S. & Amir, S. The aging clock: circadian rhythms and later life. *J Clin Invest* **127**, 437-446 (2017).

282. Turner, P.L. & Mainster, M.A. Circadian photoreception: ageing and the eye's important role in systemic health. *The British journal of ophthalmology* **92**, 1439-1444 (2008).

283. Monk, T.H., Buysse, D.J., Reynolds, C.F., 3rd & Kupfer, D.J. Inducing jet lag in older people: adjusting to a 6-hour phase advance in routine. *Exp Gerontol* **28**, 119-133 (1993).

284. Youngstedt, S.D., Kripke, D.F., Elliott, J.A. & Klauber, M.R. Circadian abnormalities in older adults. *J Pineal Res* **31**, 264-272 (2001).

285. Ancoli-Israel, S. Sleep and aging: prevalence of disturbed sleep and treatment considerations in older adults. *Journal of Clinical Psychiatry* **66**, 24 (2005).

286. Anderson, J.A.E., Campbell, K.L., Amer, T., Grady, C.L. & Hasher, L. Timing is everything: Age differences in the cognitive control network are modulated by time of day. *Psychol Aging* **29**, 648-657 (2014).

287. Asai, M*., et al.* Circadian profile of Per gene mRNA expression in the suprachiasmatic nucleus, paraventricular nucleus, and pineal body of aged rats. *J Neurosci Res* **66**, 1133-1139 (2001).

288. Jun, J.J*., et al.* Fully integrated silicon probes for high-density recording of neural activity. *Nature* **551**, 232-236 (2017).

289. Hood, B.D., Garner, B. & Truscott, R.J.W. Human Lens Coloration and Aging: EVIDENCE FOR CRYSTALLIN MODIFICATION BY THE MAJOR ULTRAVIOLET FILTER, 3-HYDROXY-KYNURENINEO-

β-d-GLUCOSIDE *. *Journal of Biological Chemistry* **274**, 32547-32550 (1999).

290. Kessel, L., Siganos, G., Jørgensen, T. & Larsen, M. Sleep disturbances are related to decreased transmission of blue light to the retina caused by lens yellowing. *Sleep* **34**, 1215-1219 (2011).

291. Ostrin, L.A. Ocular and systemic melatonin and the influence of light exposure. *Clinical and Experimental Optometry* **102**, 99-108 (2019).

292. Brøndsted, A.E.*, et al.* The Effect of Cataract Surgery on Circadian Photoentrainment: A Randomized Trial of Blue-Blocking versus Neutral Intraocular Lenses. *Ophthalmology* **122**, 2115-2124 (2015).

293. Gennuso, K.P., Gangnon, R.E., Matthews, C.E., Thraen-Borowski, K.M. & Colbert, L.H. Sedentary behavior, physical activity, and markers of health in older adults. *Med Sci Sports Exerc* **45**, 1493-1500 (2013).

294. Matthews, C.E.*, et al.* Amount of time spent in sedentary behaviors in the United States, 2003-2004. *Am J Epidemiol* **167**, 875-881 (2008).

295. Boettger, S.F.*, et al.* Prevalence and predictors of vitamin D-deficiency in frail older hospitalized patients. *BMC Geriatrics* **18**, 219 (2018).

296. Huang, C.-H., Huang, Y.-T.A., Lai, Y.-C. & Sun, C.-K. Prevalence and predictors of hypovitaminosis D among the elderly in subtropical region. *PLOS ONE* **12**, e0181063 (2017).

297. Hartong, D.T., Berson, E.L. & Dryja, T.P. Retinitis pigmentosa. *Lancet* **368**, 1795-1809 (2006).

298. García-Ayuso, D.*, et al.* Retinal ganglion cell numbers and delayed retinal ganglion cell death in the P23H rat retina. *Exp Eye Res* **91**, 800-810 (2010).

299. Roska, B. & Sahel, J.-A. Restoring vision. *Nature* **557**, 359-367 (2018).

300. Semo, M.a.*, et al.* Melanopsin retinal ganglion cells and the maintenance of circadian and pupillary responses to light in aged rodless/coneless (rd/rd cl) mice. *European Journal of Neuroscience* **17**, 1793-1801 (2003).

301. McDougal, D.H. & Gamlin, P.D. The influence of intrinsically-photosensitive retinal ganglion cells on the spectral sensitivity and response dynamics of the human pupillary light reflex. *Vision Res* **50**, 72-87 (2010).

302. Zele, A.J., Adhikari, P., Cao, D. & Feigl, B. Melanopsin and Cone Photoreceptor Inputs to the Afferent Pupil Light Response. *Frontiers in Neurology* **10**(2019).

303. Charng, J.*, et al.* Pupillary Light Reflexes in Severe Photoreceptor Blindness Isolate the Melanopic Component of Intrinsically Photosensitive Retinal Ganglion Cells. *Investigative Ophthalmology & Visual Science* **58**, 3215-3224 (2017).

304. Tsuey Tse, M. Circadian rhythm drug approved. *Nature Biotechnology* **32**, 303-303 (2014).

305. Quigley, H.A. Number of people with glaucoma worldwide. *Br J Ophthalmol* **80**, 389-393 (1996).

306. Gracitelli, C.P., *et al.* Intrinsically photosensitive retinal ganglion cell activity is associated with decreased sleep quality in patients with glaucoma. *Ophthalmology* **122**, 1139-1148 (2015).

307. Weinreb, R.N., Aung, T. & Medeiros, F.A. The pathophysiology and treatment of glaucoma: a review. *JAMA* **311**, 1901-1911 (2014).

308. Kaback, M.B., Burde, R.M. & Becker, B. Relative afferent pupillary defect in glaucoma. *Am J Ophthalmol* **81**, 462-468 (1976).

309. Kohn, A.N., Moss, A.P. & Podos, S.M. Relative afferent pupillary defects in glaucoma without characteristic field loss. *Arch Ophthalmol* **97**, 294-296 (1979).

310. Gracitelli, C.P.B., *et al.* Relationship between Daytime Sleepiness and Intrinsically Photosensitive Retinal Ganglion Cells in Glaucomatous Disease. *Journal of Ophthalmology* **2016**, 5317371 (2016).

311. Rukmini, A.V., *et al.* Pupillary Responses to High-Irradiance Blue Light Correlate with Glaucoma Severity. *Ophthalmology* **122**, 1777-1785 (2015).

312. Chaitanya, A., Pai, V.H., Mohapatra, A.K. & Ve, R.S. Glaucoma and its association with obstructive sleep apnea: A narrative review. *Oman J Ophthalmol* **9**, 125-134 (2016).

313. Entzian, P., Linnemann, K., Schlaak, M. & Zabel, P. Obstructive sleep apnea syndrome and circadian rhythms of hormones and cytokines. *Am J Respir Crit Care Med* **153**, 1080-1086 (1996).

314. Butler, M.P.*, et al.* The Circadian System Contributes to Apnea Lengthening across the Night in Obstructive Sleep Apnea. *Sleep* **38**, 1793-1801 (2015).

315. Obara, E.A., Hannibal, J., Heegaard, S. & Fahrenkrug, J. Loss of melanopsin-expressing retinal ganglion cells in severely staged glaucoma patients. *Investigative Ophthalmology & Visual Science* **57**, 4661-4667 (2016).

316. Vidal-Sanz, M.*, et al.* Retinal neurodegeneration in experimental glaucoma. *Prog Brain Res* **220**, 1-35 (2015).

317. Vidal-Sanz, M.*, et al.* Shared and differential retinal responses against optic nerve injury and ocular hypertension. *Frontiers in Neuroscience* **11**, 235 (2017).

318. Rovere, G.*, et al.* Melanopsin-Containing or Non-Melanopsin–Containing Retinal Ganglion Cells Response to Acute Ocular Hypertension With or Without Brain-Derived Neurotrophic Factor Neuroprotection. *Investigative ophthalmology & visual science* **57**, 6652-6661 (2016).

319. Green, D.R., Galluzzi, L. & Kroemer, G. Cell biology. Metabolic control of cell death. *Science (New York, N.Y.)* **345**, 1250256-1250256 (2014).

320. Trenholm, S. & Awatramani, G.B. Origins of spontaneous activity in the degenerating retina. *Frontiers in Cellular Neuroscience* **9**, 277 (2015).

321. Goo, Y.S.*, et al.* Spontaneous oscillatory rhythm in retinal activities of two retinal degeneration (rd1 and rd10) mice. *The Korean Journal of Physiology & Pharmacology* **15**, 415-422 (2011).